

THE DEVELOPMENT OF FINITE ELEMENT MODELING AND
EXPERIMENTAL TECHNIQUES FOR DYNAMIC
ANALYSIS OF READ/WRITE HEAD
DESIGNS ON FLOPPY DISK
MEDIA

By

JAMES KEITH GOOD

Bachelor of Science in Mechanical Engineering
Oklahoma State University
Stillwater, Oklahoma
1977

Master of Mechanical Engineering
Oklahoma State University
Stillwater, Oklahoma
1979

Submitted to the Faculty of the Graduate College
of the Oklahoma State University
in partial fulfillment of the requirements
for the Degree of
DOCTOR OF PHILOSOPHY
July, 1983

Thesis
1983D
G646d
cop. 2



THE DEVELOPMENT OF FINITE ELEMENT MODELING AND
EXPERIMENTAL TECHNIQUES FOR DYNAMIC
ANALYSIS OF READ/WRITE HEAD
DESIGNS ON FLOPPY DISK
MEDIA

Thesis Approved:

Richard L. Lowery

Thesis Adviser

B. E. Price

J. J. Allen

C. E. Kelly

C. L. Young

Norman D. Durham

Dean of the Graduate College

ACKNOWLEDGMENTS

The aid of those who helped during this study is greatly appreciated. I would like to thank and express my appreciation to Dr. R. L. Lowery, my graduate adviser, for his advice, instruction, and moral support during my graduate study. I would also like to thank Drs. J. J. Allen, A. E. Kelly, C. E. Price, and C. T. Young for participation as committee members.

I would like to acknowledge the engineering group of Magnetic Peripherals Incorporated for their cooperation in providing data and insight.

My appreciation is expressed to Ms. Becky Farrell for her assistance in preparing this manuscript.

I owe special words of gratitude to my wife, Linda, for her sacrifices, encouragement, and patience during this study. I would also like to thank my parents who have encouraged and inspired my educational endeavors.

I would also like to acknowledge the School of Mechanical and Aerospace Engineering for providing an Instructorship which made this study possible.

TABLE OF CONTENTS

Chapter	Page
I. INTRODUCTION	1
Overview	1
Approach to the Problem	2
Organization	2
II. LITERATURE SURVEY	4
Background History	4
Experimental Studies	5
Summary	6
III. ANALYTICAL STUDY	9
Purpose and Objective	9
Approach to the Problem	9
Model Details	16
IV. ANALYTICAL RESULTS	28
V. EXPERIMENTAL STUDIES	59
VI. EXPERIMENTAL RESULTS	89
VII. CORRELATION BETWEEN ANALYTICAL AND EXPERIMENTAL STUDIES	118
VIII. CONCLUSIONS	121
Overview	121
Conclusions Regarding Design Characteristics	122
Recommendations for Future Designs	123
BIBLIOGRAPHY	125
APPENDIX	128

LIST OF TABLES

Table	Page
I. New Production Head Flexure Eigenvalue Analysis	28
II. Old Production Head Flexure Eigenvalue Analysis	30
III. New Production Read/Write Head with Disk Eigenvalue Analysis	30
IV. Old Production Read/Write Head with Disk Eigenvalue Analysis	37
V. Difference Table for Figure 52	85
VI. Experimental Eigenvalues and Eigenvectors of Single Read/Write Head Flexures	88
VII. Resonant Frequencies of Heads at an Outside Track on Various Disks.	104
VIII. Pitch and Displacement of the New Production Head on a Maxell FD2 Disk at an Outside Track	113
IX. Roll of the New Production Head on a Maxell FD2 Disk at an Outside Track	114
X. Rotation and Displacement of the Old Production Head on an IBM 2D Diskette at an Outside Track	117

LIST OF FIGURES

Figure	Page
1. Bar Element Coordinate System and Element Forces	10
2. Floppy Disk Model	12
3. Forces and Stresses in Plate Element	14
4. Rod Element Coordinate System and Element Forces	15
5. New Production Head Finite Element Model	19
6. Old Production Head Finite Element Model	20
7. Old Production Head, High Density Finite Element Model	21
8. Read/Write Head/Disk Model Coordinate System	25
9. Definition of Pitch and Roll	29
10. New Production Head Flexure, Cantilever Mode, Frequency = 23.8 Hz.	31
11. New Production Head Flexure, Pitch Mode, Frequency = 109.5 Hz.	32
12. New Production Head Flexure, Roll Mode, Frequency = 205.8 Hz.	33
13. Old Production Head Flexure, Cantilever Mode, Frequency = 32.5 Hz.	34
14. Old Production Head Flexure, Pitch Mode, Frequency = 104.7 Hz.	35
15. Old Production Head Flexure, Roll Mode, Frequency = 227.2 Hz.	36
16. New Production Head/Disk Model, First Pitch Mode, Mode 8	38

Figure	Page
17. New Production Head/Disk Model, Mode 9	39
18. New Production Head/Disk Model, Mode 11	40
19. Old Production Head/Disk Model, First Pitch Mode, Mode 8	41
20. Old Production Head/Disk Model, Mode 10	42
21. Old Production Head/Disk Model, Mode 11	43
22. Old Production Head/Disk Model, Second Pitch Mode, Mode 20	44
23. Transient Input Function	46
24. Fourier Transform of Transient Input Function	47
25. Transient Analysis, Spike Pitch, New Production Head/Disk, Pitch Motion of Head	48
26. Transient Analysis, Spike Roll, New Production Head/Disk, Roll Motion of Head	49
27. Transient Analysis, Spike Pitch, Old Production Head/Disk, Pitch Motion of Head	51
28. Transient Analysis, Spike Roll, Old Production Head/Disk, Roll Motion of Head	52
29. SEM Photograph of a Disk Surface in an Area of Relatively Low Wear	54
30. SEM Photograph of a Disk Surface in an Area of Relatively High Wear	55
31. Old Production Head, High Element Density Flexure Model, Third Pitch Mode, Frequency = 1377 Hz.	56
32. Old Production Head/Complete Disk Model, First Pitch Mode, Frequency = 120.5 Hz.	58
33. Semiconductor Strain Gage Installed on Center Load Spring	60
34. Time Response of Center Load Spring	61
35. Response of Photocell to Translation	64
36. Response of Photocell to Rotation	64

Figure	Page
37. Dual Channel Response to Translation	65
38. Dual Channel Response to Rotation	65
39. Dual Channel System Output for Translation and Rotation	66
40. Dual Channel System Detector Block	66
41. Linear Tape Drive Schematic	68
42. Dual Beam LAMDA System Setup	70
43. Axes About Which Pitch and Roll are Defined	71
44. One of the Motion Detector Blocks for the Dual Beam LAMDA System	72
45. Response of Dual Beam LAMDA System to Translation	73
46. Response of Dual Beam LAMDA System to Rotation	75
47. Response of Dual Beam LAMDA System to Translation and Rotation	76
48. Translation Response for Front-Top Detector	78
49. Compensator Schematic with Frequency Response and Transfer Function	80
50. Experimental Frequency Response of the Front-Top Compensator	81
51. Average Translatory Frequency Response for the Front-Top Detector with Reflective Surface Positioned to Simulate the New Production Head	82
52. Translation Calibration for Front-Top Detector Positioned for the New Production Head	84
53. Schematic of Instrumentation for Dual Beam LAMDA Apparatus	87
54. Voltage versus Time Traces for the New Production Head on Disks of Various Manufacturers	90
55. Spectral Plots Corresponding to Voltage versus Time Traces of Figure 54	91

Figure	Page
56. Voltage versus Time Traces for the Old Production Head on Disks of Various Manufacturers	92
57. Spectral Plots corresponding to Voltage versus Time Traces of Figure 56	94
58. Voltage versus Time Traces for the New Production Head at Various Drive Speeds	95
59. Spectral Plots Corresponding to Voltage versus Time Traces of Figure 58	97
60. Voltage versus Time Traces for the Old Production Head at Various Drive Speeds	99
61. Spectral Plots Corresponding to Voltage versus Time Traces of Figure 60	102
62. Composite Modeshape for First Diametral Mode of Disk	106
63. Flowchart to Implement Trial and Error Method to Calculate the Translation and Pitch of the Read/Write Heads	108
64. Flowchart to Implement Trial and Error Method to Calculate the Roll of the Read/Write Heads	109
65. New Production Head on an Outside Track of a Maxell FD2 Disk, Chart Speed = 32 in/sec.	111
66. New Production Head on an Outside Track of a Maxell FD2 Disk, Chart Speed = 8 in/sec.	112
67. Old Production Head on an Outside Track of an IBM 2D Diskette, Chart Speed = 32 in/sec.	115
68. Old Production Head on an Outside Track of an IBM 2D Diskette, Chart Speed = 8 in/sec.	116

CHAPTER I

INTRODUCTION

Overview

The micro- and mini-computer industry has been developing and producing two types of magnetic disk drive storage devices over the last decade. One type, known as "Winchester", is a hard, relatively inflexible disk, which is capable of recording and retrieving data at rates of 937.5 kilobytes/sec and has storage capacities of up to 120 megabytes.¹ The second type of disk is denoted as the "floppy". As the name suggests, the floppy is a very flexible disk compared to the Winchester. The advantage of the floppy compared to the Winchester is low unit cost, sometimes as much as one order of magnitude. The disadvantages of the floppy are its low data transfer rate of 23 kilobytes/sec and storage capacity of 1.18 megabytes.

At present, each disk, Winchester and floppy, have a certain domain in the marketplace. These domains are controlled by the computer user's needs and by what he can afford. The floppy disk drive unit has seen many iterations in past years as competing manufacturers have investigated means of increasing storage capacity as well as data transfer rate while retaining disk surface quality and low wear upon the read/write heads.² Some read/write head designs have witnessed vibration phenomena which lead to signal loss and excessive wearing of the disk media.³ Understanding these phenomena

could result in extended disk and read/write head life and allow an increase in rotational drive speed which could increase the data transfer rate.

This study will be an attempt to determine the interaction of the read/write heads with the floppy disk media in effort to determine design characteristics which may make the head/disk system susceptible to vibration phenomena.

Approach to the Problem

The approach to the problem will be twofold. An analytical study will be performed using the technique of finite elements to model read/write head - floppy disk systems. Experimental studies will be performed in effort to develop experimental apparatus that can detect the motion and frequency content thereof of the read/write heads. Data obtained from such experiments will be compared to results of the analytical study. Other experiments will be performed to verify assumptions made in the analytical study.

Organization

Chapter II consists of a literature survey in which topics concerning floppy disk systems are discussed. Chapter III discusses the analytical study of the system and Chapter IV presents the results of that study. Chapter V describes the experiments performed and Chapter VI presents the results of experiments which were successful. Chapter VII discusses the correlation between the analytical results of Chapter IV and the experimental results of

Chapter VI. Chapter VIII presents conclusions formulated during the study.

CHAPTER II

LITERATURE SURVEY

Background History

The topic of deflection of a spinning disk under an out-of-plane load has long been of engineering interest. Early interest was stimulated by applications such as turbine rotor and circular saw vibrations. More recently, these studies have been extended into the area of disks of greater flexibility than the early studies considered. The floppy disk drive system has been primarily responsible for these studies.

Early work on the vibration of spinning disks explored the free vibration phenomena. Perhaps the earliest known study was by Lamb and Southwell⁴ who derive linear equations of transverse (i.e., out-of-plane) deflections of a spinning disk. Furthermore, they derive the contributions to the equations from bending and membrane stresses due to rotation. The purpose of this study and a later study by Southwell⁵ was to determine the eigenvalues and their vectors of free vibration for disks which were either very stiff or very flexible. Prescott⁶ extended Lamb and Southwell's analysis to disks of varied clamp geometries. The effect of large amplitude vibrations which induce nonlinearities into the equations of motion was studied by Tobias⁷ and Nowinski.⁸

Iwan and Moeller⁹ attacked the problem of stability of a transverse loaded spinning disk. The load was distributed over a small area of the disk and was modeled as a mass connected to a rigid base by parallel spring and damper components. Solutions of the equations of motion were sought in the form of a Fourier series. Benson¹⁰ and a subsequent paper by Benson and Bogy¹¹ extended the work of Iwan and Moeller to higher order modeshapes by employing a numerical solution technique.

The finite element technique has been employed in recent analyses of rotating disks.¹²⁻¹⁶ Pardoen¹² has developed annular ring elements used in a study of asymmetric bending of circular plates. Srinivasan and Ramamurti¹³ have extended Pardoen's technique to investigate the in-plane, free vibration of annular disks. Nigh and Olson¹⁴ studied the critical speeds of rotating disks and what effect damping and static transverse loads have on critical speed.

Experimental Studies

The earliest documented study of flexible disks was performed by Pelech and Shapiro.¹⁷ The first flexible disk magnetic recording devices consisted of a flexible disk rotating over a flat plate. Separation was maintained between disk and plate by injecting gas through the plate at the center of rotation of the disk. The disks were not encased in jackets and were not easily removable. The recording heads were implanted in the plate at fixed radial locations. Pelech and Shapiro were interested in the radial flow and pressure distribution of the gas between the disk and plate. To solve their problem gap width, the distance between plate and disk, had to

be determined as it varied radially. This was accomplished by projecting an image onto the plate and focusing a microscope on that image. The disk was then mounted and spun at which point the microscope was focused upon the image on the disk. The difference in elevation of the microscope from focus on the plate to focus on the disk was recorded by a dial indicator. All experimentation was performed at 3600 R.P.M. on disks cut from 2 mil Mylar film.

Krauter and Bulkeley¹⁸ investigated the effect of central clamping on free transverse vibrations of spinning membrane disks. The experimental apparatus consisted of an annular membrane disk (18 mil Neoprene) clamped about the inside radius by a vertical arbor. The arbor was driven by a D.C. motor and set atop an eccentric driven shake table. The entire apparatus was enclosed within a bell jar to eliminate aerodynamic effects. Typical residual pressures were less than 1 mm Hg during experimentation. Resonant frequencies were determined with the aid of a Strobotac.

Lin and Sullivan¹⁹ used white light interferometry to study the flying height of the read/write head stylus over the disk media. Increases in bit density generally require reduction of flying height. The white light interferometry technique can resolve flying heights less than 1 μm . This technique required that the stylus material be transparent (usually glass). Incident white light was directed through the stylus, part of which is reflected at the stylus-air interface while the remaining part is refracted through the thin air film toward the disk. The disk reflects this light and an observer views the two reflected light rays. As the two rays follow optical paths of different lengths they must have a phase difference

which will cause interference patterns. Using white light, some wavelengths will remain undiminished by constructive interference while other wavelength's intensities will be diminished by destructive interference. The color viewed by the observer is a function of the air film thickness and can be compared to Newton's Color Scale²⁰ to determine the film thickness.

Waddell²¹ examined strain patterns in rotating annular disks. In this study, Waddell developed what was later denoted as an "image derotator" to view fringes in a spinning photoelastic disk. The effect of the derotator was to cancel the rotary motion of the disk allowing the observer to view stationary fringes in the disk. The derotator is a prism rotating at half the disk's angular velocity through which the disk's image is viewed. The image derotator was employed by Stetson and Elkins²² and later by MacBain, Horner, Stauge, and Ogg²³ in conjunction with holographic interferometry. These studies were concerned with the vibration analysis of a spinning disk. Experiments were performed on a 10 inch diameter 1018 steel disk that was 0.0625 inches thick. The disk was rotated at speeds ranging from 2000 to 8000 R.P.M. and resonance was established by a electromagnet controlled by an oscillator. Using this technique the first five diametral modes and one complex (ring) mode were obtained at various angular velocities.

Kita, Kogure, Mitsuva, and Nakanishi²⁴ have developed a method of detecting contact between the read/write head and disk using acoustic emission. Although a Winchester drive was used during tests, this method is easily extended to other disk drives as the acoustic emission sensor is unobtrusive.

Summary

Engh²⁵ has compiled a review of the IBM diskette and disk drive development history in the 1971-1979 period. Of particular interest is the progression from fixed read/write head designs to read/write heads on flexible suspensions. Floppy disk drives typically rotate at 360 R.P.M.. Engh describes a 720 R.P.M. drive in which the previous dual-sided heads became unstable and had to be altered. Most of the design work was verified by the use of white light interferometry.

There is a wealth of information concerning the aerodynamic pressure profile developed between the stylus and disk by analytic and experimental means. Some of these experimental techniques have already been discussed, Greenberg²⁶ and Adams²⁷ have discussed analytical techniques.

The literature is scant on the subject of head suspension design. Therefore, a need exists for design tools which can analytically or experimentally perform dynamic analyses on read/write head-floppy disk systems and to aid in the stability analysis thereof.

CHAPTER III

ANALYTICAL STUDY

Purpose and Objective

The purpose of this study is to model a system consisting of the floppy disk and the read/write head. The model will be experimentally verified and used to determine the characteristics of read/write head designs which contribute to signal loss or excessive wearing of the disk media.

Approach to the Problem

The method of finite elements was chosen to model the system. The finite element code known as NASTRAN which is an acronym for NASA Structural Analysis, was employed. The version of NASTRAN used was COSMIC level 17.6.

The method of analysis chosen was to first isolate a read/write head spring and perform a finite element eigenvalue analysis. This analysis was verified by shaking isolated head springs on an electromagnetic shaker and determining the natural frequencies. The model was then iterated to produce the experimental eigenvalue. The read/write head flexures were easily modeled using bar elements as depicted in Figure 1. Moments of inertia, cross sectional area, and the polar moment of inertia were determined from engineering drawings :

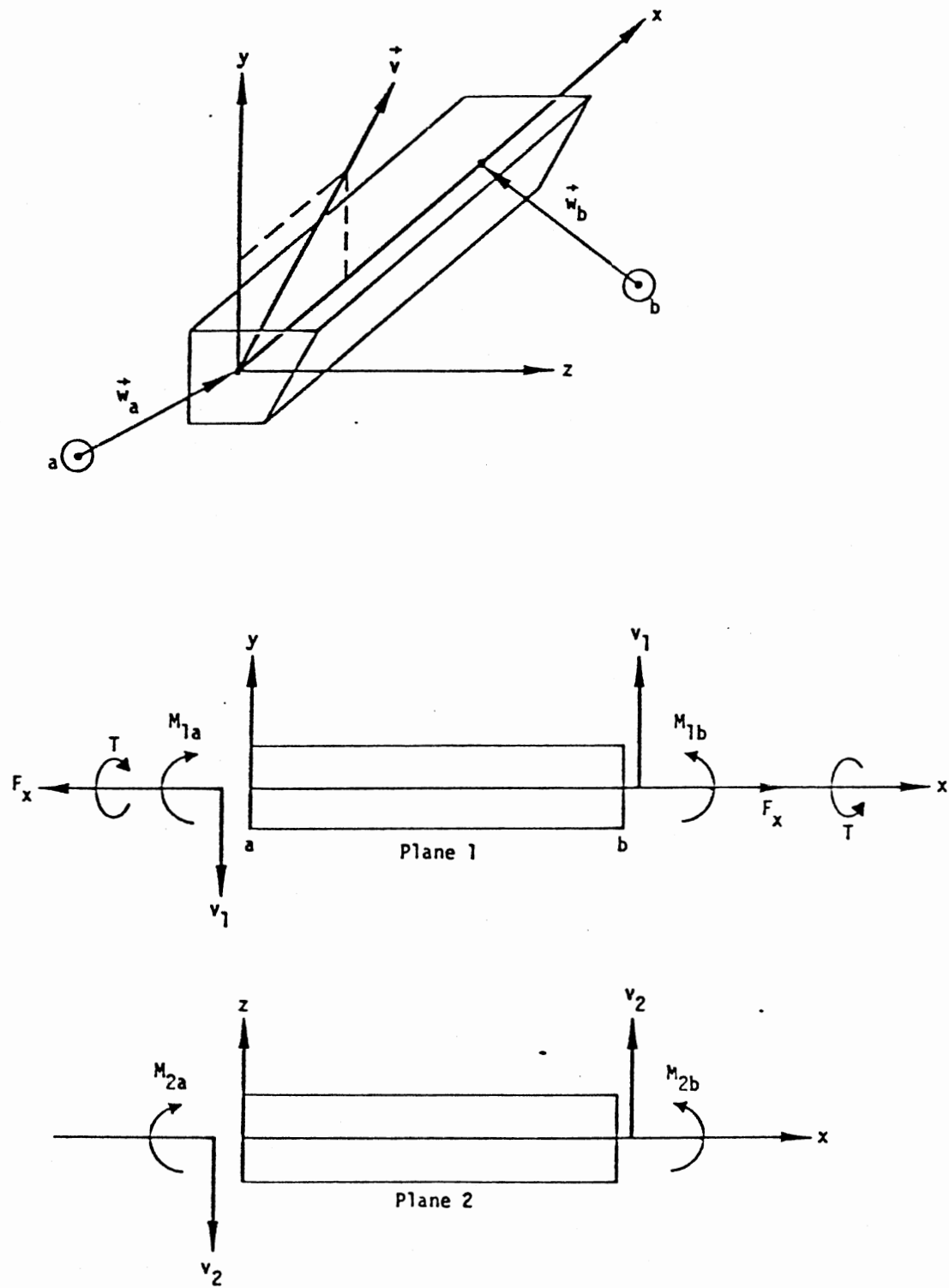


Figure 1. Bar Element Coordinate System and Element Forces

of state of the art designs supplied by MPI.* The only difficult area to model was the stylus in the determination of its mass and mass moments of inertia. Rough calculations were input and then iterated until the computed natural frequencies were reasonably close to the experimental values. Consequently, a verified model of isolated read/write head springs was developed for two designs, denoted as the old and new production heads.

The floppy disk was first modeled as a disk in its entirety to study buckling phenomena and natural frequencies. This model, portrayed in Figure 2, incorporated a high element density in one sector while the rest of the disk was of low element density. The solution cost of this model made it impractical for use in the head/disk analysis.

Before analysis could proceed, an assumption of high risk had to be made. This entailed modeling the disk and head in a fixed reference system. Only the results would prove the validity of this assumption.

An assumption was made that perhaps a sector of the disk would be adequate to model the head/disk interaction. An automatic mesh generation technique was developed to generate a disk sector as a function of inside and outside radius, sector size in degrees, maximum frequency and rotational speed. In addition, an option to logarithmically decrement the element size as a function of radius was included. The inside radius of the disk was clamped to simulate the

*Magnetic Peripherals Inc., Oklahoma City, Oklahoma.

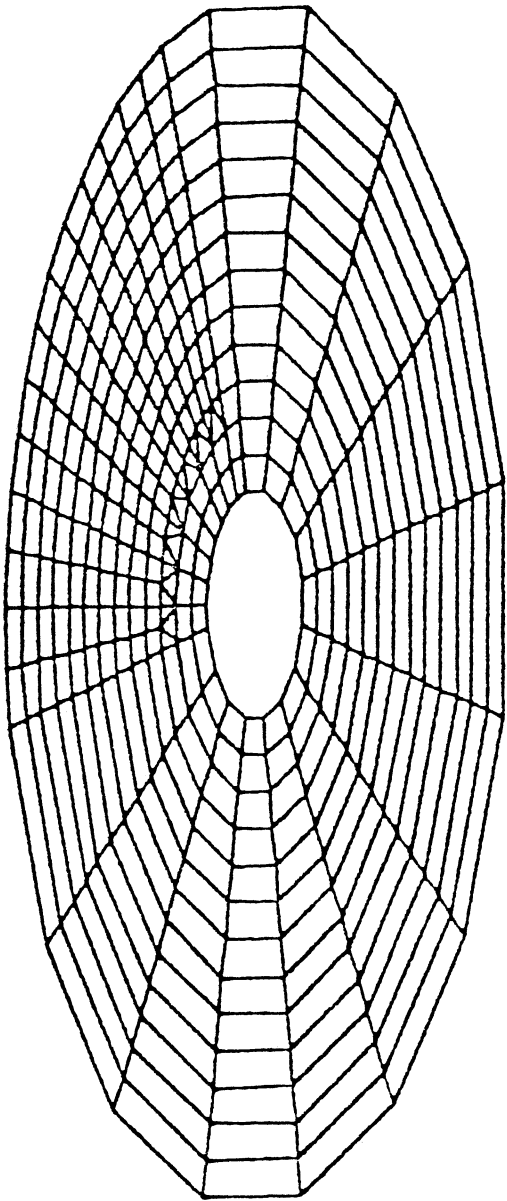


Figure 2. Floppy Disk Model

clamping to the disk hub. The straight edges of the sector were simply supported, while later iterations had clamped edges.

The disk was modeled of plate elements having both in-plane and bending stiffness. This element, shown in Figure 3, has the capability of directional material properties. This is convenient as the disk material, Mylar_{TM}, has directional properties as a substrate and due to rolling processes during production. Experimental tests in which coupons of several orientations were tested showed a range in modulus of elasticity of 40,000 psi. Mylar has a modulus of elasticity of approximately 312,000 psi so the 40,000 psi constitutes a 13% change. This change is deemed insignificant since the disk is rotating such that the read/write head senses a mean value of material properties. The disk is assumed to have isotropic properties for purposes of this study.

A 45 degree sector of an eight-inch diameter disk was generated. The log decrement option was designated for a case having a drive speed of 360 rpm and a maximum wave frequency of 200 Hz.. One of the experimentally verified head models was placed at mid-sector at an outer track. The mirror image of that head was placed on the opposite side of the disk. To complete the model, a fictitious connection had to be made between the head and disk. This was to simulate a preload that exists in the read/write head flexures. To accomplish this, rod elements capable of resisting axial but not bending loads were connected between the head and disk. Figure 4 depicts this element. The stiffness of these rod members were determined by equating the bending stiffness at the flexure ends to an axial stiffness. This assumption was deemed valid as no pressure can

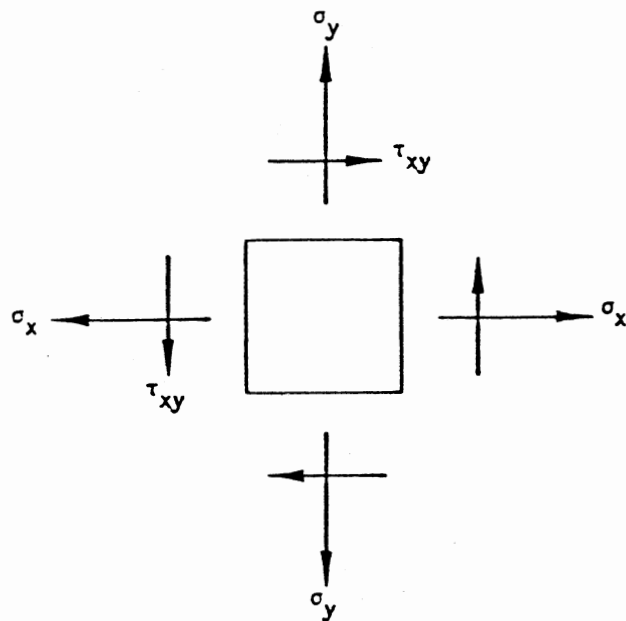
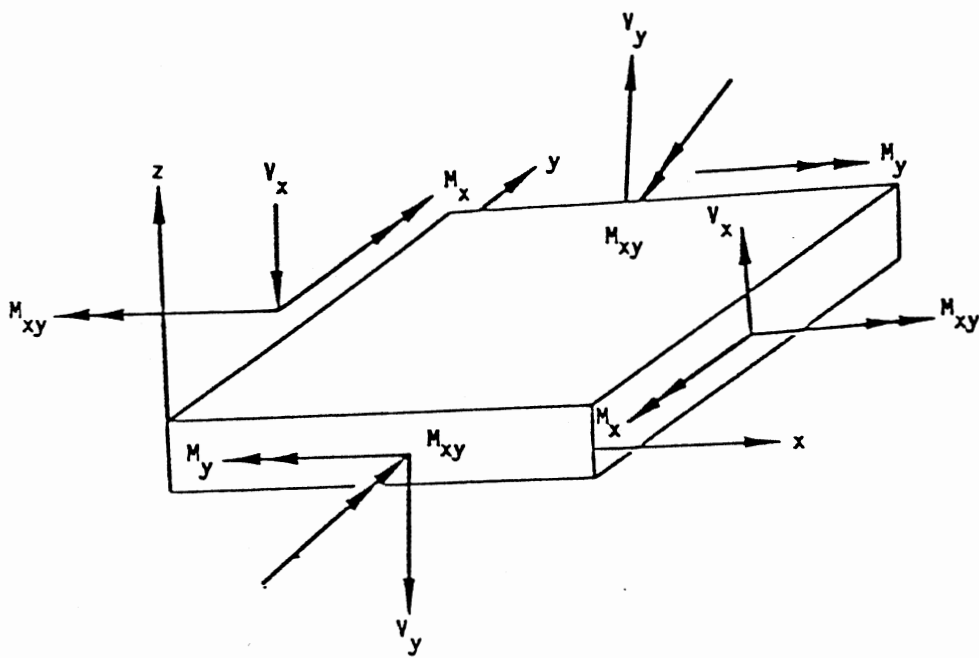


Figure 3. Forces and Stresses in Plate Elements

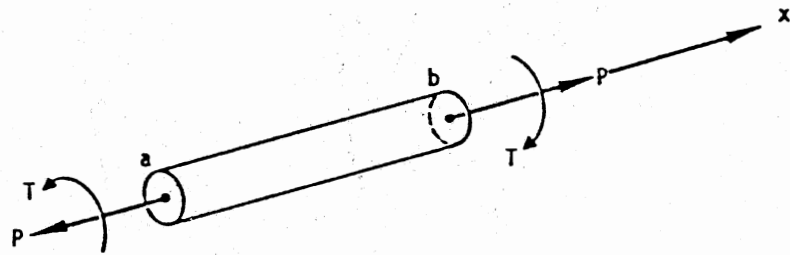


Figure 4. Rod Element Coordinate System and Element Forces

be exerted on the disk greater than the bending stiffness of the flexures will allow.

With the models complete, a method of analysis was planned. The natural frequencies would be determined for head/disk combinations with both fixed and free boundary conditions at the sector edges. In addition, natural frequencies of the head on the full disk model would be determined. If the natural frequencies were unaffected by boundary conditions, confidence could be established that a large enough sector had been chosen to well represent the disk. Providing the prior analyses proved fruitful, transient analyses would be performed. These analyses will yield the modal contribution to pulse inputs about selected axes.

Model Details

The forementioned models were first configured of single flexures for the new and old production heads. Pertinent data was accumulated from MPI Engineering Drawing No. 75889335 for the new production head and from No. 75889440 for the old production head.

The first step was to discretize the flexure in terms of geometric grid points located in a Cartesian coordinate system. These grid points were typically located at points where the flexure structure changes in either direction or cross sectional properties. These points can have from zero to six degrees of freedom in a particular coordinate system.

The second step included choosing the elements of which the flexure would be composed. Per the description in the Approach to the Problem, elements denoted as bars (CBAR) were used in these

analyses.²⁸ These elements are capable of resisting bending moments about two axes, an axially concentric torque, as well as shear on two axes and finally an axial load. The input data includes such things as element and section property identification, connectivities (i.e., identification of grid points which the element connects), a reference plane for the section properties (this can be accomplished by designating a vector or a third grid point), and finally restraint releases which can remove the ability to resist one of the forementioned loads at either end of the bar.

The third step is defining the structural properties of the bar (PBAR).²⁸ Property and material identification are required as well as cross sectional area, moments of inertia, torsional constants and offsets for centroids if not coincidental with the grid points. A time saving feature is that elements with identical properties need not have these properties repeated. Thus, several bar elements may reference one set of property data. This is also true for material properties (i.e., several structural properties may refer to one set of material data). This data (MAT1) includes such entities as Young's Modulus, Poisson's ratio or the shear modulus, and density.²⁸

Concentrated masses (CONM2) can be located at or offset from grid points and if desired mass moments of inertia can be included.²⁸

In the fashion described, models were prepared for the new and old production head. A concentrated mass was placed at the centroid of the ceramic portion of the read/write head. The roots of the center and side flexures were fixed with respect to the coordinate system as the assembly in which the read/write heads are mounted are considerably stiffer (i.e., relatively high moments of inertia) when

compared to the flexures. At the point at which the center flexure meets the dimple on the back of the read/write head a ball joint was created by not allowing the end of the center flexure to resist moments or torques.

After experimentally determining the first few natural frequencies of the flexures, the concentrated mass and the corresponding mass moments of inertia were iterated until reasonable correlation was obtained between experiment and analysis. Figures 5, 6, and 7 are line drawings of head flexure models used in these analyses. The model shown in Figure 7 is a high element density version of the old production head whose purpose is forthcoming in the Analytical Results of Chapter IV.

With verified head flexure models modeling of the floppy disk became imminent. As noted in the Approach to the Problem, the disk was discretized into quadrilateral plates (CQUAD2) capable of resisting bending moments in addition to membrane forces.²⁸ These elements were selected in particular as even though the bending stiffness of the disk is small it is hardly trivial when compared to the bending stiffness of the head flexures. The bending stiffness per unit width for a plate is denoted as:²⁹

$$D = \frac{Eh^3}{12(1 - \nu^2)} = \frac{312,000(.003)^3}{12(1 - (.3)^2)} = 7.7 \times 10^{-4} \text{ LB} - \text{IN}^2 \quad (3.1)$$

The bending stiffness of parts of the new production head flexures is:

$$\begin{aligned} EI &= (3.0 \times 10^7)(6.0 \times 10^{-11}) \\ &= 1.8 \times 10^{-3} \text{ LB} - \text{IN}^2 \end{aligned} \quad (3.2)$$

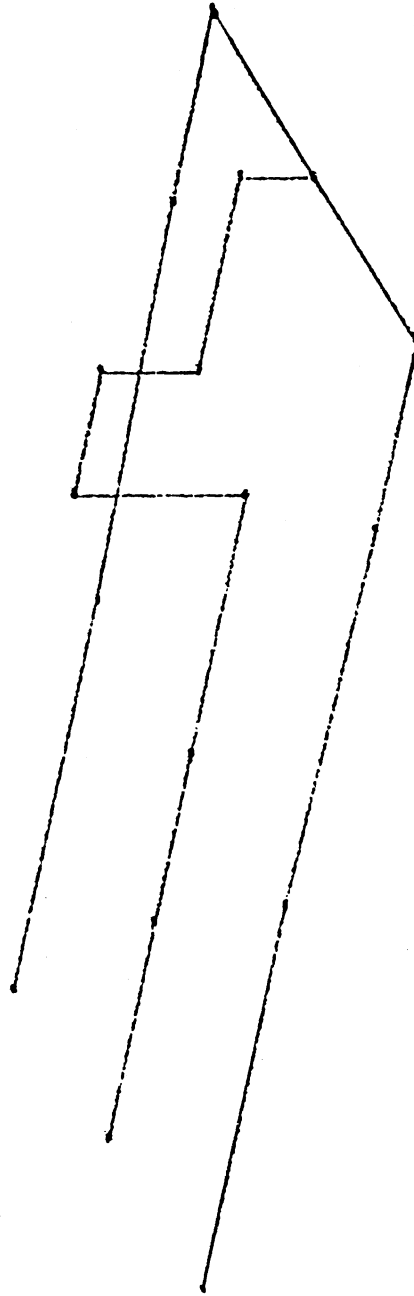


Figure 5. New Production Head Finite Element Model

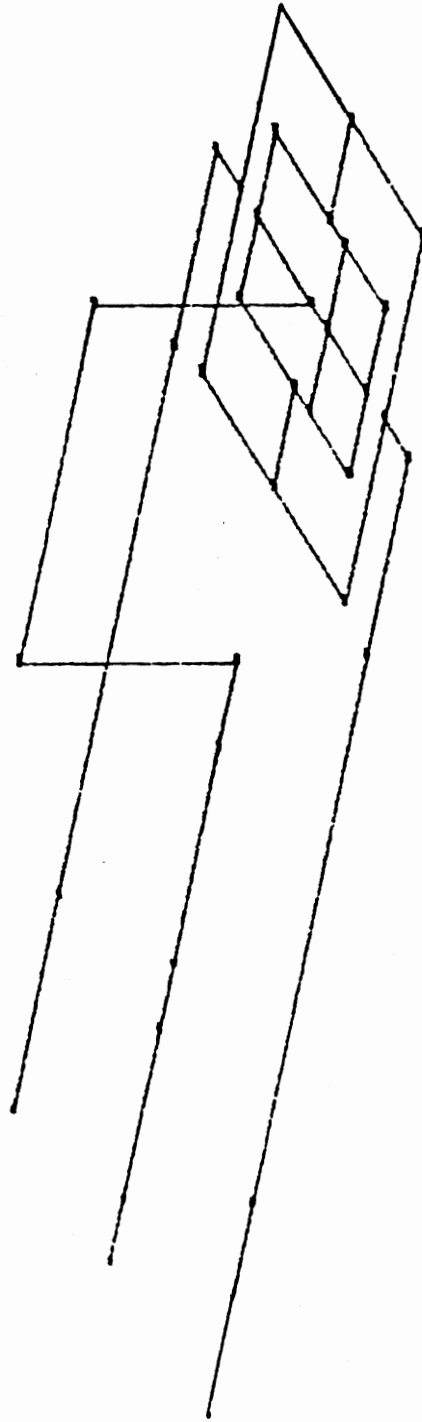


Figure 6. Old Production Head Finite Element Model

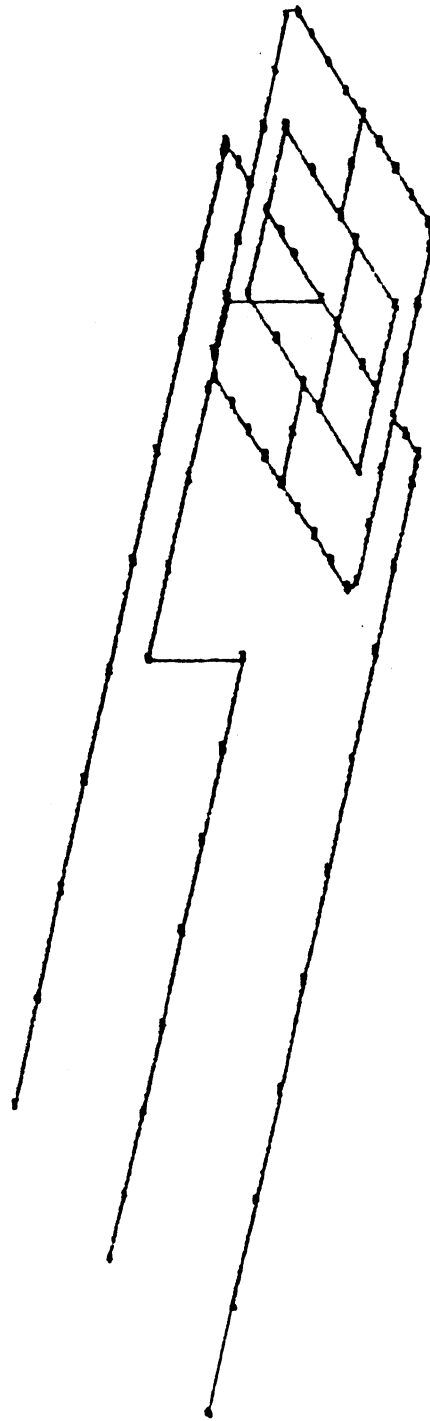


Figure 7. Old Production Head, High Density
Finite Element Model

In an effort to decrease solution cost the disk was modeled as an annular sector. To speed the modeling process an automatic mesh generation technique was developed and implemented. Mesh generation techniques aid in discretizing the model by locating grid points and by establishing connectivities for the elements. This particular technique also enforces boundary conditions.

The disk jacket can be seen to inflate during operation of the disk drive. This phenomena is analogous to the operation of a centrifugal vane pump. In this instance, the vanes are represented by diametral waves in the disk. This promoted the hypothesis that the jacket has little or no effect on the disk in the region of the read/write head. Thus, the boundary conditions selected for the disk were:

1. A clamped or fixed condition at the inside radius of the annular sector was chosen to model the clamping action of the drive spindle.
2. The sector edges were simply supported. Later models had a fixed condition to determine the effect of restraint.
3. Each grid point of the disk was restrained from rotation about axes orthogonal to the plane of the disk. This must be done as these rotations are undefined for this element.

A printoff of the automatic mesh generation program is located in the Appendix. Input data include:

- RI, RO: Inside and outside radius of the annulus (inches)
QI, QF: Angles defining the beginning and end of the sector
(degrees)
FREQM: Maximum frequency of a standing wave in the disk (Hz.)

ITYPE: Either 0 or 1
 0 - all elements will have the same radial dimension
 1 - with increase in radius the radial dimension of the elements will decrease in a logarithmic decrement fashion.

OMEGA: Rotational speed of disk drive (R.P.M.)

TH: Disk thickness (in.)

E: Young's Modulus (psi)

NU: Poisson's Ratio (Dimensionless)

RHO: Mass Density = $\frac{\text{Weight Density (lb/in}^3\text{)}}{386}$

Caution must be used in regard to units. NASTRAN and most other finite element programs allow the use of any system of units one wishes. The user must take care to keep units consistent throughout this model. For instance, if the model is described in a Cartesian coordinate system in units of feet then Young's Modulus must be given in units of lb/ft³ providing that the input loads are in units of pounds.

The mesh generation technique develops the disk model in a cylindrical coordinate system. NASTRAN has the ability to have models generated in several coordinate systems (Cartesian, cylindrical, spherical) and combined models can be made by referencing the origin of one coordinate system to another. For instance, the head/disk models entail three coordinate systems:

1. A basic Cartesian system
2. The cylindrical system of the disk, which is defined with respect to system 1

3. The Cartesian system of the read/write head, also defined with respect to system 1

Figure 8 portrays the geometrical relationship between the three systems. The origins of all three systems lie in the X_1Y_1 plane.

To complete the head/disk models, fictitious springs were connected between the head and the disk to represent the preloads on the flexures. The springs are rod elements (CROD) with negligible bending strength so that the spring stiffness is a function of cross sectional area.²⁸ It was surmised that these axial springs should have stiffness approximately that of the stiffness of the side flexures of the heads. For a cantilever beam with a load applied at the end the relationship to displacement is:³⁰

$$\Delta = \frac{PL_1^3}{3EI} \quad K = \frac{3EI}{L_1^3} \quad (3.3)$$

where:

P is the applied load

L_1 is the length

K is the stiffness

E is Young's Modulus

For a rod:

$$\Delta = \frac{PL_2}{AE} \quad K = \frac{AE}{L_2} \quad (3.4)$$

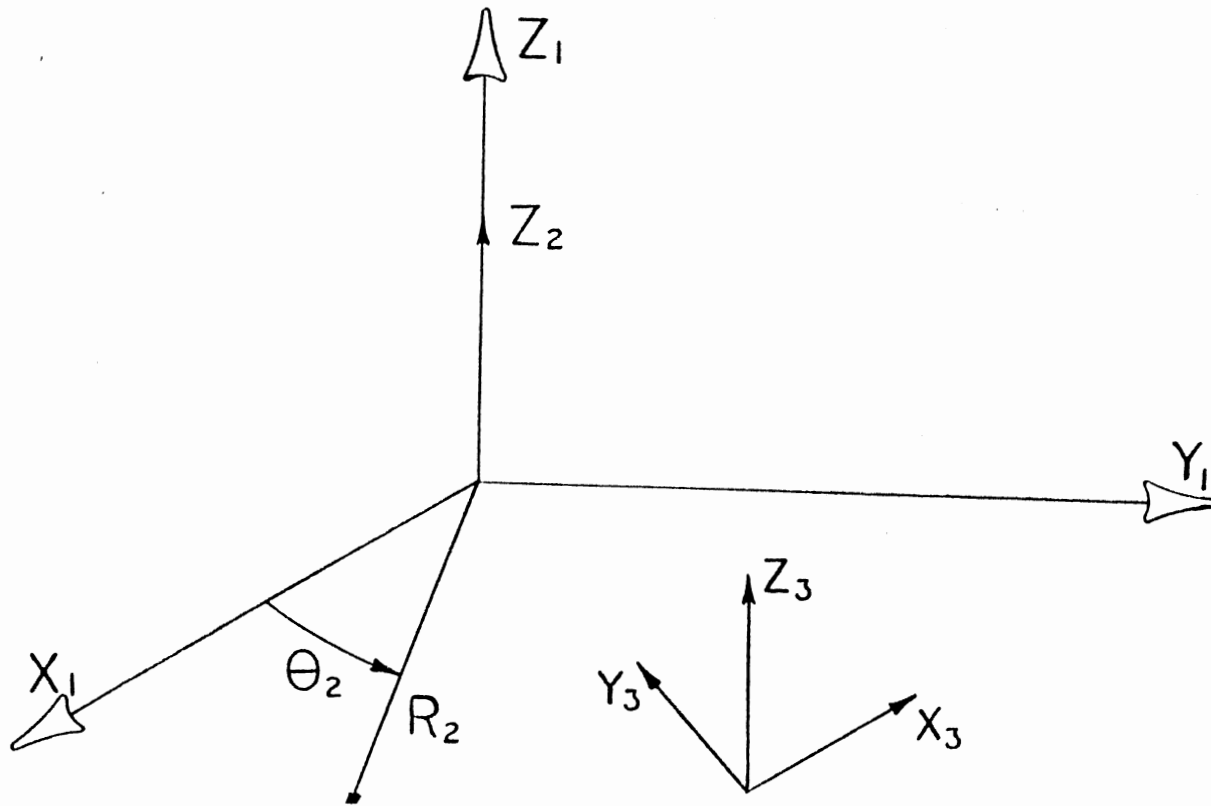


Figure 8. Read/Write Head/Disk Model
Coordinate Systems

where:

A is the cross-sectional area

L_2 is the length

Equating the stiffnesses it can be seen that:

$$\frac{AE}{L_2} = \frac{3EI}{L_1^3} \quad (3.5)$$

Assume E to be constant:

$$A = \frac{EIL_2}{L_1^3} = \frac{3I(.075)}{(.895)^3} = (.3138)I \text{ in}^2 \quad (3.6)$$

An average value of I for the side flexures is approximately $9.5 \times 10^{-10} \text{ in}^4$. The corresponding value for A would be $9.5 \times 10^{-10}(.3138) = 3.0 \times 10^{-10} \text{ in}^2$.

In regard to cost optimization it should be noted that finite elements is a technique which simultaneously solves several algebraic equations in lieu of solving complex differential equations of motion. The program manipulates matrices which are at least as large as the number of grid points multiplied by the number of degrees of freedom for those grid points. A significant amount of cost can be saved if these matrices are kept to a minimal bandwidth. The automatic mesh generator for the disk keeps as narrow a bandwidth as is possible. All of the head/disk models have approximately three hundred grid points for the disk and are numbered 1 through 300. For convenience, the head grid points start numbering at 2000. If left as is, the computer would have to store large fields of zeroes for the nonexistent grid points between 300 and 2000. This is solved by using grid point sequencing (SEQGP) which renumbers the grid points to

minimize bandwidth.²⁸ This can be done manually or by a NASTRAN preprocessor known as BANDIT.

CHAPTER IV

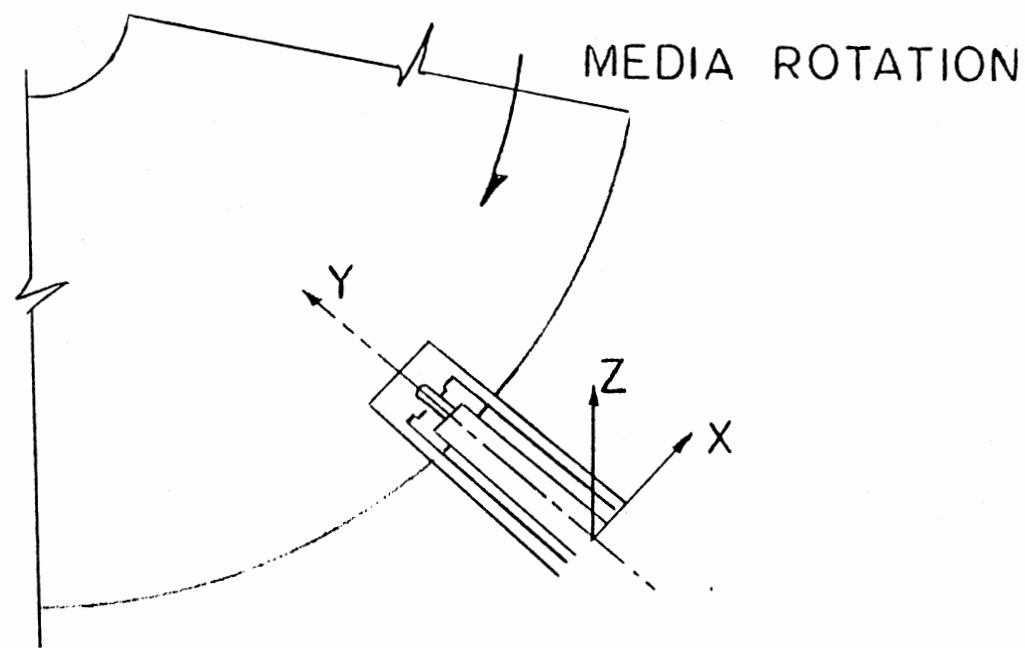
ANALYTICAL RESULTS

As stated in the approach to the problem the first task was to obtain experimentally verified models of the read/write heads. The verification was done in terms of an eigenvalue analysis of single head flexures. The results compared with experimental data are contained in Tables I and II for the new and old production heads. Figure 9 portrays the directions of roll and pitch with respect to the head.

TABLE I
NEW PRODUCTION HEAD FLEXURE EIGENVALUE ANALYSIS

Eigenvector	Eigenvalue (Hz.)	Experimental (Hz.)
Cantilever	23.8	24.7
Pitch	109.5	110.2
Roll	205.8	260.0*

* The roll mode frequency is highly dependent on the position of the input lead ribbons.



θ_{yy} - Pitch - Rotation about Y Axis

θ_{xx} - Roll - Rotation about X Axis

Figure 9. Definition of Pitch and Roll

TABLE II
OLD PRODUCTION HEAD FLEXURE EIGENVALUE ANALYSIS

Eigenvector	Eigenvalue (Hz.)	Experimental (Hz.)
Cantilever	32.5	32.2
Pitch	104.7	108.1
Roll	227.2	256.0

Figures 10 through 15 depict the eigenvectors listed in Tables I and II. With the verified head models analysis could proceed. As previously stated, a 45° sector of a 3 mil thick Mylar disk was discretized and the head flexures (upper and lower) were placed at an outside track. Both pinned and fixed boundaries were analyzed. Tables III and IV contain the eigenvalues of the dual read/write heads on an outer track of the disk.

TABLE III
NEW PRODUCTION READ/WRITE HEAD WITH DISK EIGENVALUE ANALYSIS

Eigenvector	Eigenvalue (Hz.)	
	<u>Pinned Boundary</u>	<u>Fixed Boundary</u>
Cantilever	23.6	24.8
Pitch	121.6	125.6
Roll	227.2	243.9

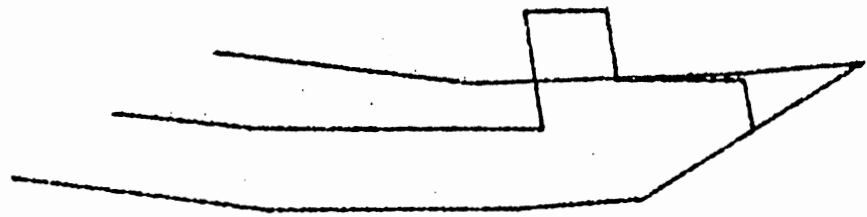


Figure 10. New Production Head Flexure,
Cantilever Mode, Frequency =
23.8 Hz.

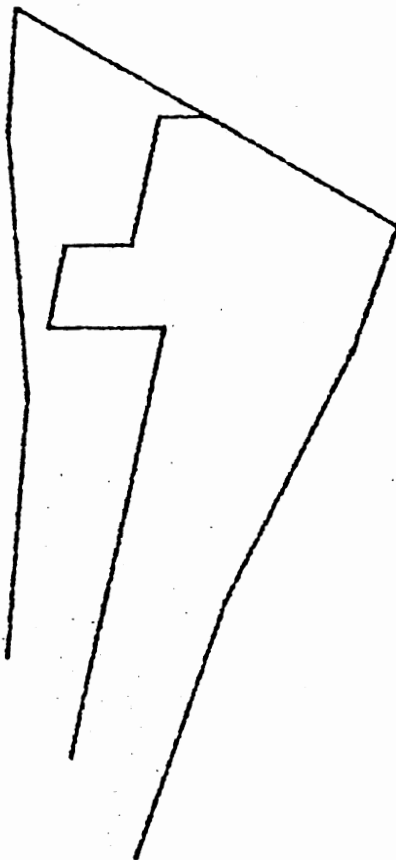


Figure 11. New Production Head Flexure,
Pitch Mode, Frequency =
109.5 Hz.

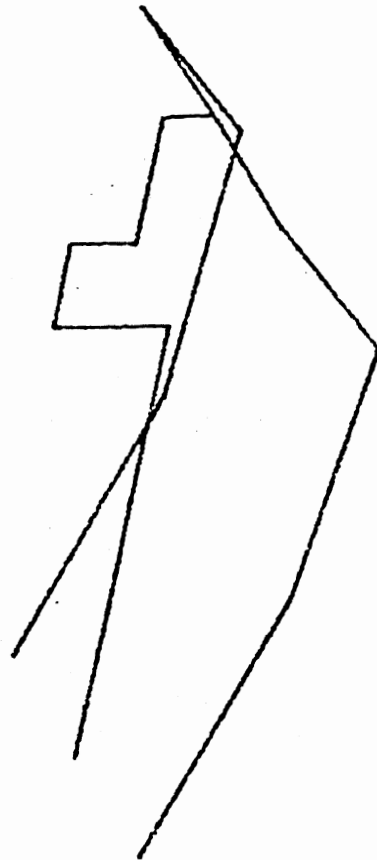


Figure 12. New Production Head Flexure,
Ro11 Mode, Frequency = 205.8
Hz.

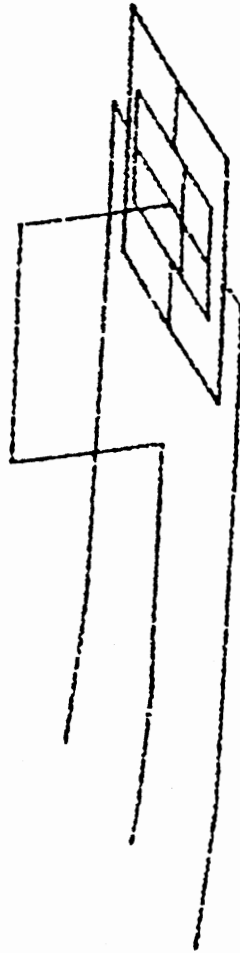


Figure 13. Old Production Head Flexure,
Cantilever Mode, Frequency =
32.5 Hz.

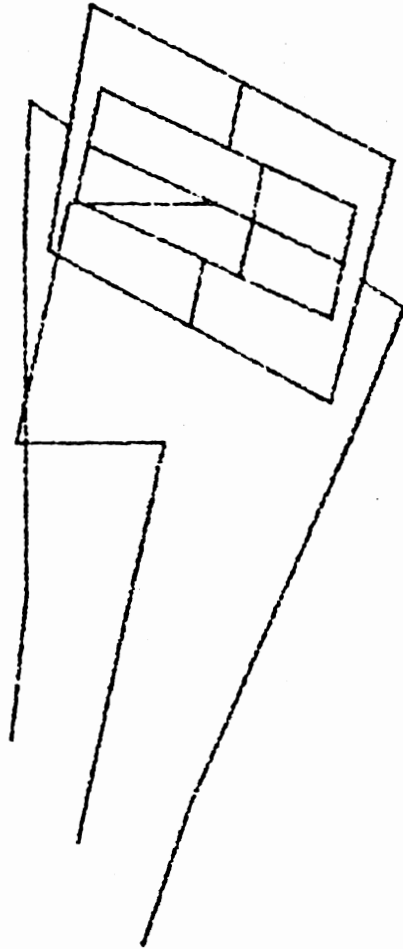


Figure 14. Old Production Head Flexure,
Pitch Mode, Frequency =
104.7 Hz.

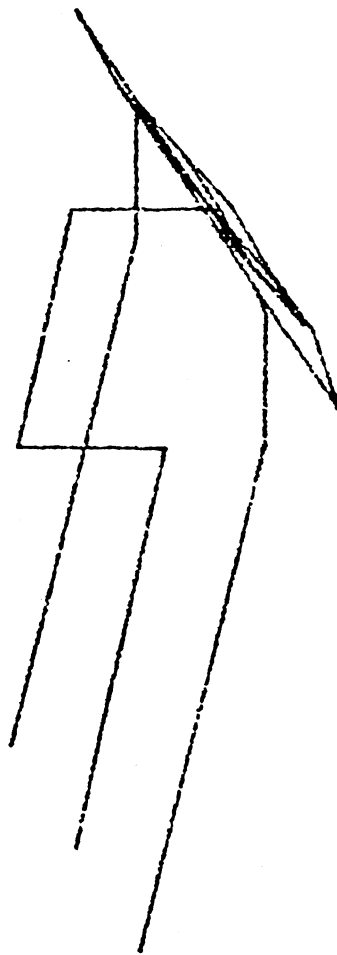


Figure 15. Old Production Head Flexure,
Roll Mode, Frequency =
227.2 Hz.

TABLE IV
 OLD PRODUCTION READ/WRITE HEAD WITH DISK EIGENVALUE ANALYSIS

Eigenvector	Eigenvalue (Hz.)	
	<u>Pinned Boundary</u>	<u>Fixed Boundary</u>
Cantilever	30.0	32.0
Pitch	120.9	131.5
Roll	246.3	281.0

Initially, the read/write head pitch mode was of interest as experimentation had shown that the largest displacements are associated with the pitch mode. The eigenvalue analysis has shown that there are several eigenvalues that contribute to the pitch motion of the head.

For instance, consider the new production head with pinned boundaries. Modes 8, 9, and 11, corresponding to 121.6, 143.5, and 163.2 Hz., respectively, all contribute to pitch motion of the head. The respective mode shapes may be viewed in Figures 16, 17, and 18.

Consider the old production head/disk with pinned boundaries. Modes 8, 10, and 11, corresponding to 120.9, 167.3, and 169.1 Hz., respectively, contribute to the pitch of the head. Also note mode 20 at 295.3 Hz., which is the second pitch frequency of the head (i.e., the inner stylus is no longer in phase with the outer gimbal). The respective mode shapes may be viewed in Figures 19, 20, 21, and 22.

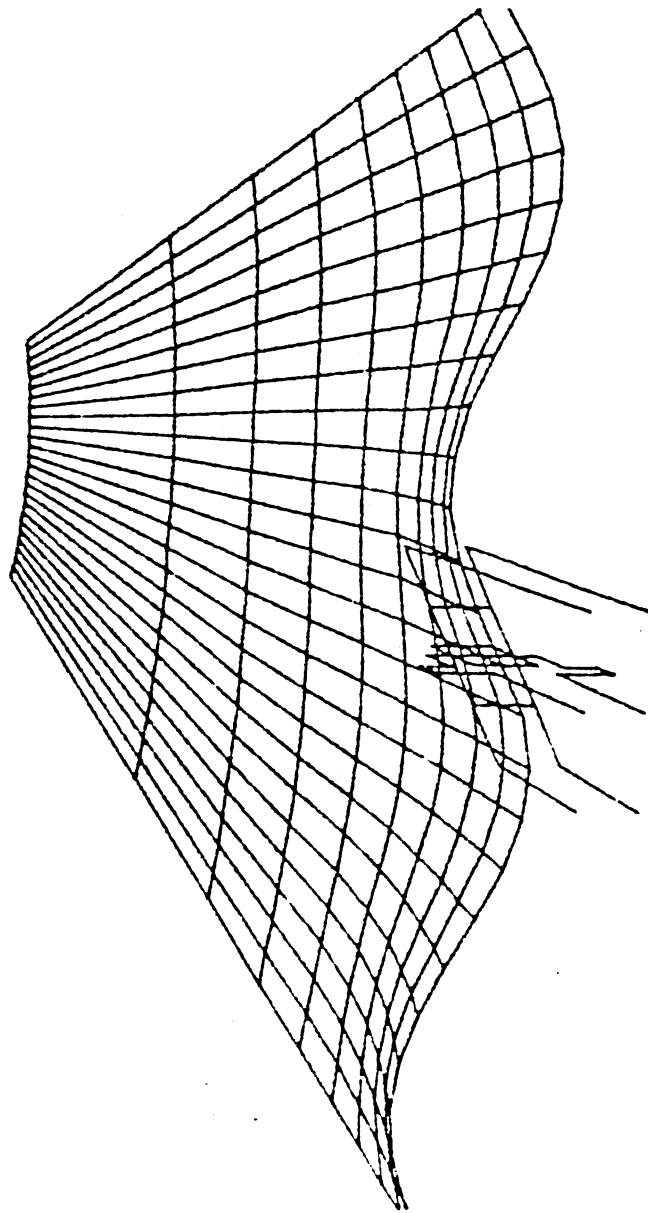


Figure 16. New Production Head/Disk
Model, First Pitch Mode,
Mode 8.

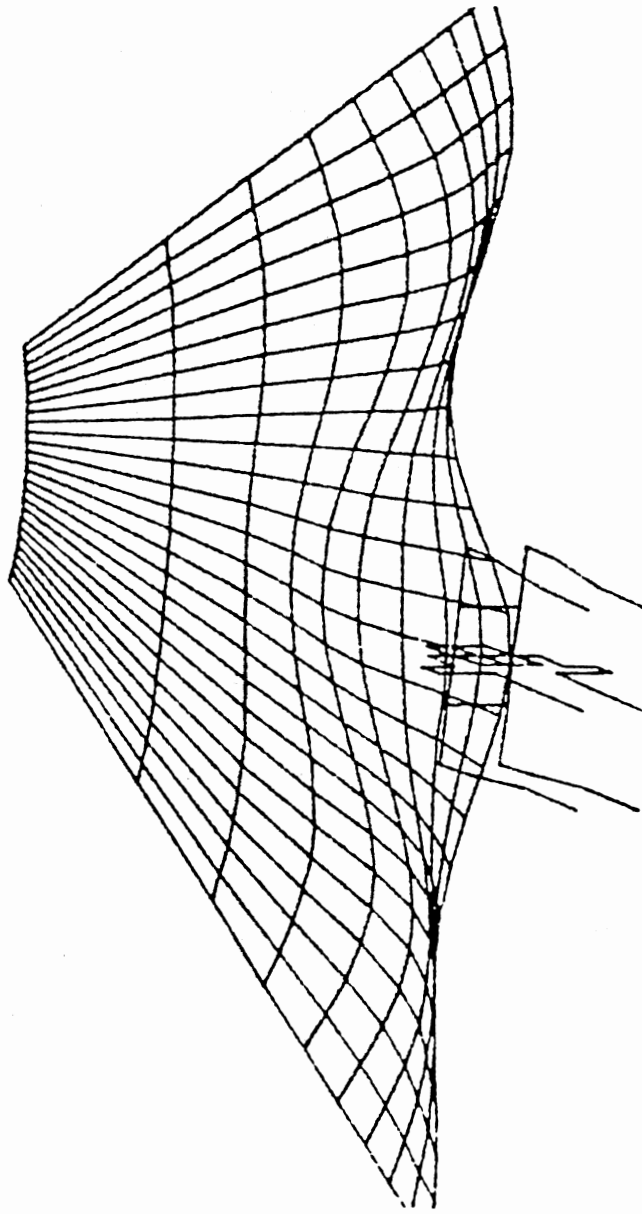


Figure 17. New Production Head/Disk
Model, Mode 9

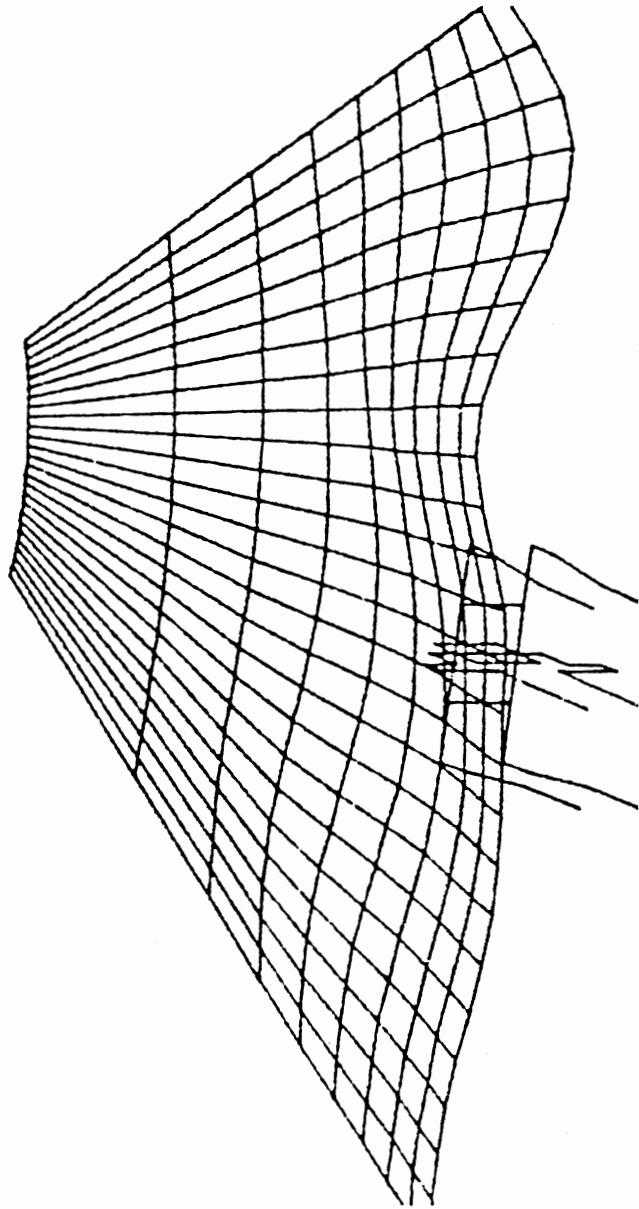


Figure 18. New Production Head/Disk
Model, Mode 11

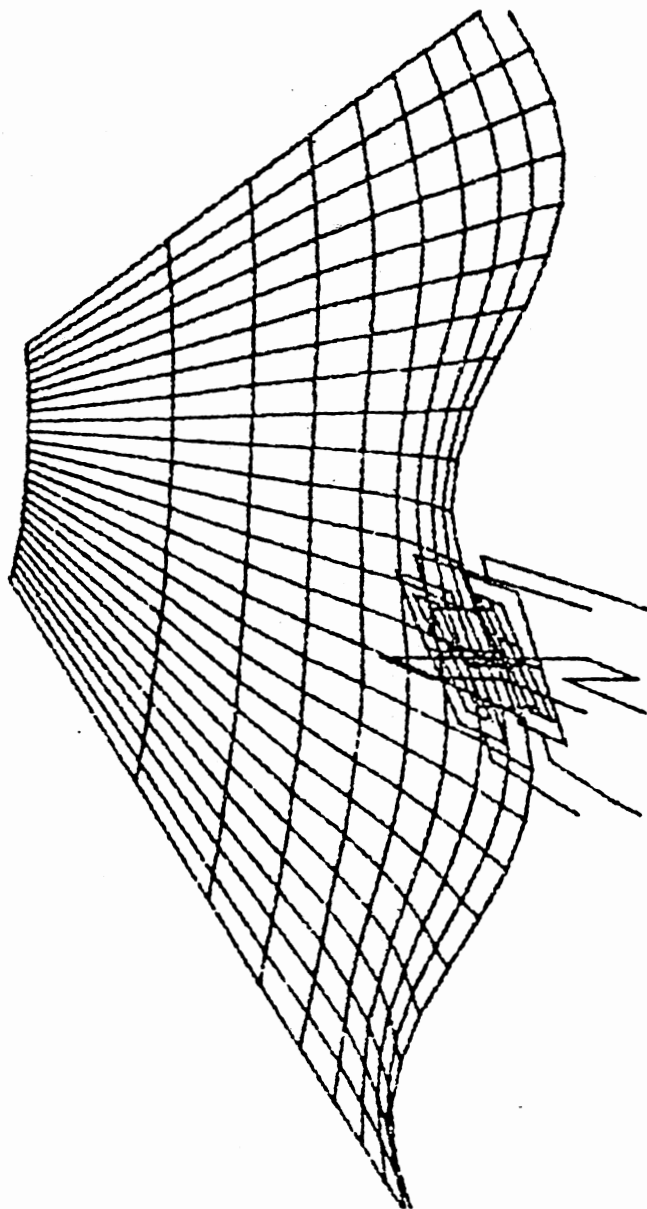


Figure 19. Old Production Head/Disk Model,
First Pitch Model, Mode 8

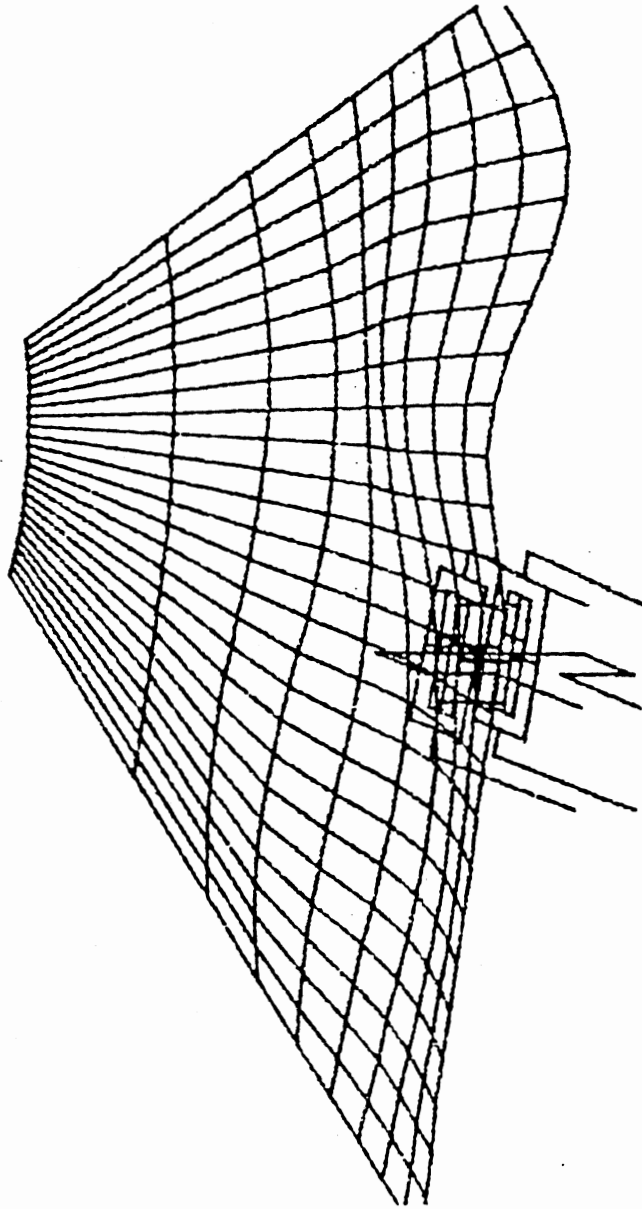


Figure 20. Old Production Head/Disk
Model, Mode 10

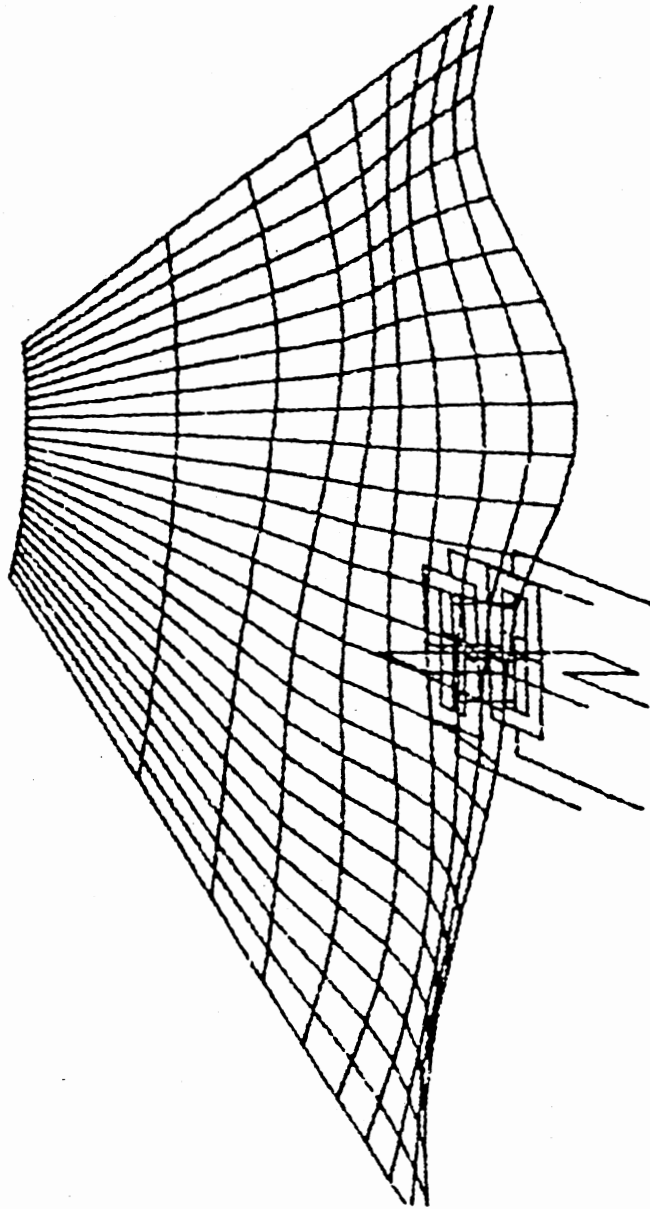


Figure 21. 01d Production Head/Disk
Model, Mode 11

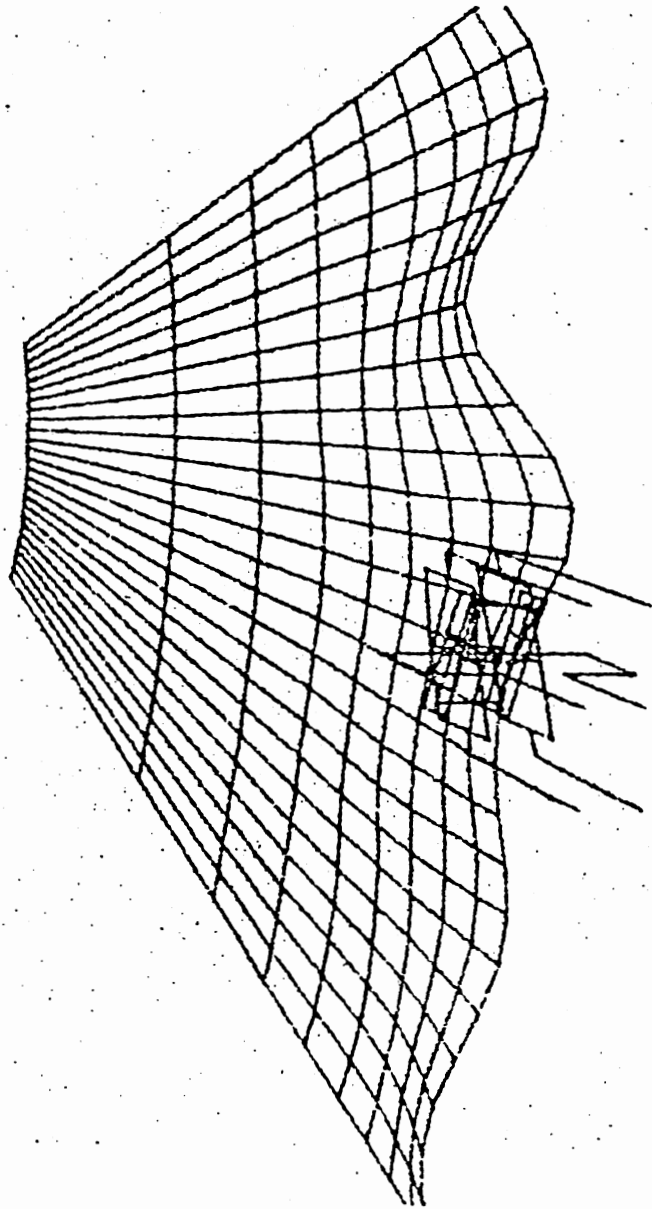


Figure 22. Old Production Head/Disk
Model, Second Pitch Mode,
Mode 20

This suggests that broad band pitch response may occur in the head/disk systems in the 120 to 170 Hz. band, depending on which modes are excited.

In an effort to reduce solution cost, transient analyses were implemented. Spike rotations were input at a central grid point on the disk under the read/write head in directions which would cause pitch and roll response of the heads. A typical forcing function is shown in Figure 23. The Fourier transform of a spike is constant amplitude white noise. The Fourier transform of a spike of finite width (or a rectangular pulse) for the duration and amplitude of the pulse in Figure 23 is shown in Figure 24.

For the new production head/disk the response of the head to a spike pitch is shown in Figure 25. Figure 25 is a plot of pitch rotation of a point at the plan view center of the ceramic stylus. The dominant feature of Figure 25 is the first pitch mode of the head at approximately 121.9 Hz.. All of the transient analyses were performed on disks with pinned edge boundary conditions on the sector sides. The 121.9 Hz. determined from the transient analysis correlates well with the 121.6 Hz. from the eigenvalue analysis.

The response of the new production head/disk to a spike roll is shown in Figure 26. Figure 26 is a plot of the same point of Figure 25 except that roll rotation is the dependent variable. The transient analysis indicates that the first roll mode should be approximately 212.8 Hz.. The eigenvalue analysis produced the first roll mode at 227.2 Hz. which is reasonable correlation. An interesting beating effect is present in Figure 26. A frequency of approximately 25 Hz.

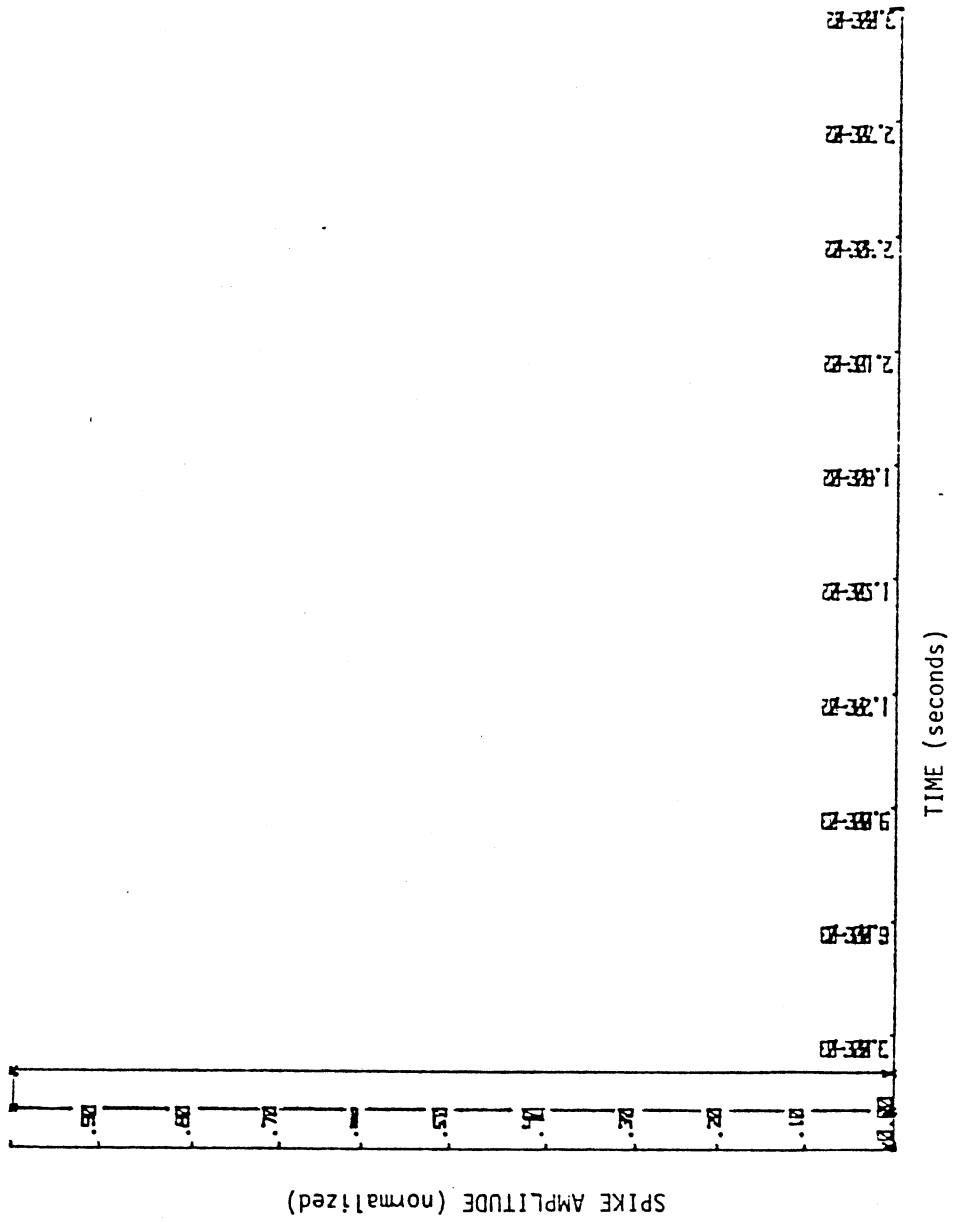


Figure 23. Transient Input Function

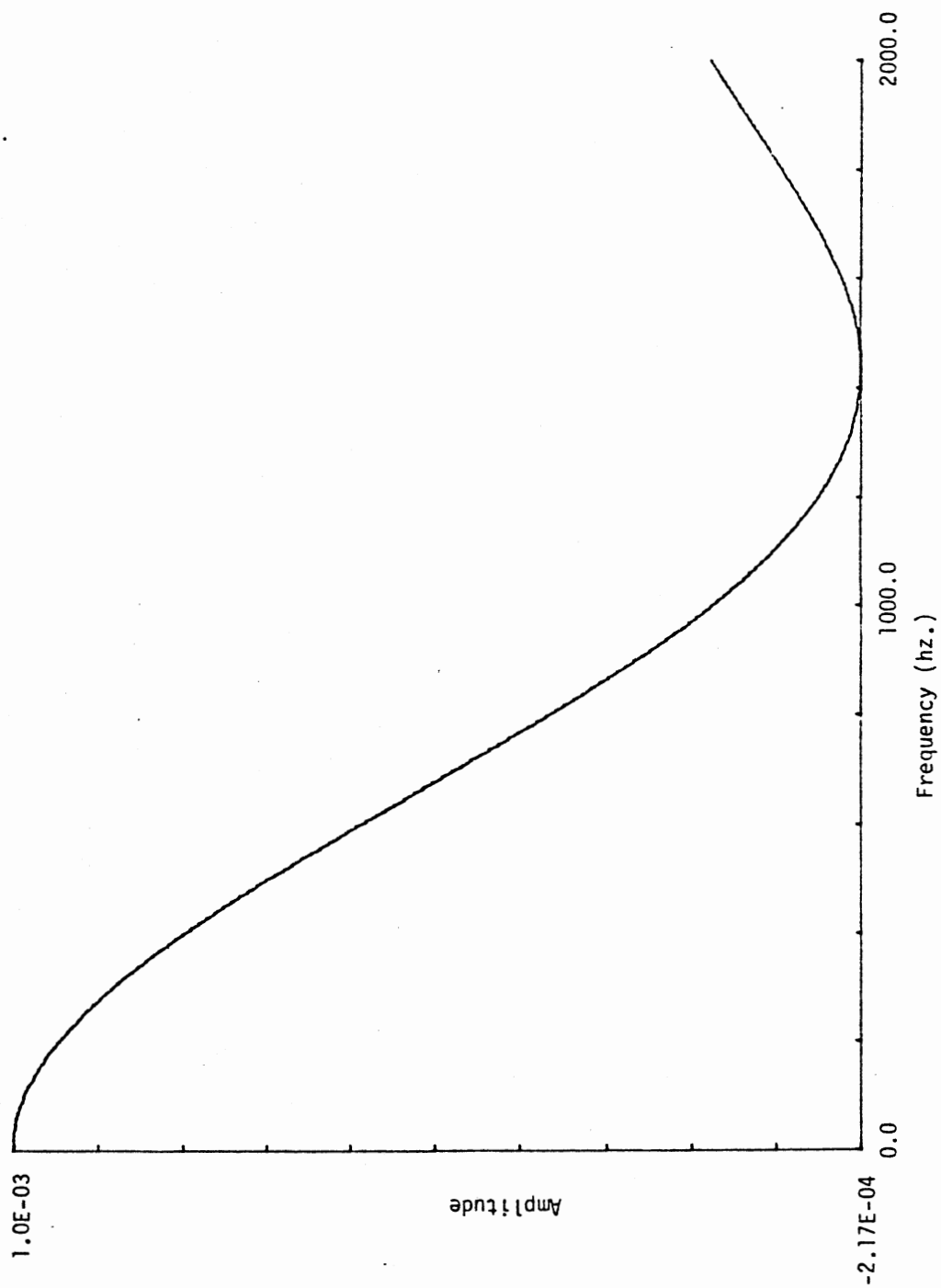
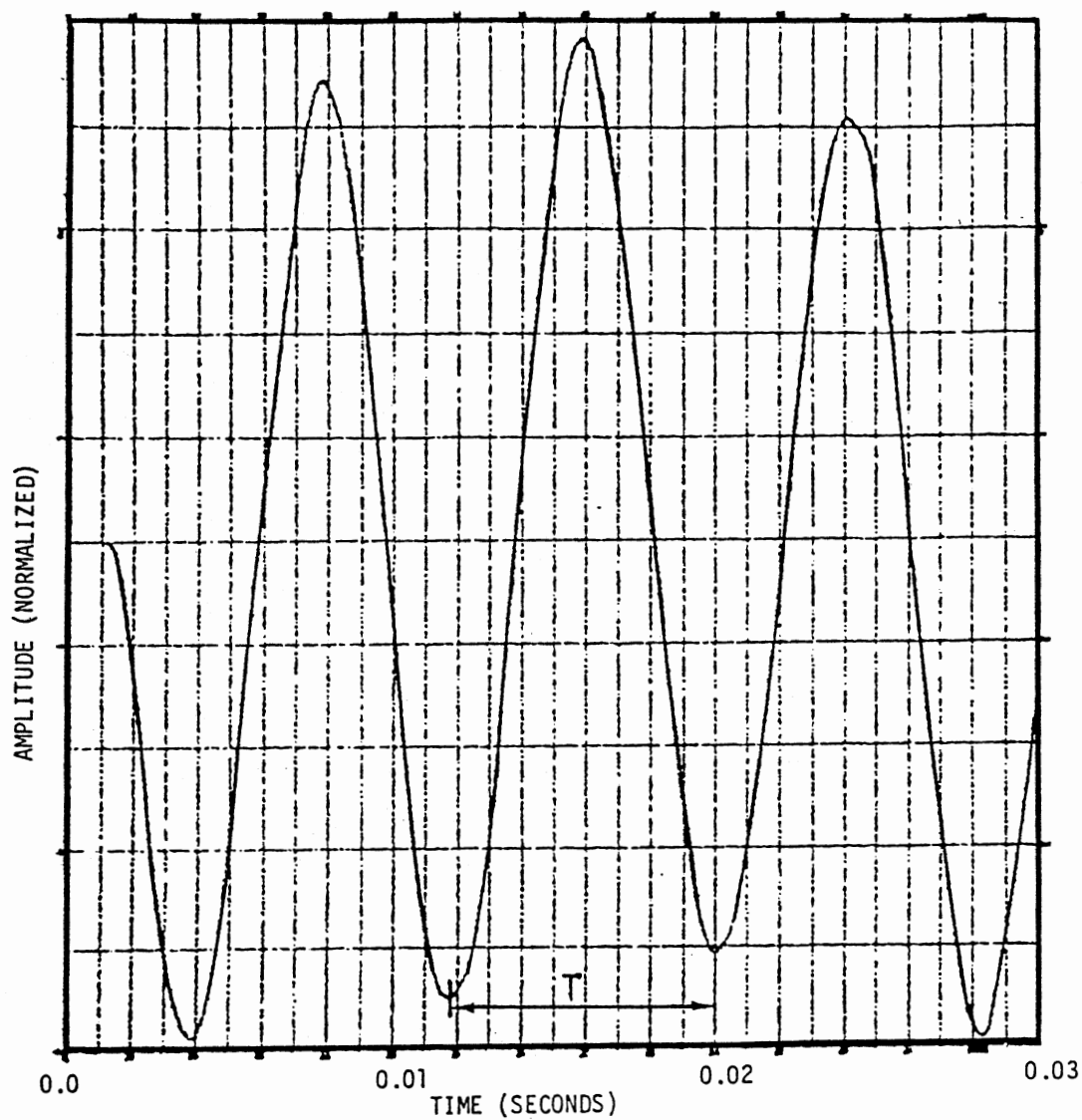


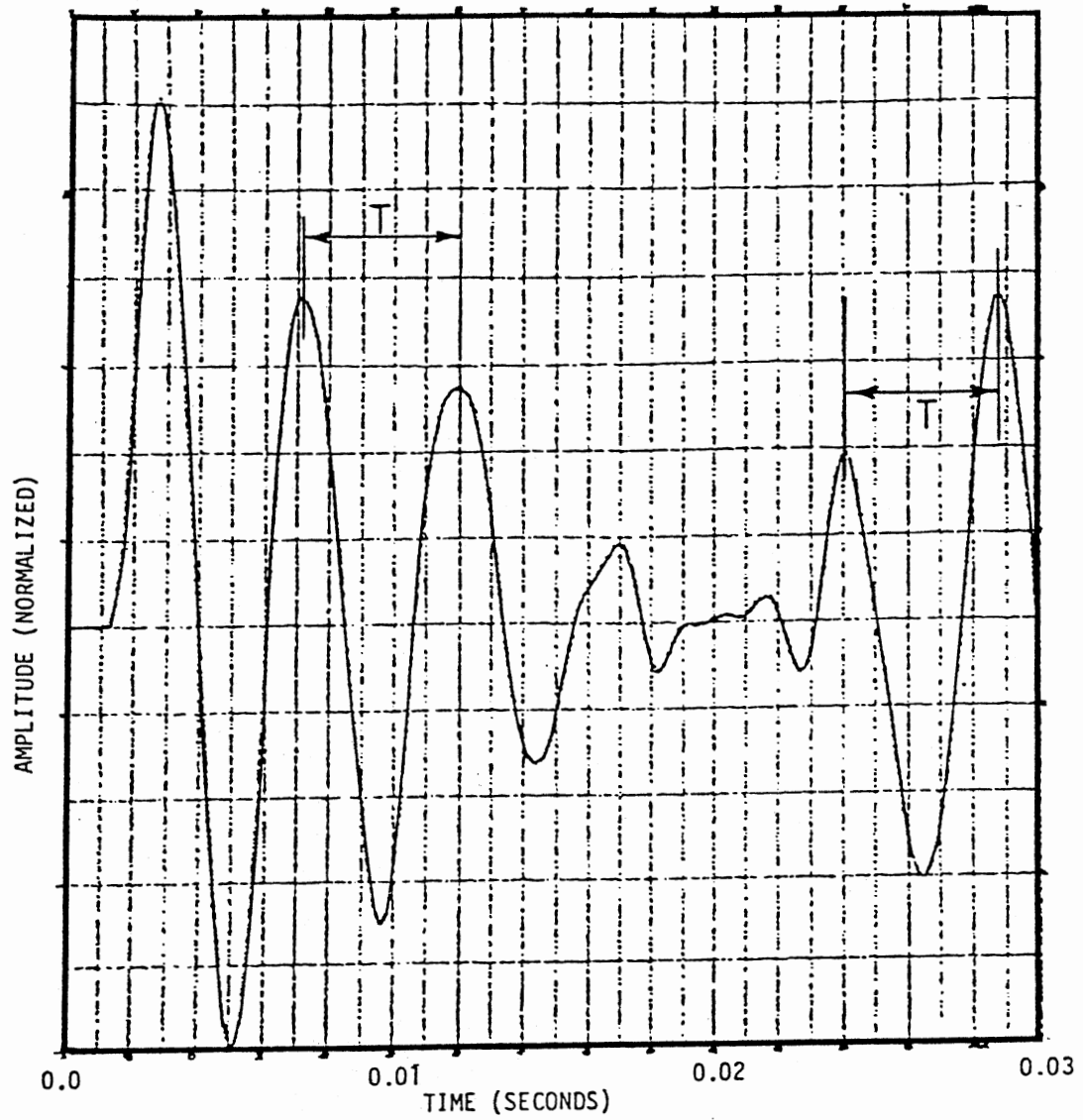
Figure 24. Fourier Transform of Transient Input Function



$T \approx 0.0082$ sec.

$f \approx 121.9$ Hz.

Figure 25. Transient Analysis, Spike Pitch,
New Production Head/Disk, Pitch
Motion of Head



$$T \approx 0.0047 \text{ sec.}$$

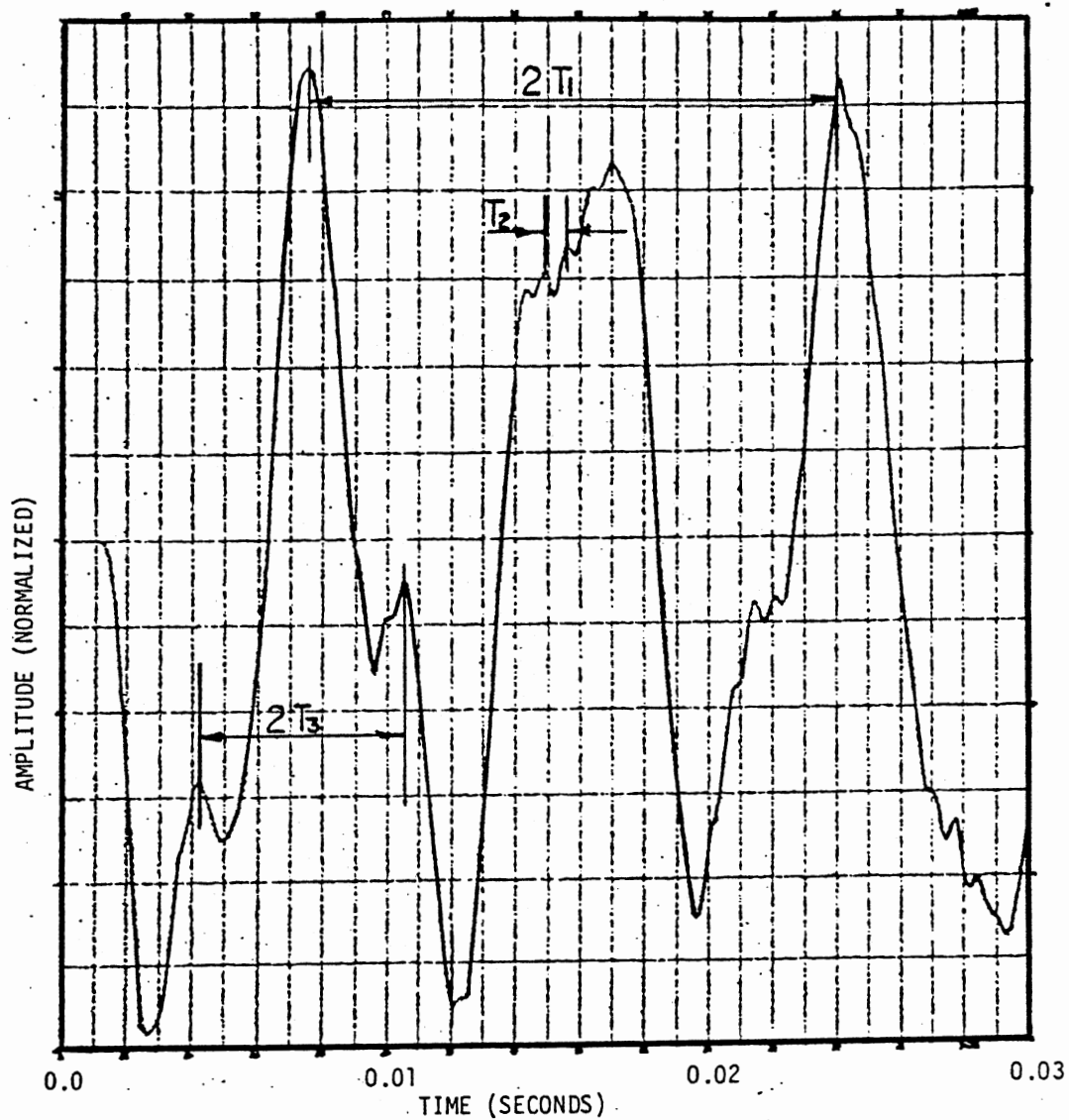
$$f \approx 212.8 \text{ Hz.}$$

Figure 26. Transient Analysis, Spike Roll,
New Production Head/Disk, Roll
Motion of Head

is present which represents the roll of the stylus during the first cantilever mode.

Figure 27 is a plot of pitch rotation of the old production head/disk due to a spike pitch input. The plot is for a point of the same geometric location as that of Figure 25 and 26 for the new production head. A first observation is that the pitch response of the old production head is of varied frequency content, especially when compared to Figure 25 of the new production head. A 122 Hz. frequency is present corresponding to the first pitch mode which was determined to be 120.9 Hz. in the eigenvalue analysis. A 315.0 Hz. frequency is present corresponding to the second pitch mode which was determined to be 295.3 Hz. in the eigenvalue analysis. This 315 Hz. component fades quickly as it has difficulty existing in conjunction with the first pitch mode. This is due to the stylus and outside gimbal frame being in phase in the first pitch mode which is contrary to the second pitch mode where the stylus and outside gimbal frame are rotating in opposite directions. An interesting high frequency component was apparent at 1428 Hz.. As no eigenvalue analysis had been performed in this frequency range it was impossible to determine an associated eigenvector. This became the subject of later analyses.

The response of the old production head to a spike roll input is portrayed in Figure 28. The first roll mode is approximately 224.7 Hz. compared to 246.3 Hz. obtained in the eigenvalue analysis. Although some beating between the first cantilever and roll mode is apparent it is not as graphic as that which was discussed earlier in Figure 26.



$$T_1 \approx 0.0082 \text{ sec.}$$

$$T_2 \approx 0.0007 \text{ sec.}$$

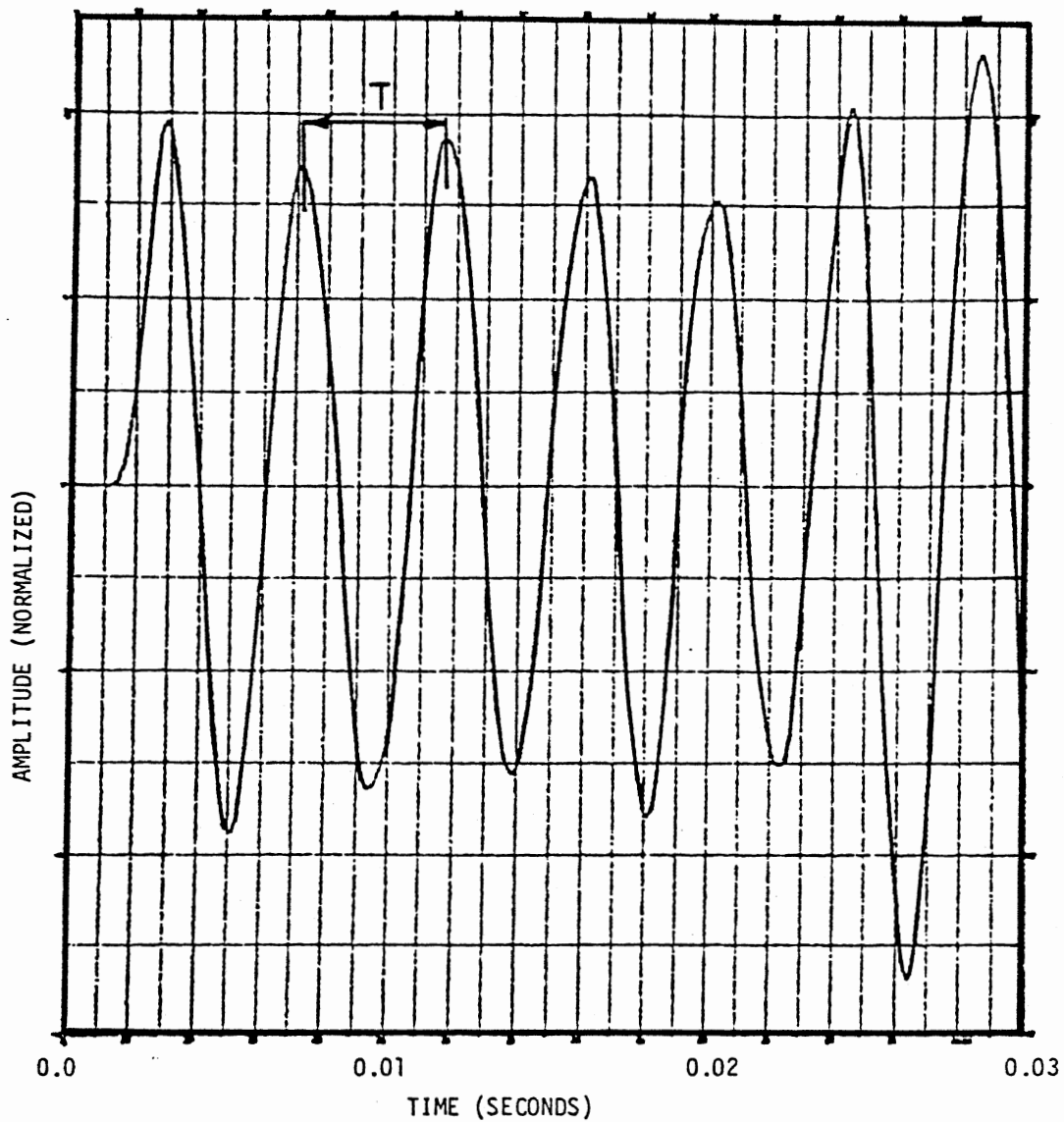
$$f_1 \approx 122.0 \text{ Hz.}$$

$$f_2 \approx 1428.0 \text{ Hz.}$$

$$T_3 \approx 0.0032 \text{ sec.}$$

$$f_3 \approx 315.0 \text{ Hz.}$$

Figure 27. Transient Analysis, Spike Pitch,
Old Production Head/Disk, Pitch
Motion of Head



$$T \approx 0.0044 \text{ sec.}$$

$$f \approx 224.7 \text{ Hz.}$$

Figure 28. Transient Analysis, Spike Roll,
Old Production Head/Disk, Roll
Motion of Head

Discussions with engineers of MPI disclosed that the old production head has inherent high frequency characteristics which generated a "whine", or "squeal", when excited. This "squeal" accelerated wear of the disk surface but when the head is left in the same track location for extended periods of time the squeal would diminish. This indicates that the phenomena is excited by the oxide surface of the disk which presumably becomes smoother with wear. Figure 29 is a photograph taken on a scanning electron microscope in an area of low wear on a used IBM diskette. Figure 30 is a photograph taken in an area of high wear at the same magnification as Figure 29.

This prompted the development of a high element density model of the old production head flexure for high frequency eigenvalue analysis. A line drawing of the model was shown in Figure 7 in Chapter III. The previous model was unable to portray high frequency eigenvectors due to low element density. The disk was not included in this model as the high frequency eigenvectors were of interest and it was uncertain if the additional stiffness and mass of the disk would affect the eigenvalues to any extent. Solution cost was also a factor.

The representation of the eigenvector shown in Figure 31 portrays a third pitch mode. With a natural frequency of 1377 Hz., this mode correlates well to the 1428 Hz. signal present in the transient analysis. The additional stiffness of the disk could have raised the natural frequency higher but this is of little consequence since a 3.7% difference is well within engineering accuracy.

To validify the use of a sector of disk in the modeling procedure, an eigenvalue study of the old production head on a

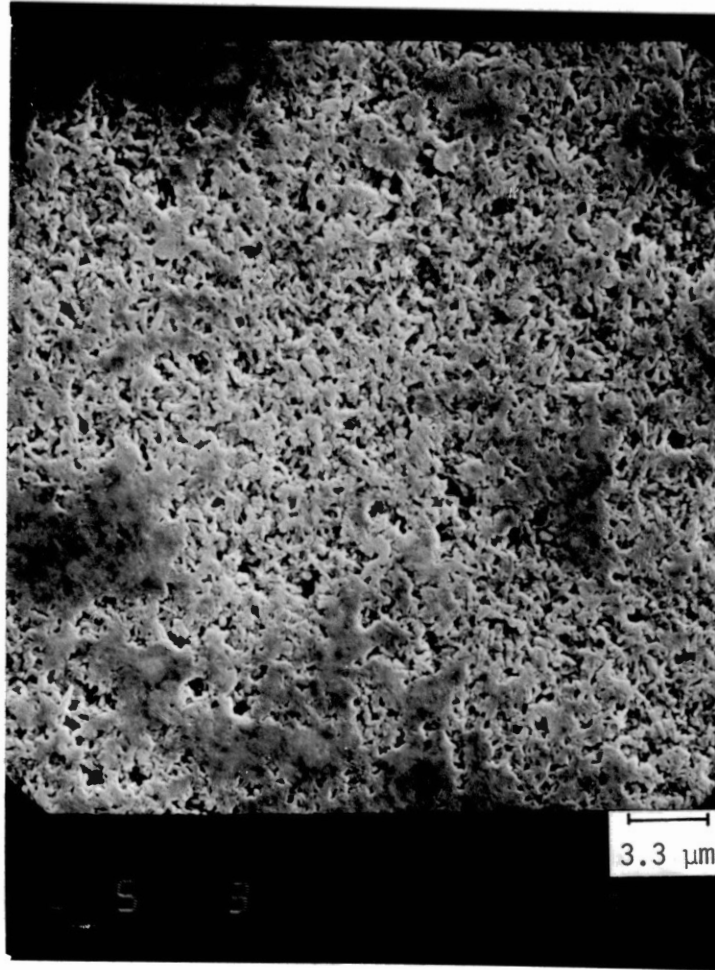


Figure 29. SEM Photograph of a Disk Surface in an Area of Relatively Low Wear

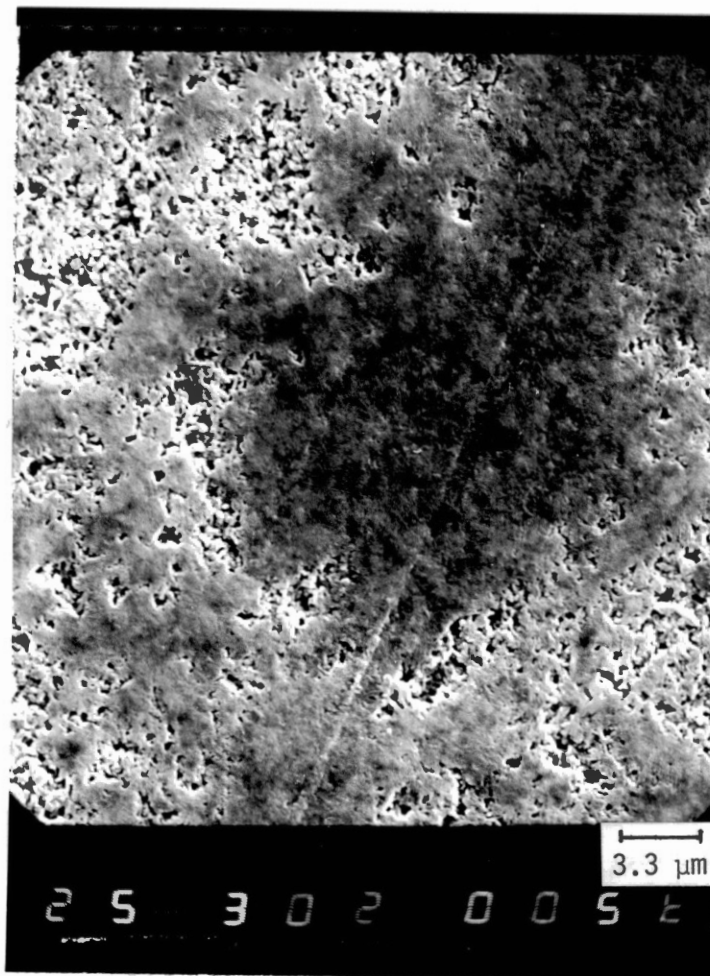


Figure 30. SEM Photograph of a Disk Surface in an Area of Relatively High Wear

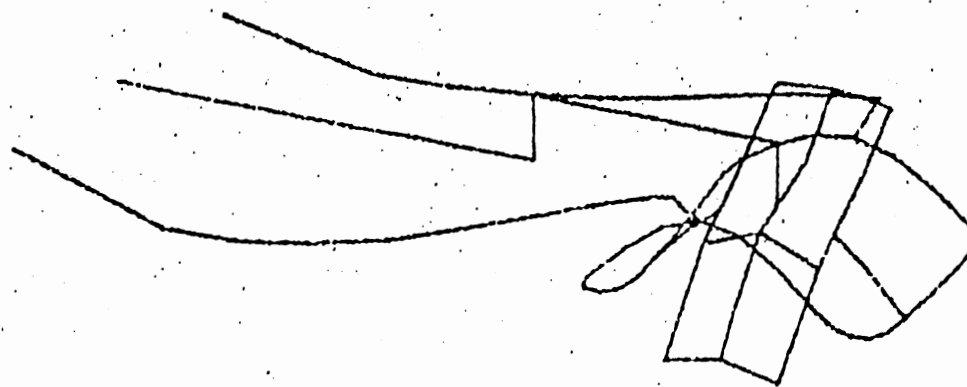


Figure 31. Old Production Head, High Element Density
Flexure Model, Third Pitch Mode,
Frequency = 1377 Hz.

complete disk was performed. The disk model already existed as was described in Chapter III. The read/write head was positioned at an outside track in the high element density portion of the disk model. The first pitch mode is depicted in Figure 32. This model predicted the first pitch mode to occur at 120.5 Hz.. This correlates nicely to the 120.9 Hz. value computed for the old production head on a disk sector with pinned boundaries presented in Table IV. The use of the sector has thus had little impact on resonance of the head, though it may have altered eigenvalues and eigenvectors of the disk to a greater extent.

Centrifugal forces acting to increase the membrane stiffness of the disk were neglected as preliminary hand calculations predicted minimal effect. To verify this, Rigid Format 13 of NASTRAN was employed to combine an eigenvalue analysis with a static radial load case. The first and second pitch resonances occurred at 120.4 and 296 Hz., respectively. Earlier analyses predicted 120.9 and 295.3 Hz., respectively, for these modes, without the centrifugal effect thereby verifying the preliminary calculations.

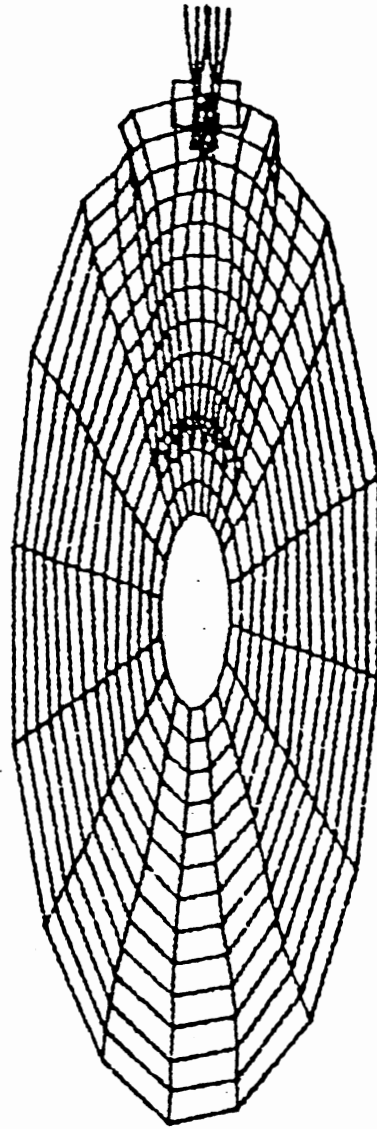


Figure 32. Old Production Head/Complete Disk Model,
First Pitch Mode, Frequency = 120.5 Hz.

CHAPTER V

EXPERIMENTAL STUDIES

Some of the first experiments performed to detect the motion of the read/write head employed the strain gage technique. The earliest of these studies were performed with foil gages, later studies employed semiconductor gages which are known to exhibit high gage factors but have a high temperature drift in addition. The semiconductor gage was used because of its high gage factor and for its small dimensions (silicon whiskers) and therefore low impact on the stiffness or the read/write head flexures.

Silicon whiskers were adhered to the center load spring as shown in Figure 33. The change in resistance of the silicon whiskers was monitored by a Vishay Ellis Bridge Amplifier Meter (BAM-1). The output signal of the BAM-1 was recorded on a Biomation Model 805 digital storage device. The Biomation would plot stored traces on a Hewlett Packard Model 7044A X-Y plotter.

Figure 34 is the product of a typical experiment. Specifically this experiment considers the old production head on a used IBM disk. The purpose of these particular tests was to determine the effect on head motion imposed by disks of various manufacturers and the effect of the pressure pad. Due to the nonlinearity of the semiconductor gage quantitative data was difficult to obtain. The

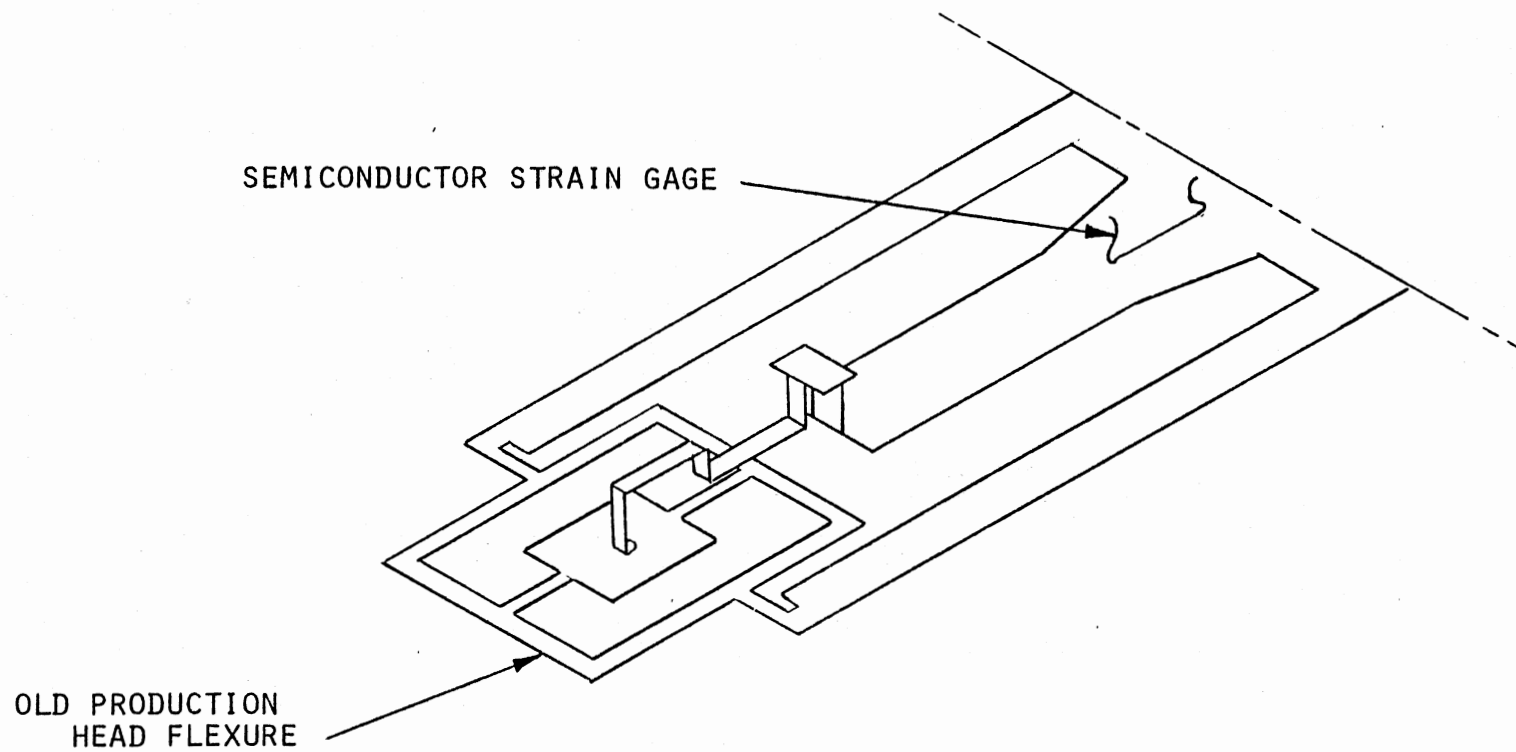


Figure 33. Semiconductor Strain Gage
Installed on Center Load Spring

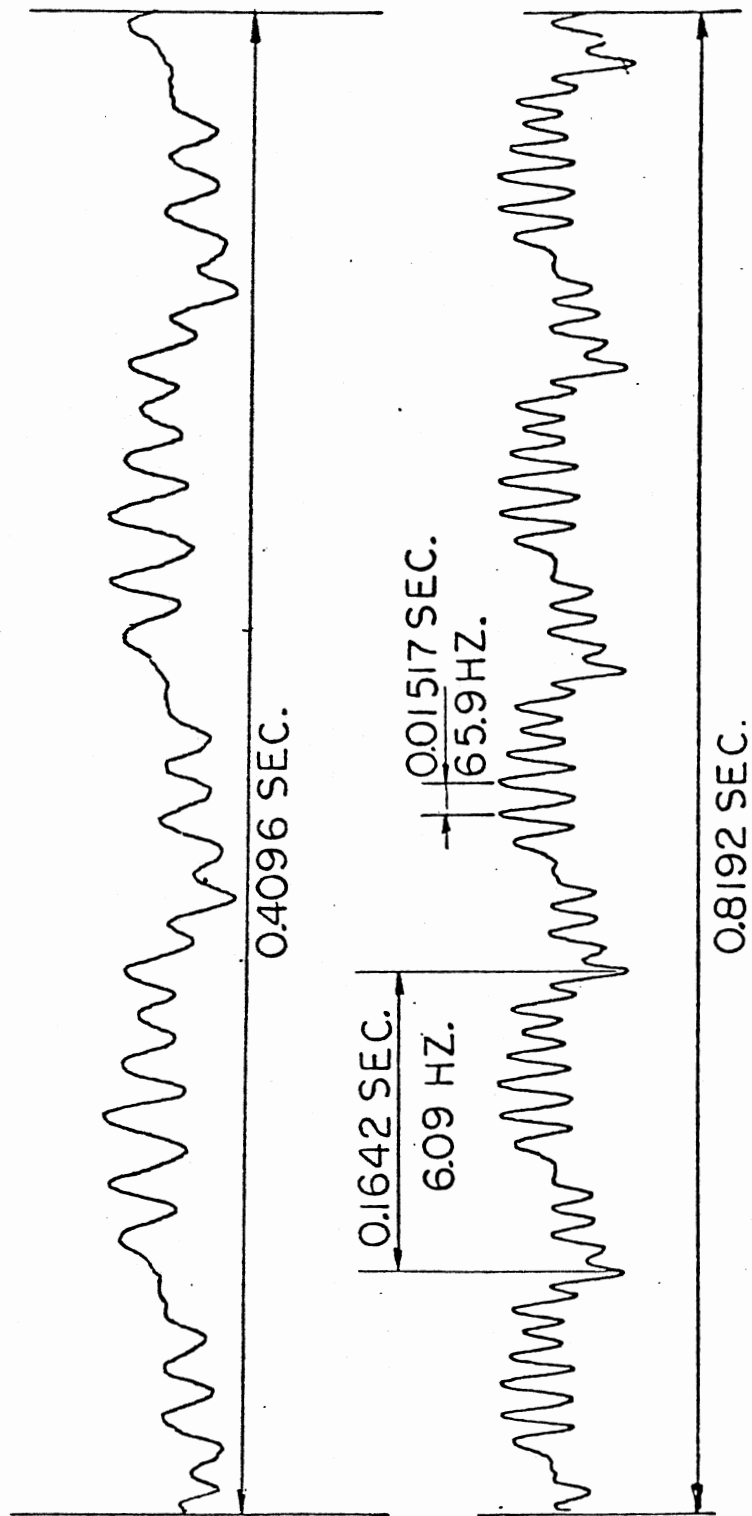


Figure 34. Time Response of Center Load Spring

additional stiffness and damping of the gage adhesive on the flexure compounded the problem.

Nevertheless, Figure 34 is informative as qualitative data. The data is notably periodic on 0.1642 second intervals. This corresponds to a frequency of 6.09 Hz. which is very similar to the angular frequency of the disk drive which is approximately 6 Hz.. Comparison between this and other data taken were inconclusive with regard to the disk's manufacturers. Frequency content was much the same in each case. Little or no change was witnessed upon engaging or disengaging the pressure pad. Frequency content and amplitudes remained much the same.

From the strain gage studies it was obvious that a less obtrusive motion detection apparatus needed to be implemented. An investigation was initiated to determine if a detection system based on the measurement of light reflected from the read/write head was feasible in this instance. Instruments denoted as photonic probes are commercially available which work on a principle of comparing a light intensity transmitted toward an object with the light intensity reflected from the object as a measure of distance between the probe and object. A fallacy with such an instrument in this circumstance is the inability to distinguish between a translation away from the probe or a rotation of the object as either case will diminish the reflected light intensity.

During the investigation an experimental apparatus was conceived in which a laser beam was directed onto a reflective surface on the read/write head. The reflected beam was attenuated by means of an adjustable knife edge prior to its final destination, a

photodetector. As the reflective surface displaces with the read/write head, the reflected beam intensity at the photodetector will either increase or decrease, depending on the orientation of the knife edge. The photodetector, in this case, a cadmium sulfide photocell, will respond with a change in resistance, and by connecting the photocell in a ballast circuit a change in voltage can be monitored as a function of displacement.

Figures 35 and 36 graphically depict how a translation or rotation of the mirror can vary the light intensity received by the photocell. These Figures also illustrate that with only one photocell, rotation cannot be distinguished from translation. The solution to this problem is to split the reflected beam with an optical beam splitter. Each beam will have a separate knife edge and photocell. The distance between knife edge and photocell will differ, thereby only one photocell will have a longer optical arm making it more sensitive to rotation. Each photocell should be equally sensitive to translation in this instance. Figures 37 and 38 show the response of such a system to translation and rotation. Figure 39 displays the significance of this concept. In the region A, the output signals for the photocells are superimposed. This signifies that a pure translation of the mirror has occurred. In region B, separation of the two signals indicates that a rotation of the mirror has taken place. Figure 40 depicts the geometry of the monitor block which houses the two photocells. The system was called the LAMDA system. LAMDA is an acronym meaning LAser BeaM Deflection Analyzer.³¹

Each of the photocells within the monitor block was connected within a ballast circuit. The voltage across the photocell was

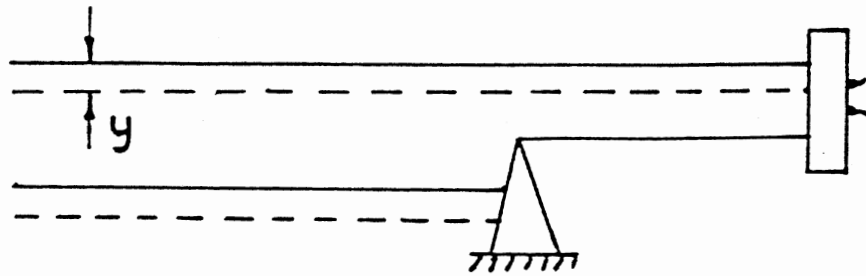


Figure 35. Response of Photocell to Translation

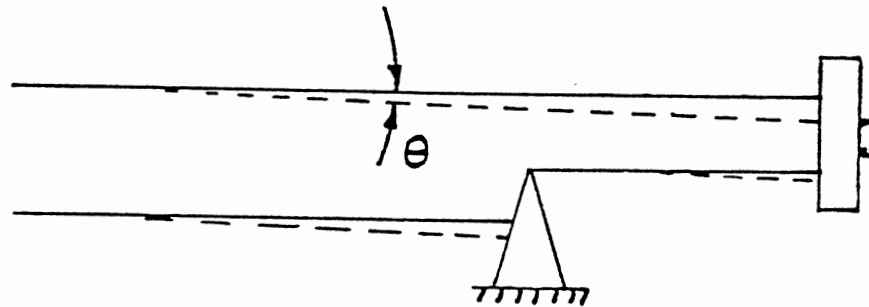


Figure 36. Response of Photocell to Rotation

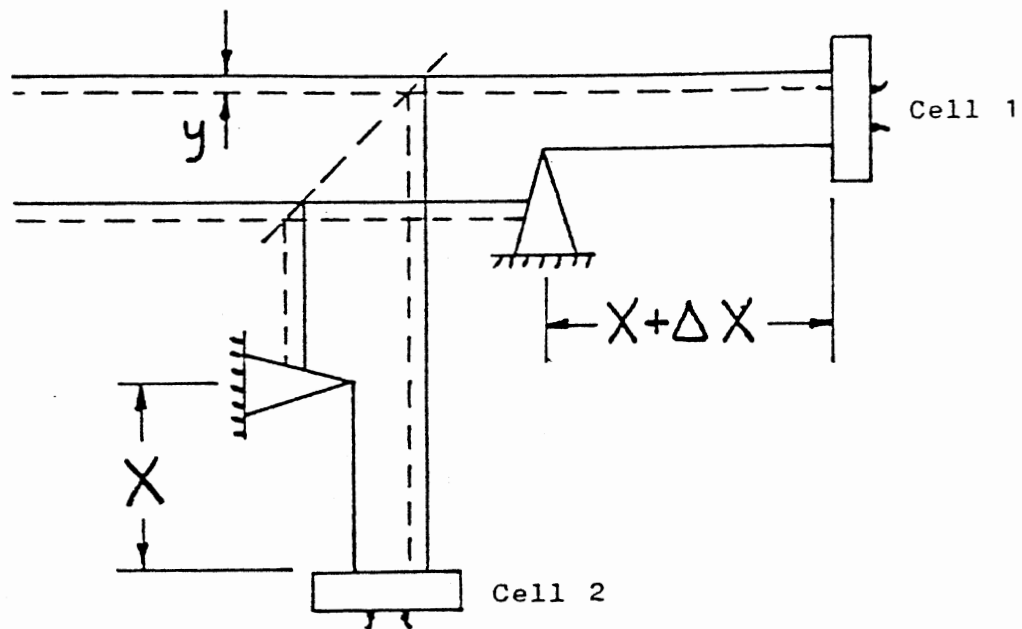


Figure 37. Dual Channel Response to Translation

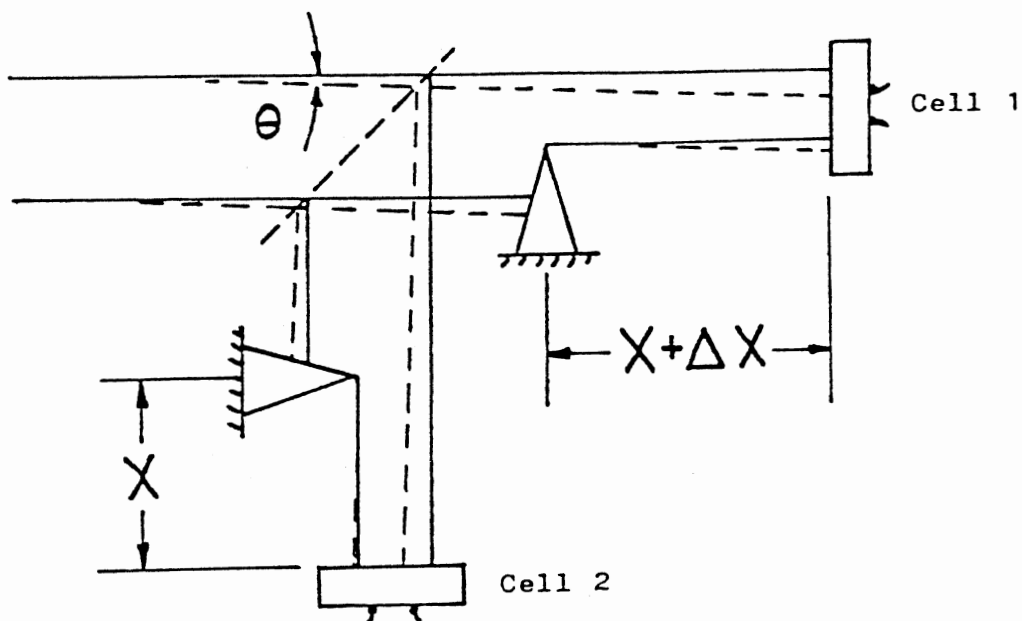


Figure 38. Dual Channel Response to Rotation

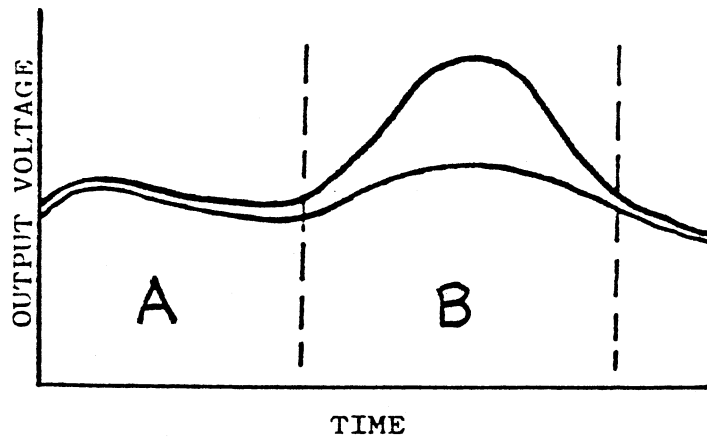


Figure 39. Dual Channel System Output for Translation and Rotation

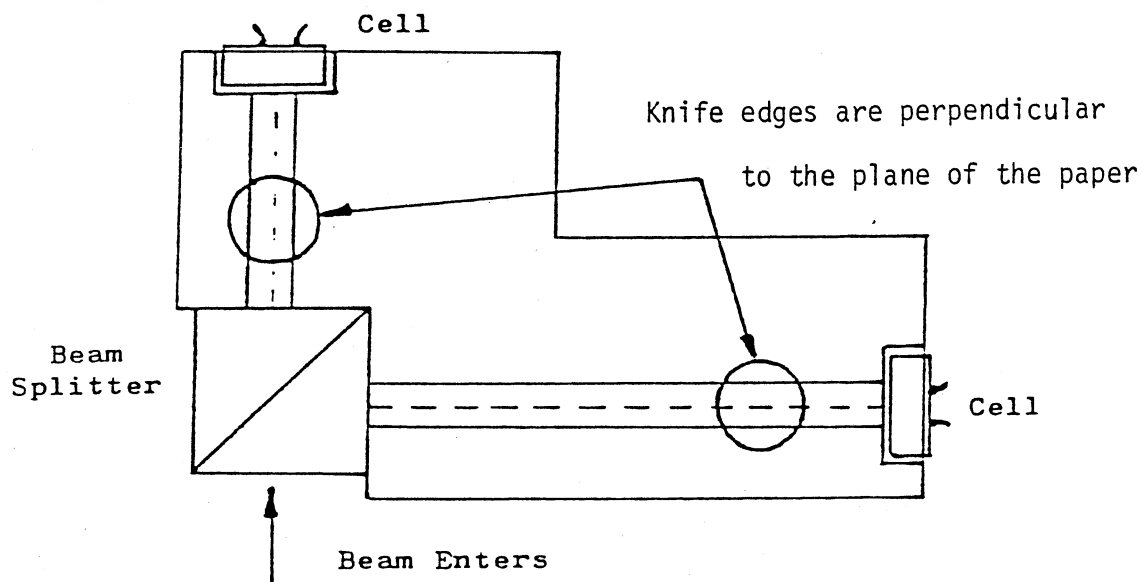


Figure 40. Dual Channel System Detector Block

monitored by the Biomation Model 805 digital storage device and a Spectral Dynamics Model 345 Spectroscope. This permitted concurrent recording of data in the frequency and time domain. The objectives of the experiments performed using the LAMDA system were to observe the effects of different manufacturer's disk surfaces, speed of disk rotation, and location of the head on the disk as factors which contribute to the frequency and amplitude of read/write head motion. The results of these experiments are presented in Chapter VI.

While the LAMDA system produced a means of studying some parameters it was unable to study one area of concern. The oxide surface of the disk is rough on a microscopic scale as shown in Figure 29. An investigation developed in which the interaction between the disk surface and the read/write head was studied. To accomplish this, the geometry of the spinning disk and its inherent waveshapes had to be eliminated from the list of possible variables. An intermediate result of the investigation was the evolution of an experimental apparatus known as the Linear Tape Drive.³² Figure 41 depicts the apparatus.

As the LAMDA system was engaged in other efforts, it was decided that strain gages would be used to sense the motion of the read/write head. Foil gages were adhered to the root of each flexure. The signal of each gage was monitored by the same experimental equipment used in the first strain gage experiment. The results of experiments performed on the LTD were inconclusive. Spectral data exhibited mainly the harmonics of the capstan angular frequency. Again the damping due to the gages compounded matters. The LTD was aborted at this point as the apparatus needed a tensioner to separate the effects

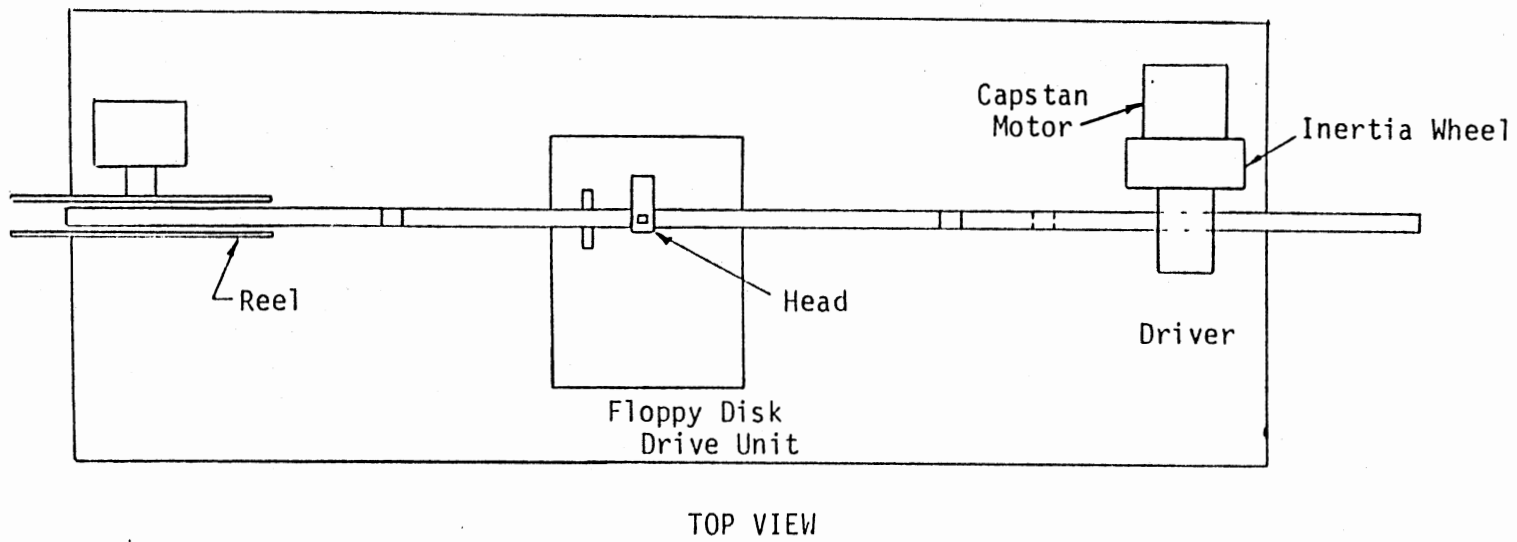
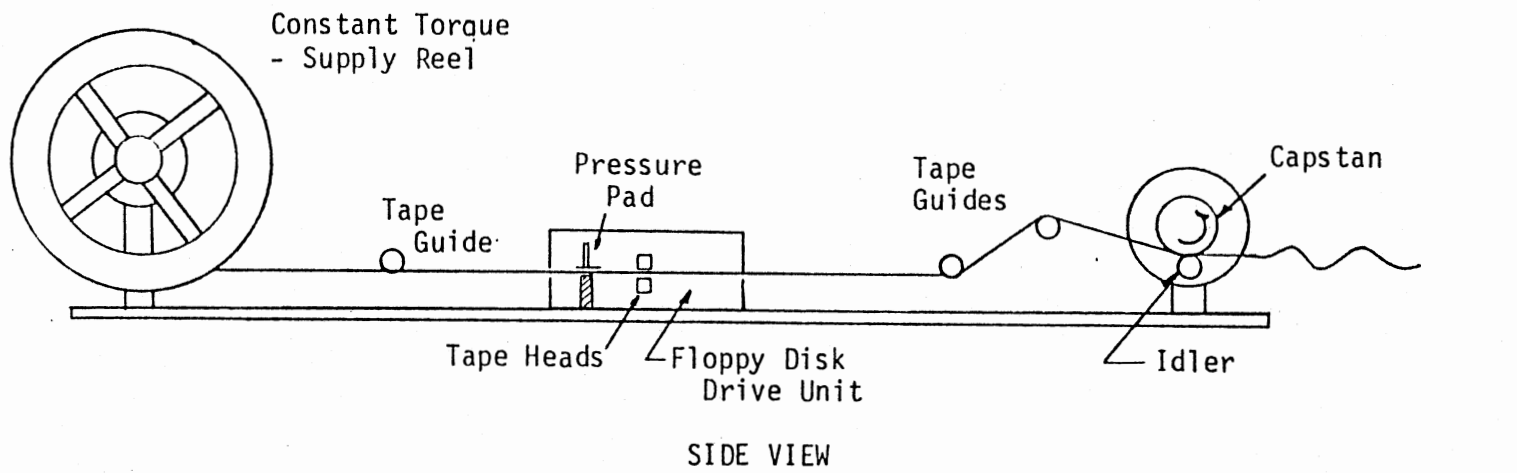


Figure 41. Linear Tape Drive Schematic

of the capstan from the region of tape in which the experiments were being performed and a better motion detector was needed. As the single beam LAMDA system had already shown success, the decision was made to design a more complex LAMDA system capable of obtaining quantitative data for roll, pitch, and vertical displacement.³³

The system developed was denoted as the dual beam LAMDA system. Figure 42 depicts the system set up. The theory of operation of the system is as follows. Figure 43 shows the coordinate axes about which roll, pitch, and vertical displacement are defined. To detect roll, an additional set of knife edges were installed to make the photocells sensitive to the roll motion. Figure 44 presents an orthographic view of one of the motion detectors. The counterpart is a mirror image. For this system, the following system of equations can be developed.

For translation and pitch:

$$\text{Signal One: } S_1 (Z, \theta_{yy}) = A_1 f(Z) + B_1 g (\theta_{yy}) \quad (5.1)$$

$$\text{Signal Two: } S_2 (Z, \theta_{yy}) = A_2 f(Z) + B_2 g (\theta_{yy}) \quad (5.2)$$

For roll:

$$\text{Signal Three: } S_3 (\theta_{xx}) = C_1 h (\theta_{xx}) \quad (5.3)$$

$$\text{Signal Four: } S_4 (\theta_{xx}) = C_2 h (\theta_{xx}) \quad (5.4)$$

To investigate how this system of equations can be formed into a viable solution, first consider a pure translation of the reflective surface atop the read/write head as shown in Figure 45. The deflection ΔZ produces unequivalent signals in motion detectors one and two. A comparison of the two signals is given in the following equations:

$$S_1 (Z, \psi_1) \propto (2 \cos \psi_1) \Delta Z = r_1 \quad (5.5)$$

$$S_2 (Z, \psi_2) \propto (2 \cos \psi_2) \Delta Z = r_2 \quad (5.6)$$

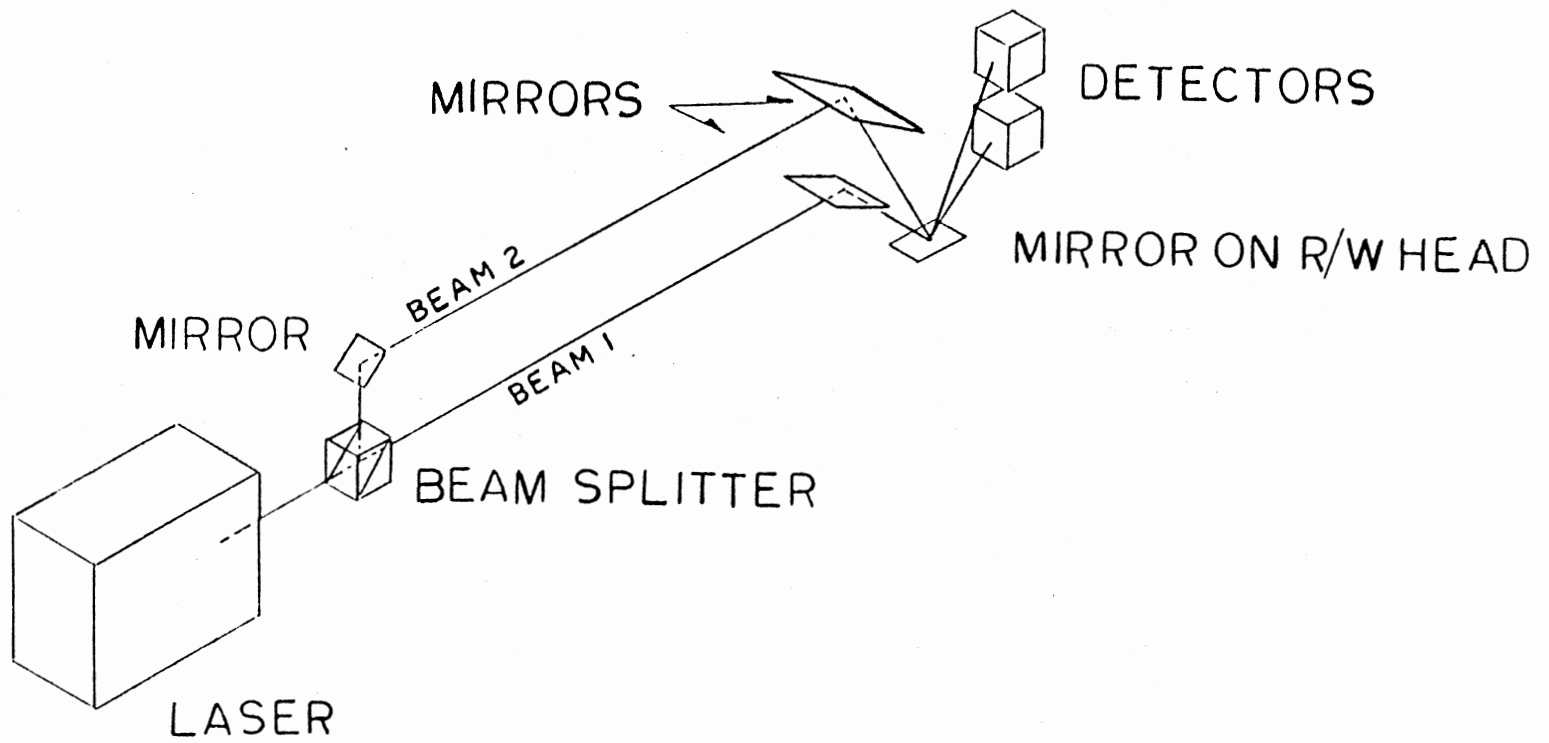


Figure 42. Dual Beam LAMDA System Setup

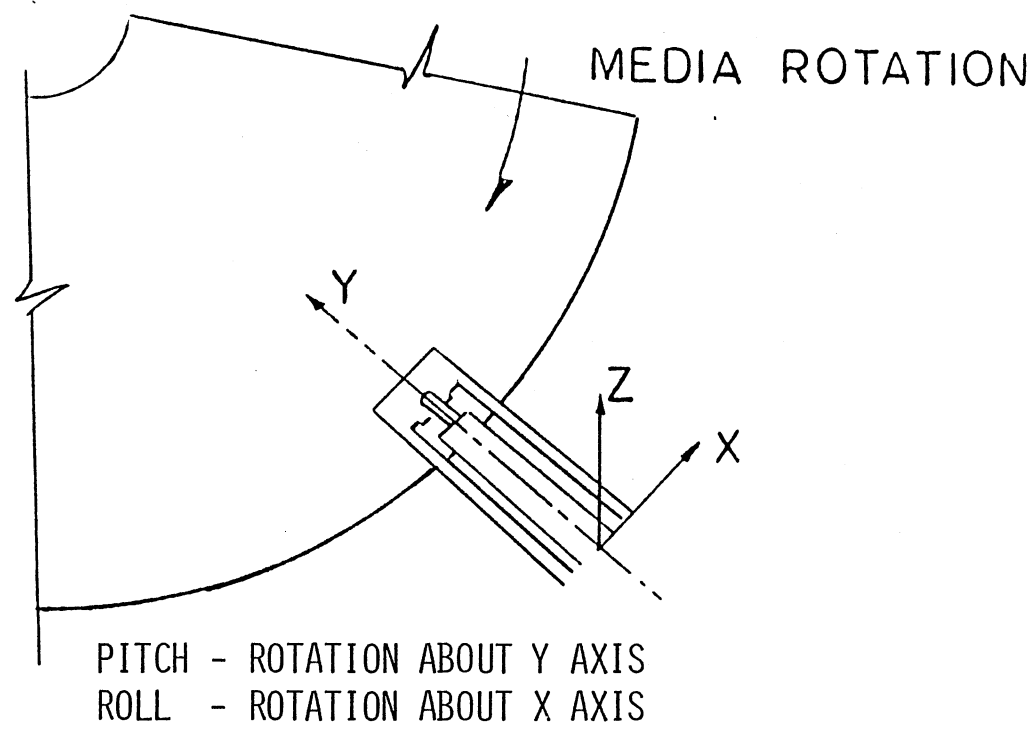


Figure 43. Axes About Which Pitch and Roll are Defined

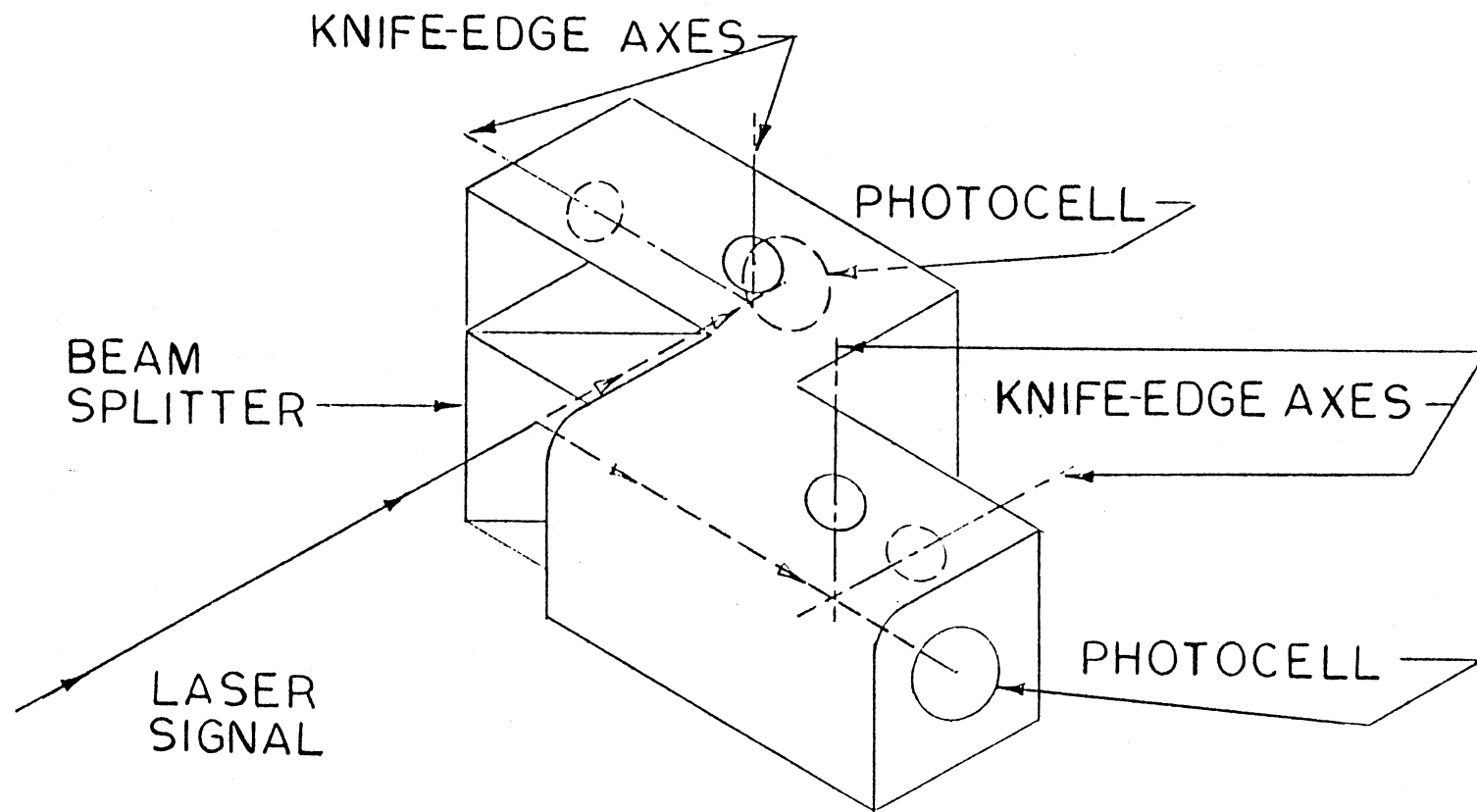


Figure 44. One of the Motion Detector Blocks for the Dual Beam LAMDA System

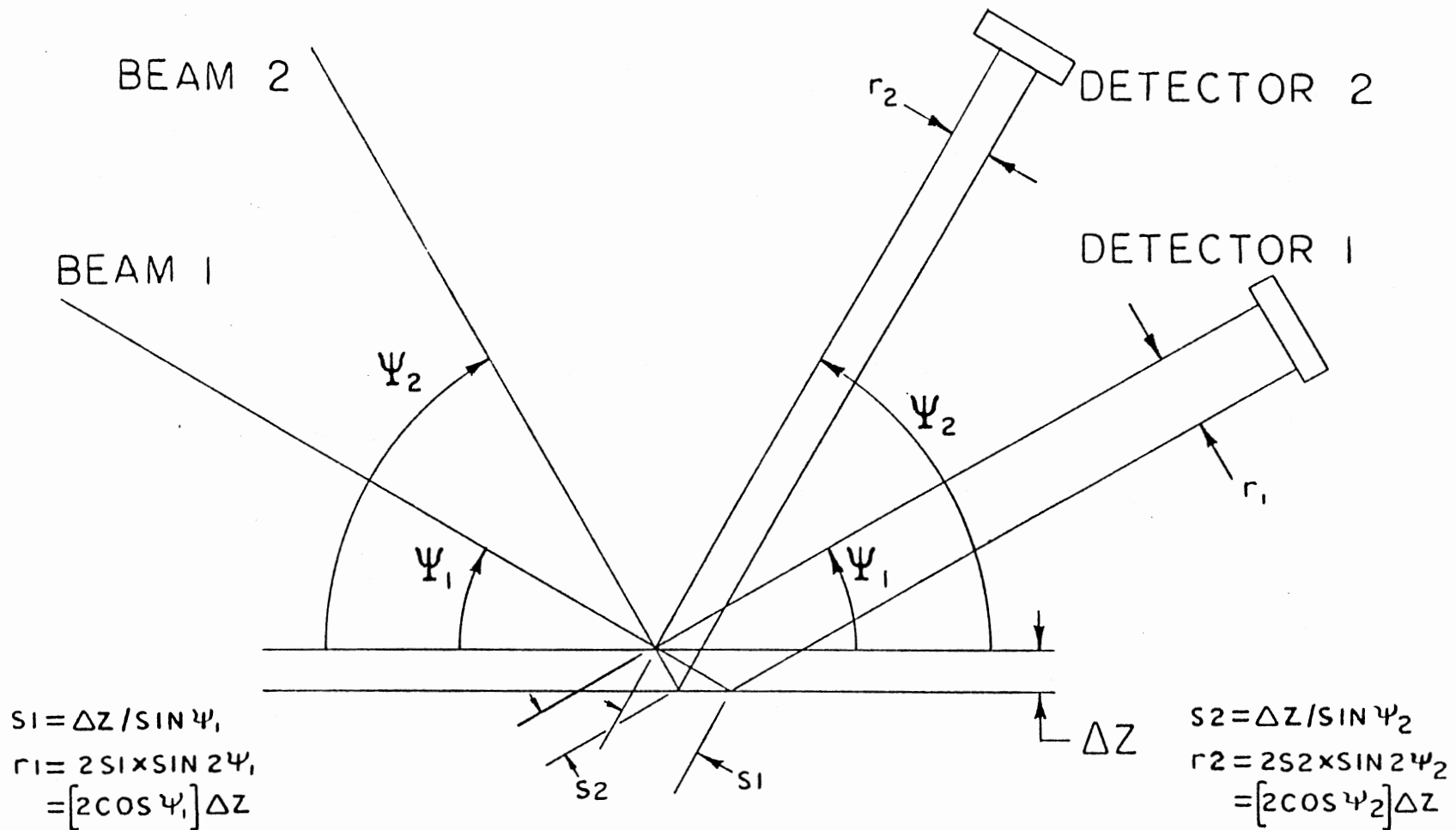


Figure 45. Response of Dual Beam LAMDA System to Translation

ψ_1 and ψ_2 are constants for pure translation thereby the signal intensity becomes directly proportional to the translation, ΔZ .

Second, consider a pure rotation of the reflective surface as shown in Figure 46. In this case let the rotation be both a plus and minus quantity. The equations governing the signals of the detectors are:

$$S_1 (\pm \theta) \propto 2R_1 \tan (\pm \theta) = L_1 \quad (5.7)$$

$$S_2 (\pm \theta) \propto 2R_2 \tan (\pm \theta) = L_2 \quad (5.8)$$

Note that if R_1 is equal to R_2 that the detected signals will be equivalent.

Now consider a combined state of translation and rotation as shown in Figure 47. From the Figure it is apparent that the amount of light striking the detectors can be obtained by superposition of the translation and rotation components. Thus, for combined rotation and translation the signal intensities become:

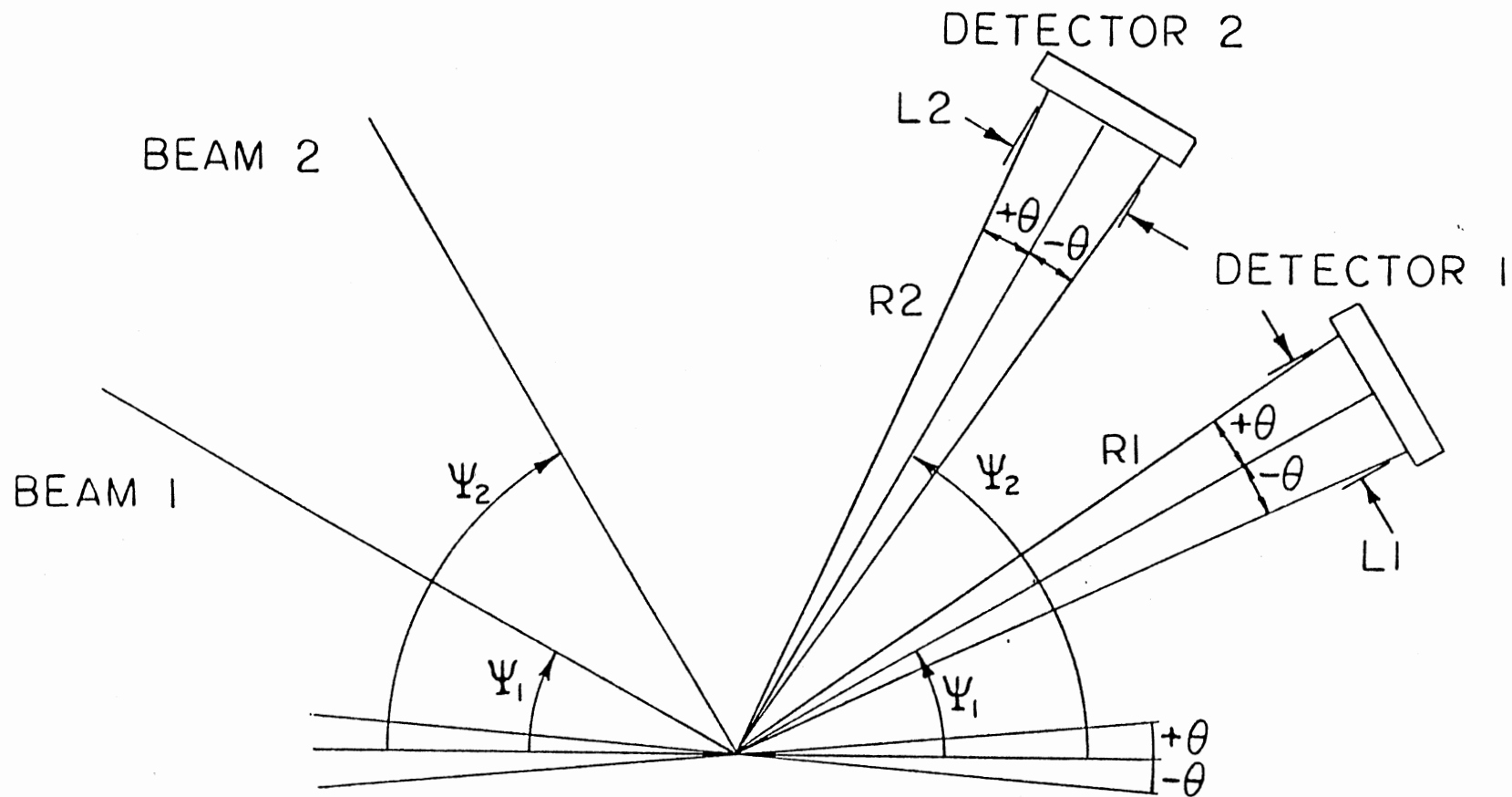
$$S_1 (Z, \pm \theta, \psi_1) \propto (2 \cos \psi_1) \Delta Z + 2 R_1 \tan (\pm \theta) = L_1 + r_1 \quad (5.9)$$

$$S_2 (Z, \pm \theta, \psi_2) \propto (2 \cos \psi_2) \Delta Z + 2 R_2 (\pm \theta) = L_2 + r_2 \quad (5.10)$$

If ψ_1 , ψ_2 , R_1 , and R_2 are constants, S_1 and S_2 become functions of ΔZ and θ alone. If R_1 and R_2 are equal the previous equations when subtracted will yield

$$S_1 (Z, \pm \theta, \psi_1) - S_2 (Z, \pm \theta, \psi_2) \propto 2 \Delta Z (\cos \psi_1 - \cos \psi_2) \quad (5.11)$$

Substituting the variables from the original system of equations derived for translation and pitch yields:



$$\text{TAN}\theta = L_2 / [2 \times R_2]$$

$$L_2 = 2R_2 \text{TAN}\theta$$

$$\text{TAN}\theta = L_1 / [2 \times R_1]$$

$$L_1 = 2R_1 \text{TAN}\theta$$

Figure 46. Response of Dual Beam LAMDA System to Rotation

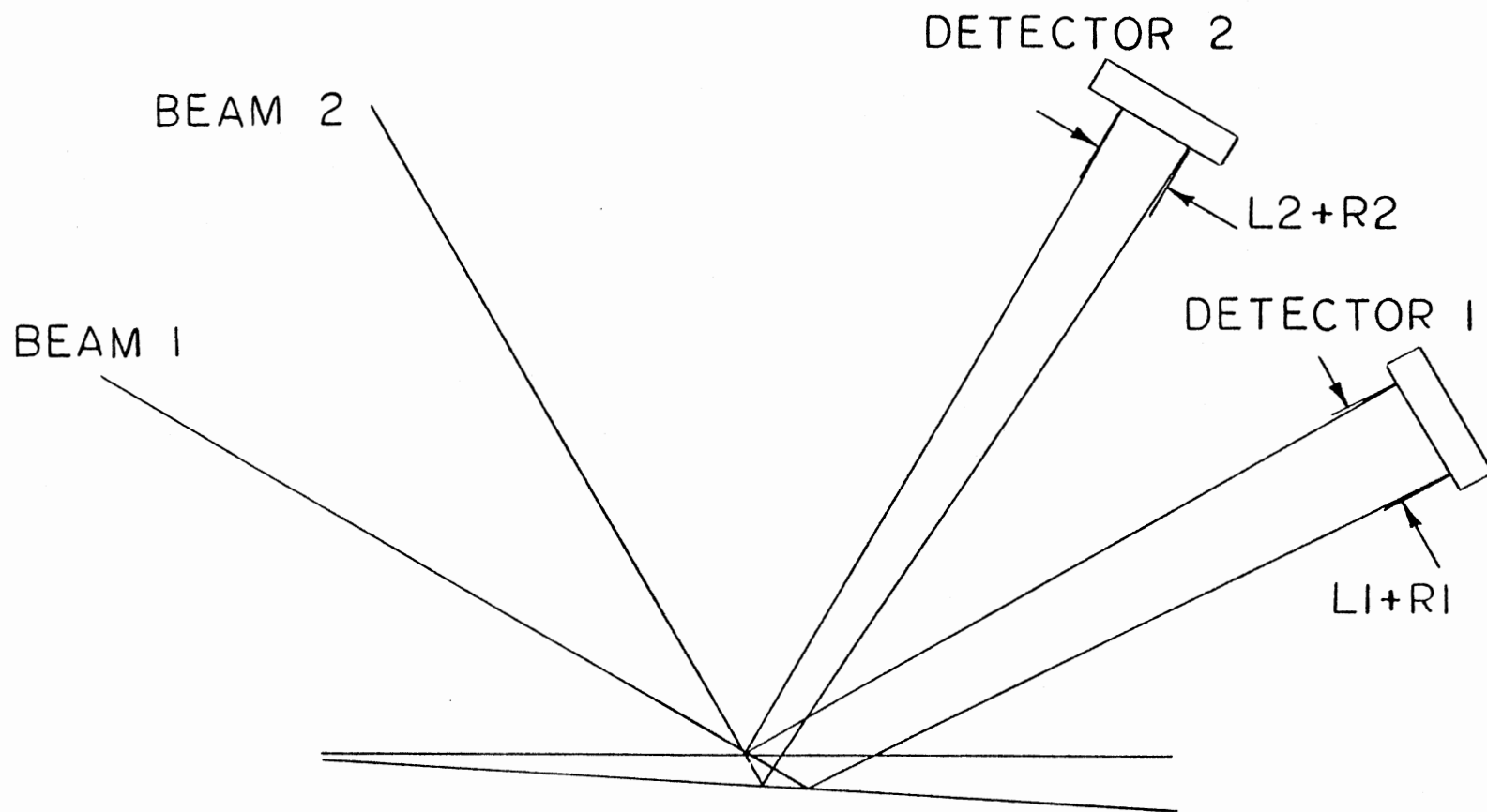


Figure 47. Response of Dual Beam LAMDA System to Translation and Rotation

$$\begin{aligned}
 S_1 (Z, \theta_{yy}, \psi_1) - S_2 (Z, \theta_{yy}, \psi_2) \\
 \alpha 2 \Delta Z (\cos \psi_1 - \cos \psi_2)
 \end{aligned}
 \tag{5.12}$$

The vertical translation, ΔZ , can be determined by subtraction of the two analog signals S_1 and S_2 .

The pitch, θ_{yy} , can be determined by substitution of ΔZ into either of the following equations

$$\begin{aligned}
 S_1 (Z, \theta_{yy}, \psi_1) \alpha (2 \cos \psi_1) \Delta Z \\
 + 2R_1 \tan \theta_{yy}
 \end{aligned}
 \tag{5.13}$$

$$\begin{aligned}
 S_2 (Z, \theta_{yy}, \psi_2) \alpha (2 \cos \psi_2) \Delta Z \\
 + 2R_2 \tan \theta_{yy}
 \end{aligned}
 \tag{5.14}$$

θ_{xx} can be determined from the equations:

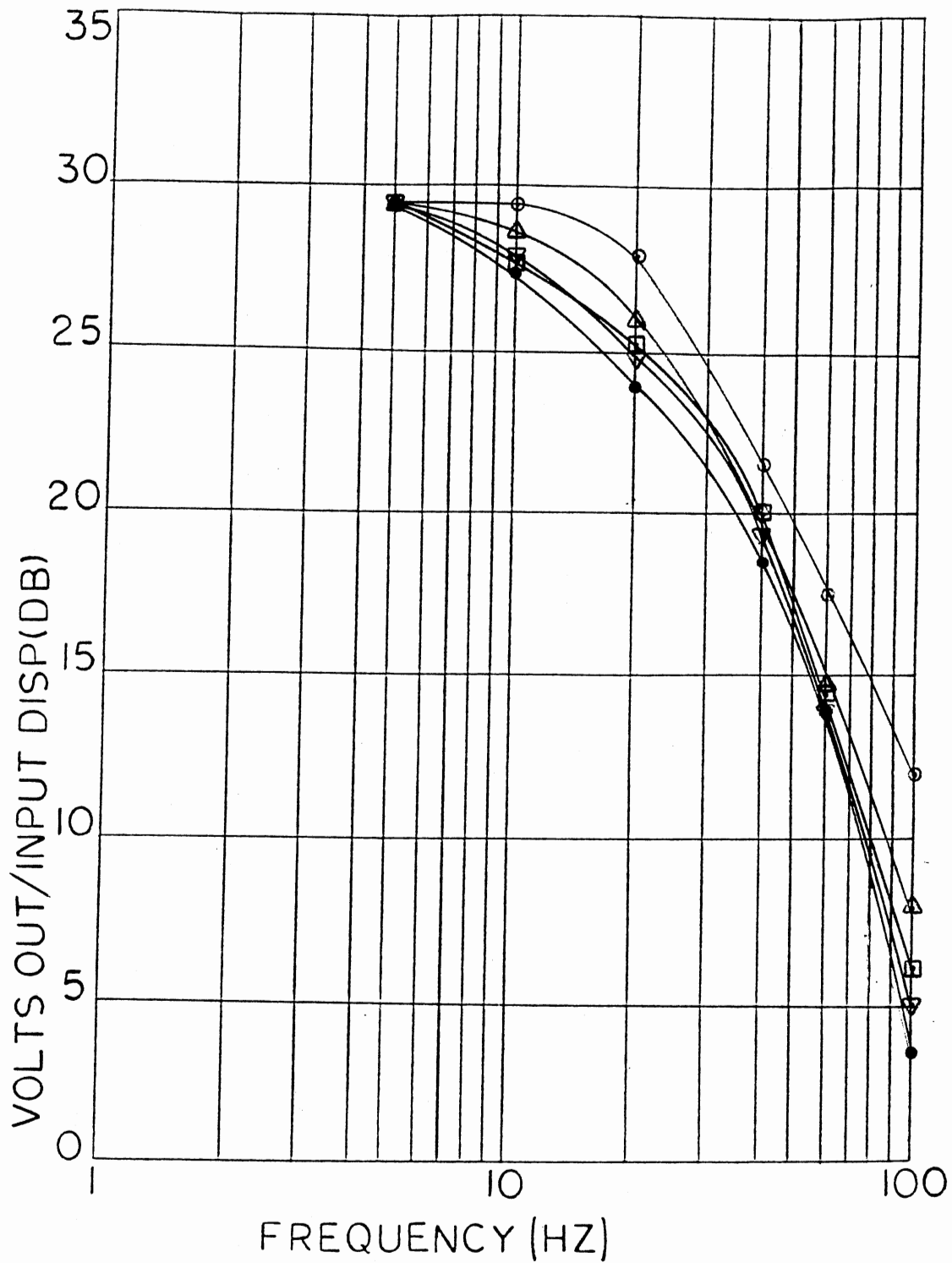
$$S_3 (\theta_{xx}) \alpha 2 R_1 \tan \theta_{xx} \tag{5.15}$$

$$S_4 (\theta_{xx}) \alpha 2 R_2 \tan \theta_{xx} \tag{5.16}$$

These equations contain only one term as the orientations of the knife edges which are sensitive to roll motion are insensitive to vertical displacement. These equations yield two values for θ_{xx} and θ_{yy} thus providing checkpoints for data.

With the detectors complete and the system equations derived the problem of determination of the constants of proportionality in the system equations was dealt with. This was accomplished by mounting a mirror atop of the exciter on a MB Electronics Model T112031 vibrational shaker. The reflective surface thus provides a calibration source for the detector system.

Figure 48 depicts the frequency responses of the front-top detector to a sinusoidal vertical translation of the reflective surface (Front-Top refers to the photosensor on the top of the front



DISPLACEMENT LEGEND

- 0.002 IN. △ 0.004 IN. ● 0.01 IN.
 □ 0.006 IN. ▽ 0.008 IN.

Figure 48. Translation Response for Front-Top Detector

detector). As shown in the Figure, these tests were run for varied displacements. This Figure is typical for rotations, pitch or roll, on this or one of the other three detectors as well. Rotational calibration was obtained by using the MB shaker to drive a rocker mechanism. The reflective surface was adhered to the rockets at the pivot point such that the mirror is submitted to pure rotation.

As it was undesirable to have system equations as a function of displacement and frequency, as well as reduced signals at high frequencies, attempts were made to extend a constant frequency response out to approximately 500 Hz.. This was accomplished by electronic compensation. Figure 49 is a schematic of a typical compensator and its transfer function. Figure 50 shows the experimentally determined frequency response for the front-top detector compensator.

With the compensation complete, a new set of calibration data was taken. In these tests displacement or rotation was held constant while frequency was varied. Alignment of the laser beams within the detector is a critical factor in the reproduction of a constant output signal for a given displacement and frequency. This meant that two sets of calibration data had to be taken as the reflective surfaces on the old and new production heads were in slightly different locations. Each test was performed three times and the data was averaged and plotted of which Figure 51 is typical. Figure 51 is atypical from other plots in that each signal curve has positive slope. This again is undesirable as frequency must become a variable in the system equations. Figure 51 is the calibration curve for the front-top detector. Other detectors exhibited a markedly flat

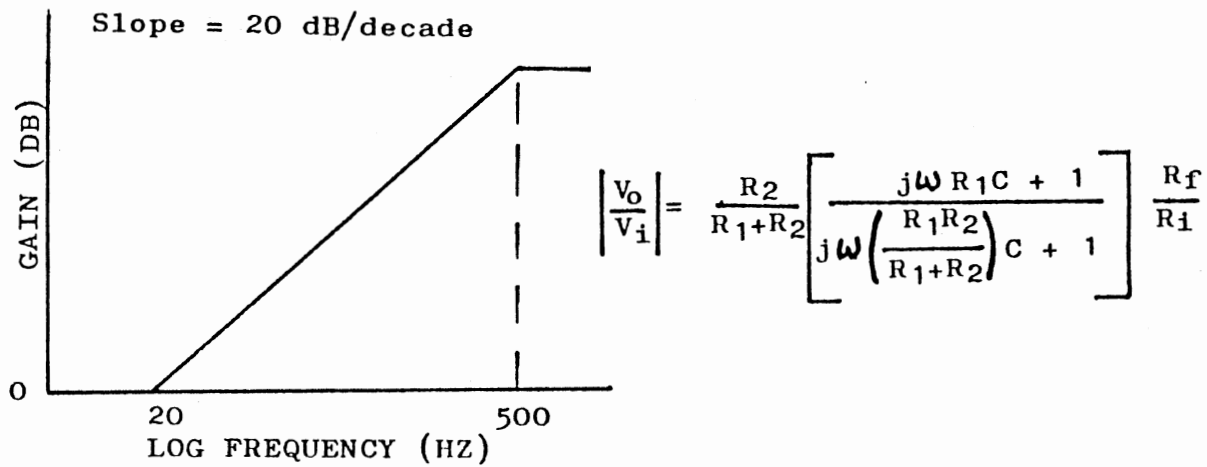
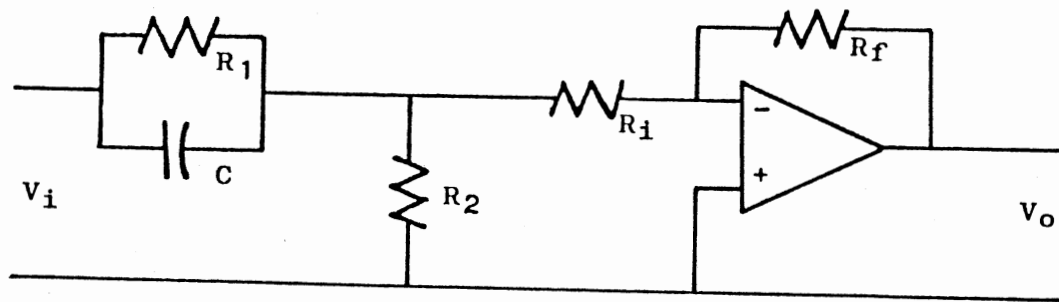


Figure 49. Compensator Schematic with Frequency Response and Transfer Function

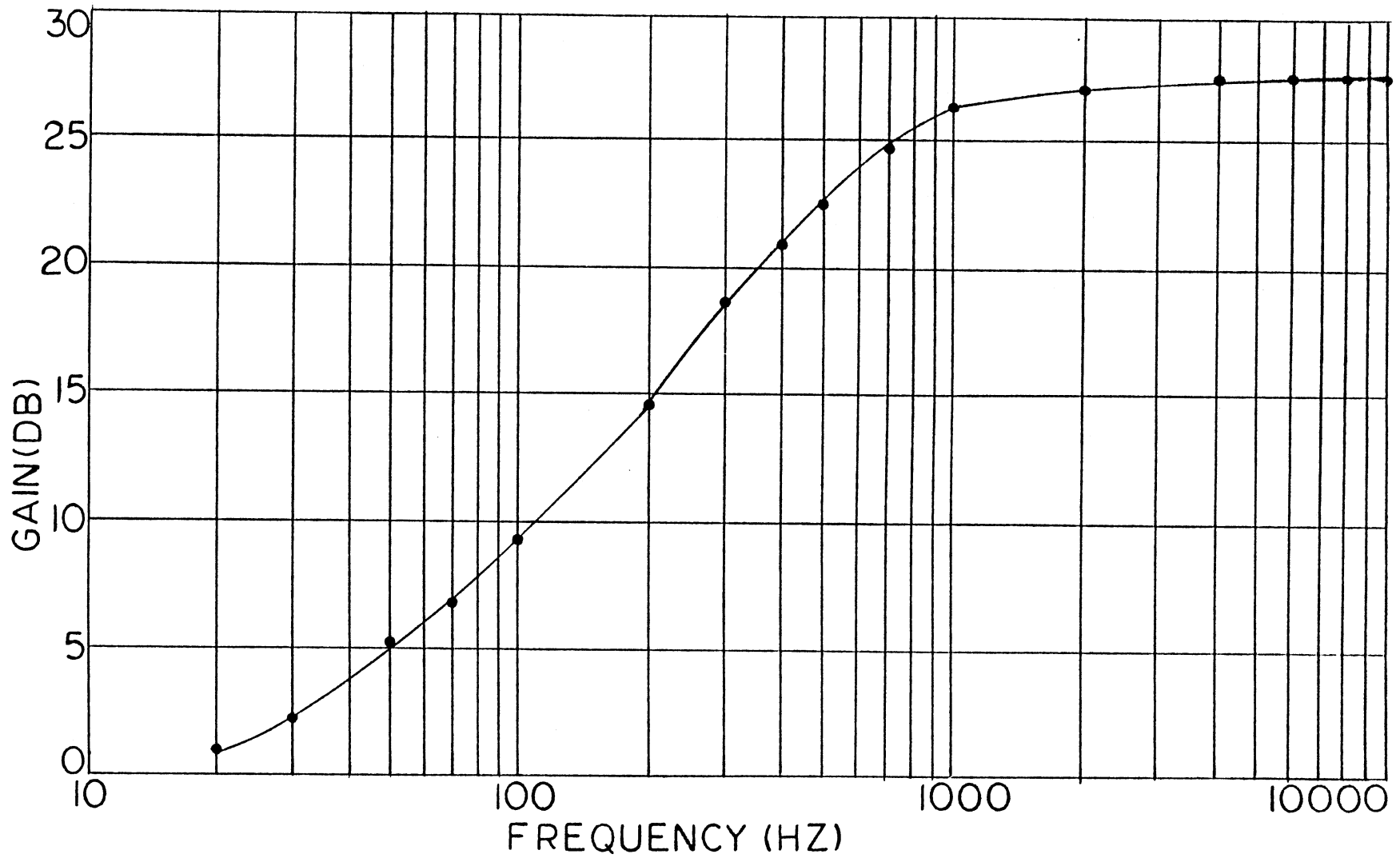


Figure 50. Experimental Frequency Response of the Front-Top Compensator.

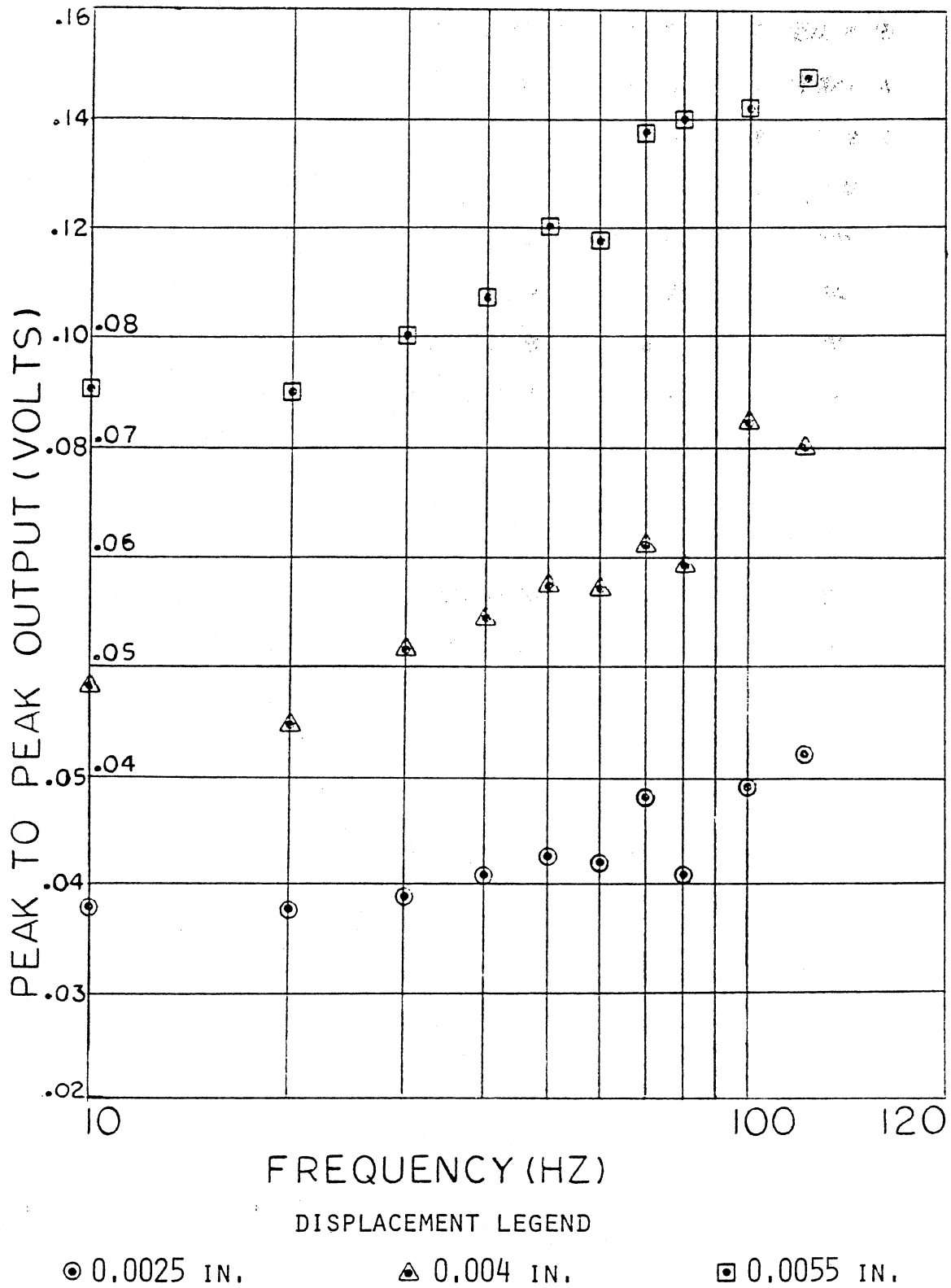


Figure 51. Average Translatory Frequency Response for the Front-Top Detector with Reflective Surface Positioned to Simulate the New Production Head

frequency response. Further perusal of Figure 51 will divulge that for a fixed frequency the output signal is nonlinear with respect to the displacement domain.

With the characteristics of the system known, some key assumptions had to be made. First, it had to be assumed the system equations (5.1 through 5.16) were at least partially invalid. These equations were developed assuming a constant signal output versus the frequency domain for a given displacement. Although three of four detectors exhibited such characteristics within reason, the front-top detector did not. In addition, the system equations assumed a linear relationship between signal output and displacement at a given frequency. After completing the calibration of the detectors (the top detectors had to be calibrated for translation and pitch), it was found that this was a poor assumption.

To render the system usable, a second key assumption was made. It was decided that the nonlinearity with respect to frequency would be partially disregarded. The calibration data, of which Figure 51 was typical, would be extrapolated to a frequency of 170 Hz. which was in the region of the first pitch mode. Extrapolation was required due resonance of the calibration shaker at 140 Hz. and limited amplitude capability of the shaker at higher frequencies. From the extrapolated data new calibration curves would be made relating signal output to displacement. Figure 52 is typical of such curves and depicts translation calibration for the front-top detector with the reflective surface positioned to simulate the New Production Head. The curve connecting the data points in Figure 52 was obtained using the Newton-

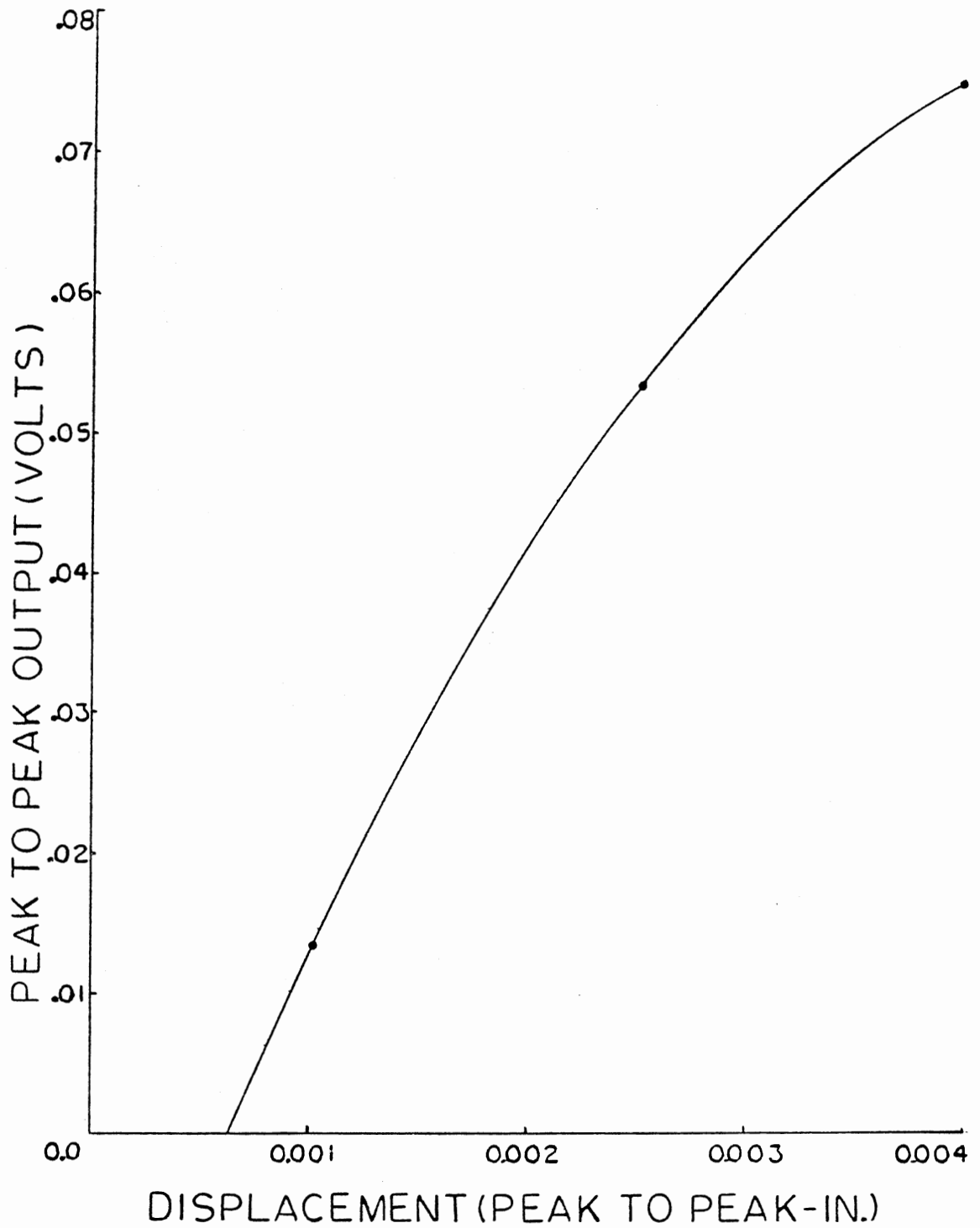


Figure 52. Translation Calibration for Front-Top Detector
Positioned for the New Production Head

Gregory method for second degree backward polynomials.³⁴ The equation for this method follows:

$$F_2(x) = f(x_0) + \binom{s}{1} f_{-1} + \binom{s+1}{2} f_{-2}; s = (x - x_0)/h \quad (5.17)$$

Demonstrating this method for the case of Figure 52 first involves the forming of a difference table.

TABLE V
DIFFERENCE TABLE FOR FIGURE 52

x	f (x)	Δf	$\Delta^2 f$
.001	.0135		
		.0405	
.0025	.0540		-.0195
		.0210	
.004	.075		

Substitution of information from Table V and the X increment of .0015 into Equation (5.17) yields:

$$\begin{aligned} F(Z) &= .075 + (1/.0015) (Z - .004) (.0210) \\ &\quad + 1/2 (1/.0015)^2 (Z - .004) (Z - .0025) (-.0195) \\ &= -.0243 + 42.17 Z - 4333.3 Z^2 \end{aligned} \quad (5.18)$$

This procedure was performed for all of the calibration data taken yielding six calibration equations per read/write head. Calibration equations for translation, pitch, and roll for two detector blocks comprises the total of six. It must be clear that the equations for the Front-Top detector are valid only for signals whose frequency content is in the 170 Hz. range.

To evaluate test data some of the theory background from the development stage of the dual beam LAMDA system can be used. The signals from the Front-Top and Back-Top detectors are a combination of a translation and pitch signal. The signals from the Front-Side and Back-Side detectors are comprised of a roll signal only. Thus, in the form of equations:

$$V \text{ (top signal)} = V \text{ (translation)} + V \text{ (pitch)} \quad (5.19)$$

$$V \text{ (side signal)} = V \text{ (roll)} \quad (5.20)$$

where $V \text{ (translation)}$, $V \text{ (pitch)}$, and $V \text{ (roll)}$ are voltages corresponding to displacements or rotations on the calibration curves. The evaluation of these signals will be discussed in Chapter VI.

During tests, four signals were monitored simultaneously. These signals were viewed on a four channel Tektronix Model 564 oscilloscope and recorded on a Consolidated Electrodynamics Corporation Model 5-124 oscillograph. Frequency analyses were performed on a Spectral Dynamics Model 345 Spectroscope whose output was plotted on a Hewlett Packard Model 7044A X-Y plotter. Figure 53 is a schematic of the instrumentation.

For the purpose of verifying the analytical head models, single read/write head flexures were studied to determine their natural

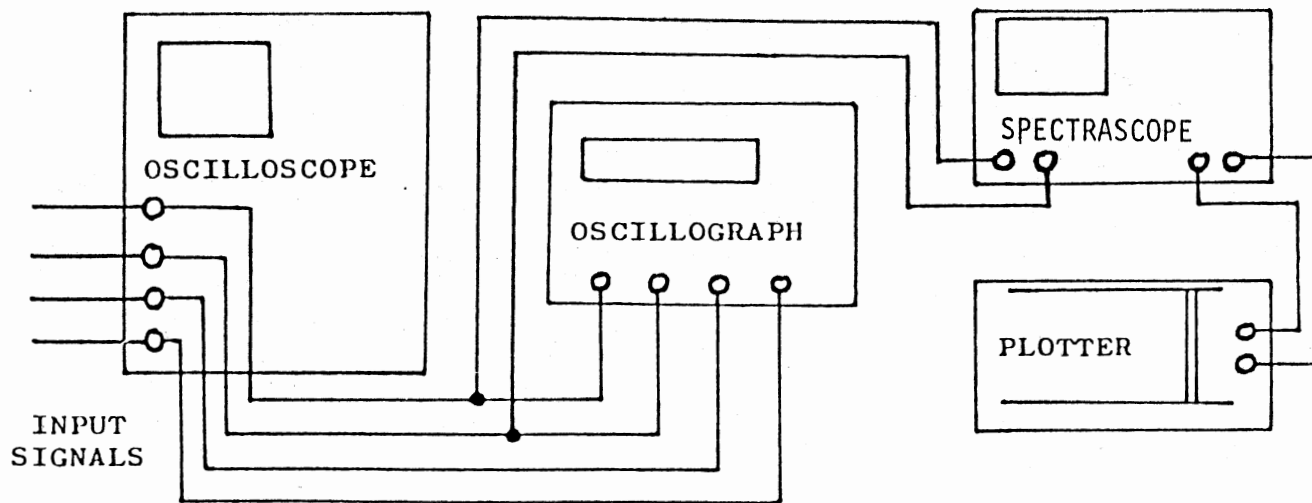


Figure 53. Schematic of Instrumentation for Dual Beam LAMDA Apparatus

frequencies. The flexures were shaken on an MB Electronics Model T 112031 electromagnetic shaker with sinusoidal input. After resonance was established the mode shape was determined by viewing the vibrating flexure with a strobe. Since the results of this work are brief they will be presented in the following table.

TABLE VI
EXPERIMENTAL EIGENVALUES AND EIGENVECTORS
OF SINGLE READ/WRITE HEAD FLEXURES

Eigenvector	Eigenvalue (Hz.)	
	<u>New Production Head</u>	<u>Old Production Head</u>
Cantilever	24.7	32.2
Pitch	110.2	108.1
Roll	260.0	256.0

CHAPTER VI

EXPERIMENTAL RESULTS

This chapter presents the results of tests performed on the floppy disk system using the single and dual beam LAMDA apparatus. The apparatus and their use are discussed in detail in Chapter V.

Some of the first tests performed using the single beam LAMDA system involved the comparison of head motion for disks of varied manufacture. Figure 54 depicts voltage versus time of the top signal for the new production head on three different disks. In this case, the top signal is monitored, as it should be sensitive to pitch and vertical motion. The three traces resemble one another little with the exception of periodicity. A perusal of each trace will divulge the periodicity of each signal as well as the consistency in base period shown in all three traces. Time scales are inferred on these traces as the base period will be the inverse of the drive speed. These traces show the read/write head deflecting to a certain position, vibrating about that position and finally returning to the initial position in the time interval of the base period. Figure 55 depicts the spectral plots of the voltage versus time plots of Figure 54. All plots show several harmonics of the drive speed and exhibit a significant frequency component at approximately 140 Hz..

Figure 56 portrays the same tests as Figure 54 with the exception that the old production head has been installed into the disk drive.

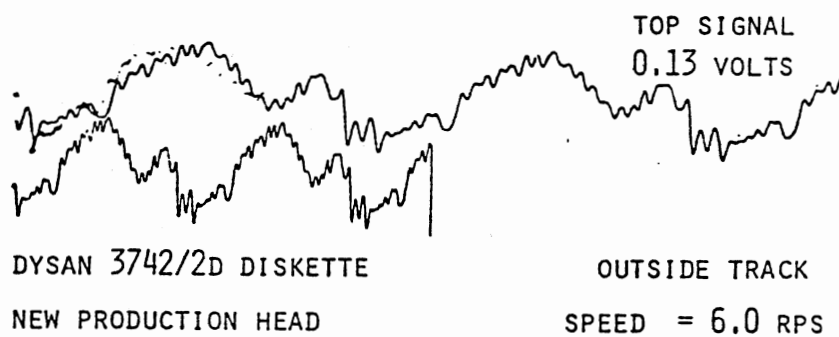
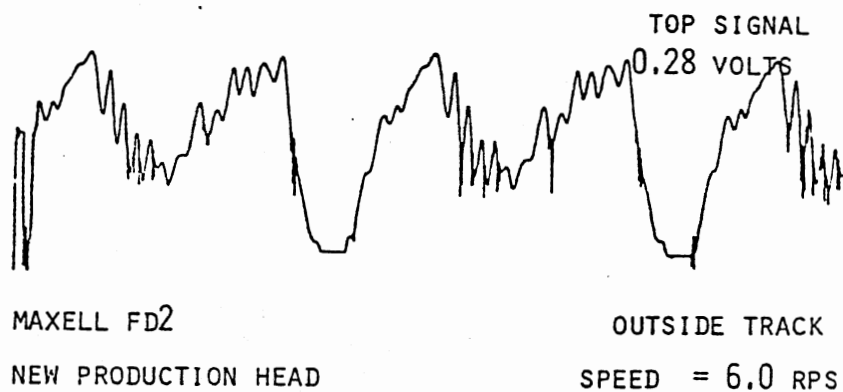
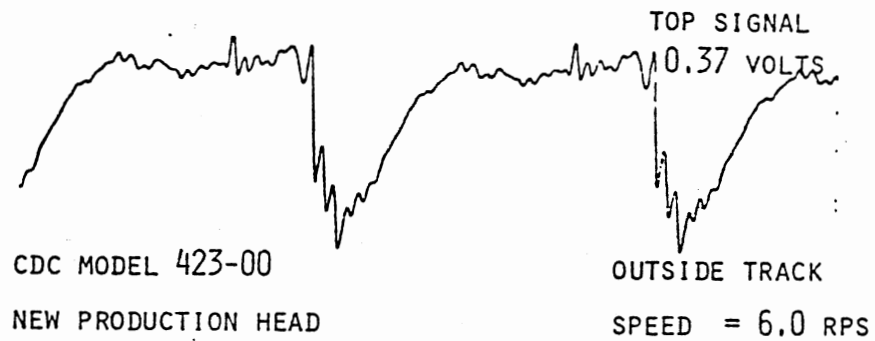


Figure 54. Voltage versus Time Traces for the New Production Head on Disks of Various Manufacturers

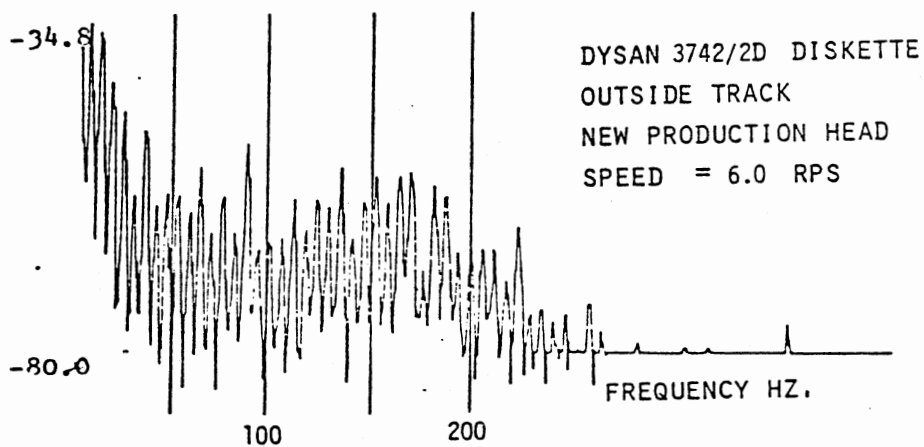
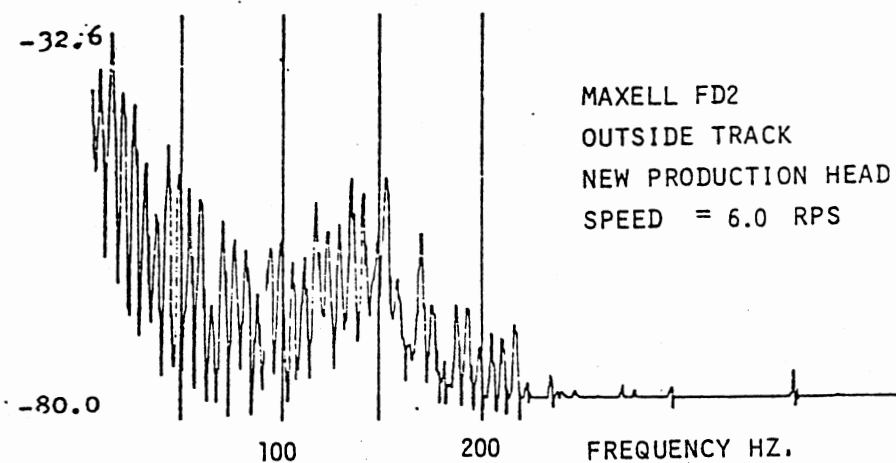
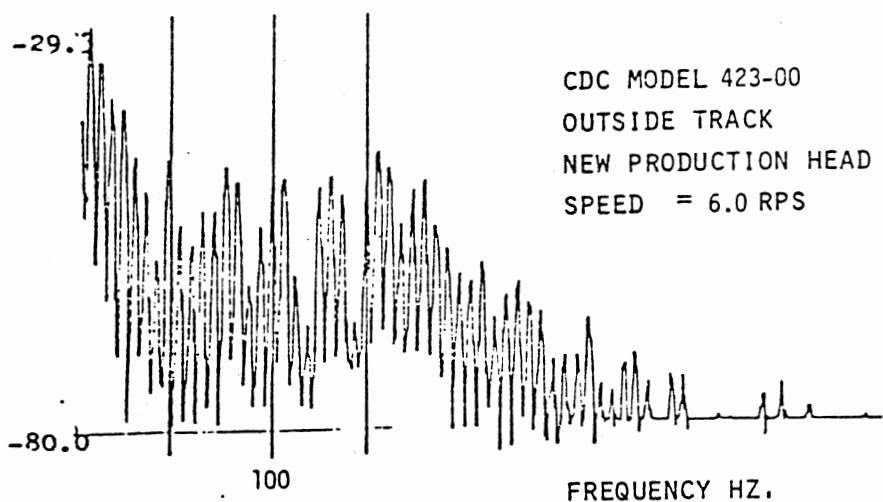


Figure 55. Spectral Plots Corresponding to Voltage versus Time Traces of Figure 54

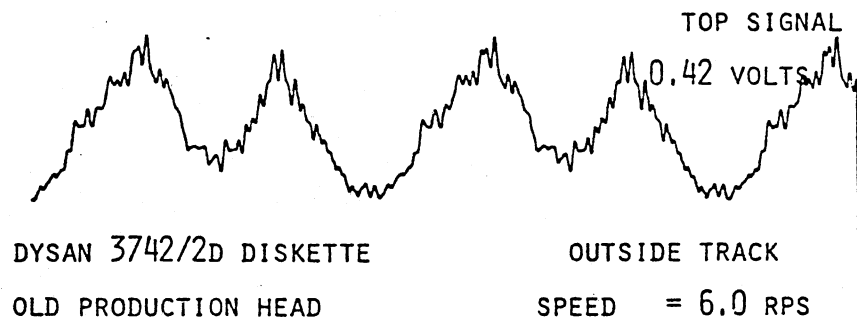
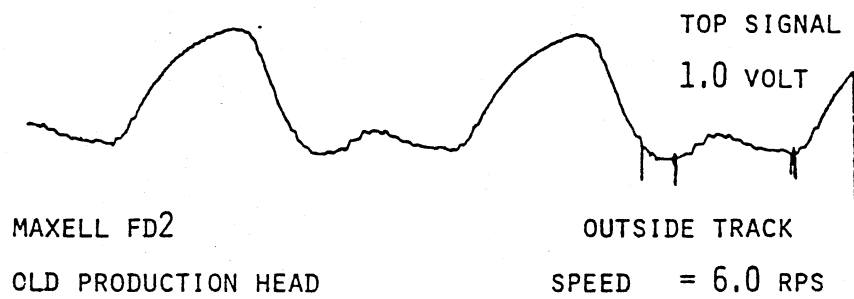
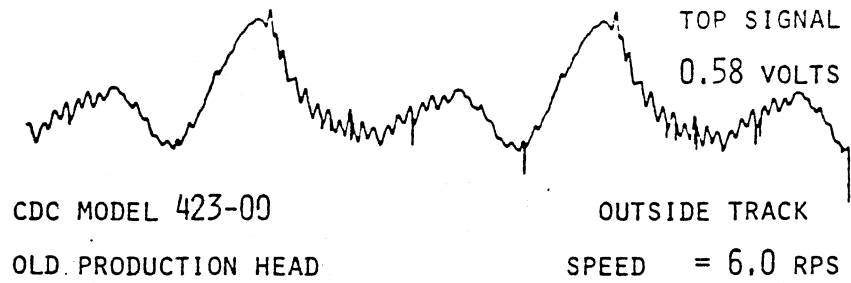


Figure 56. Voltage versus Time for the
Old Production Head on Disks
of Various Manufacturers

As the old production head is a gimbaled design a difference in behavior would be expected when compared to the non-gimbaled new production head. Perusal of Figure 56 shows the deflection increasing and decreasing which, contrary to the new head, is indicative of the flexibility of the gimbaled design in the pitch direction. Figure 57 depicts the spectral plots of Figure 56. The spectral plots show dominant frequency components in the 160 to 190 Hz. range as well as a higher frequency component in the 280 to 320 Hz. range.

Later tests involving the use of the single beam LAMDA system were performed to study the effect of drive speed on head motion. In these tests, the variance in disks due to different manufacturers was removed as a variable by performing all tests on an IBM Diskette 2D. Figure 58 displays voltage versus time traces for the new production head at drive speeds of 6.0, 7.14, 8.89 and 11.1 revolutions per second. As would be expected, the base period decreased according to the increase in drive speed. The voltage amplitude decreased with increased drive speed which is indicative that deflections decrease with increasing speed. At the highest drive speed, 161 revolutions per second, an increase in high frequency content is detectable. Figure 59 displays the spectral content of the top signals shown in Figure 58. The conclusions drawn from the voltage versus time plots may also be deduced from the spectral data.

Figure 60 depicts voltage versus time for the old production head running on a Maxell FD2 disk. The correlation between drive speed and vibration level is random when compared to the new production head data. For instance, in Figure 60, the voltage amplitude for 6.0, 7.14, and 8.89 revolutions per second is shown to increase from 0.46

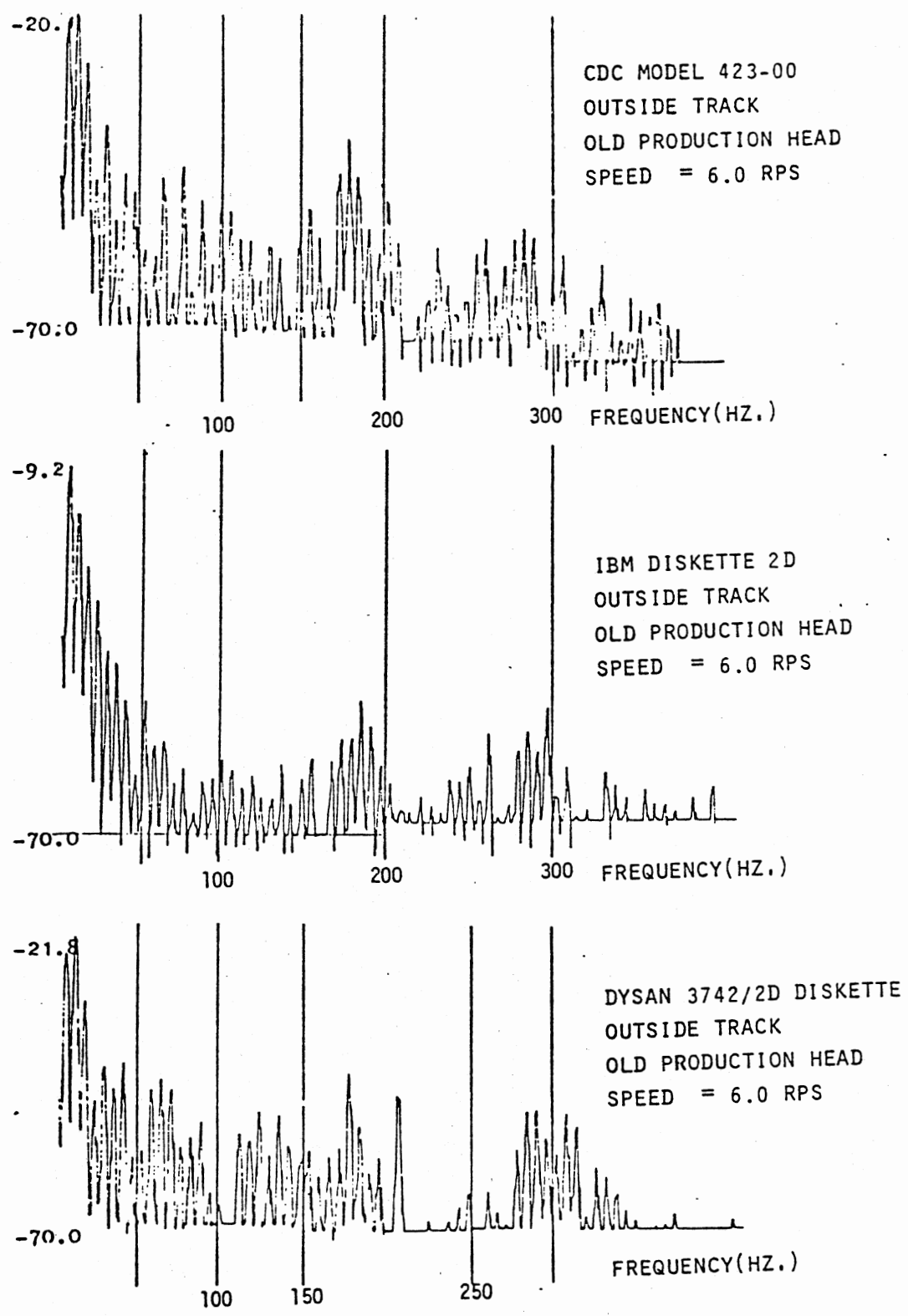


Figure 57. Spectral Plots Corresponding to Voltage versus Time Traces of Figure 56

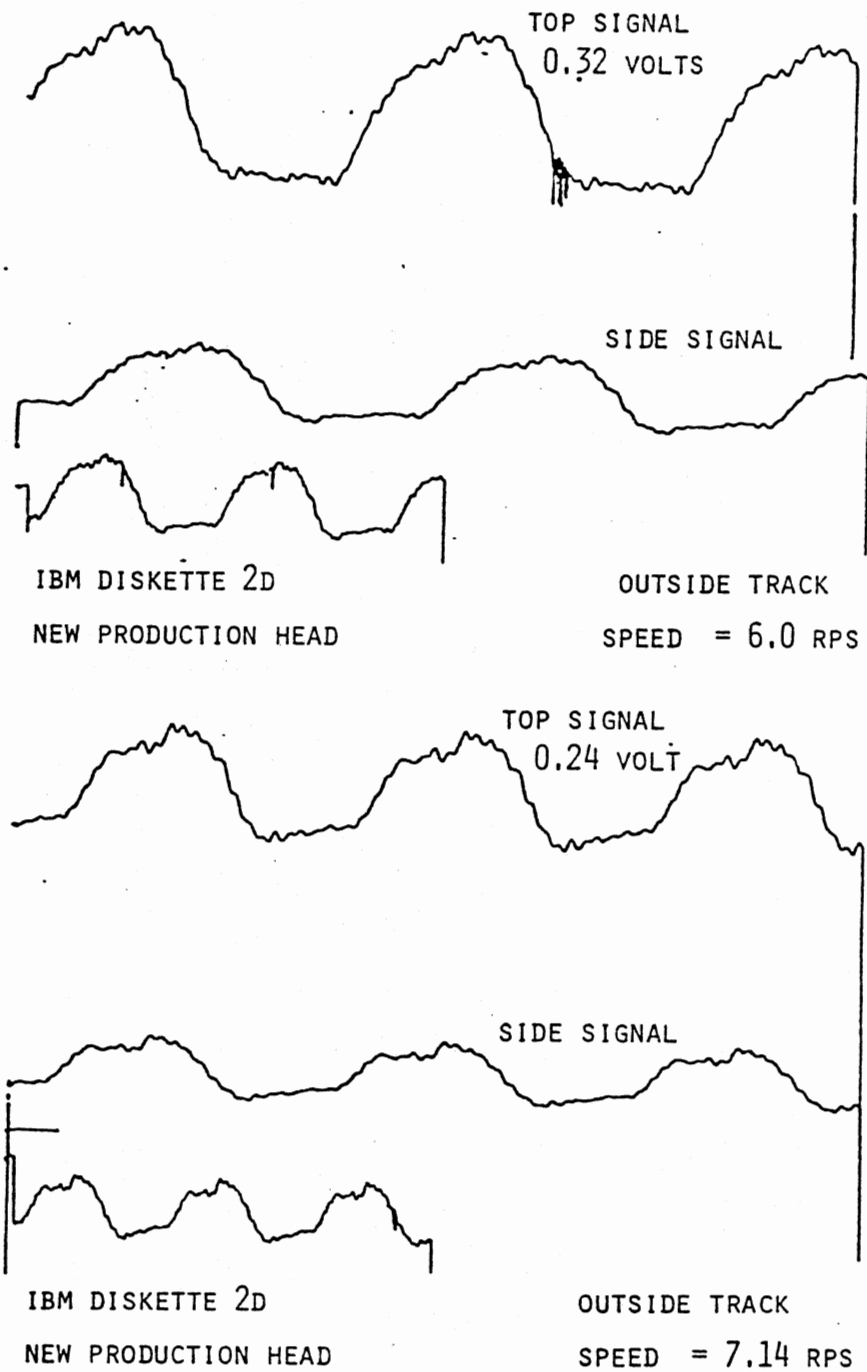


Figure 58. Voltage versus Time Traces for the New Production Head at Various Drive Speeds

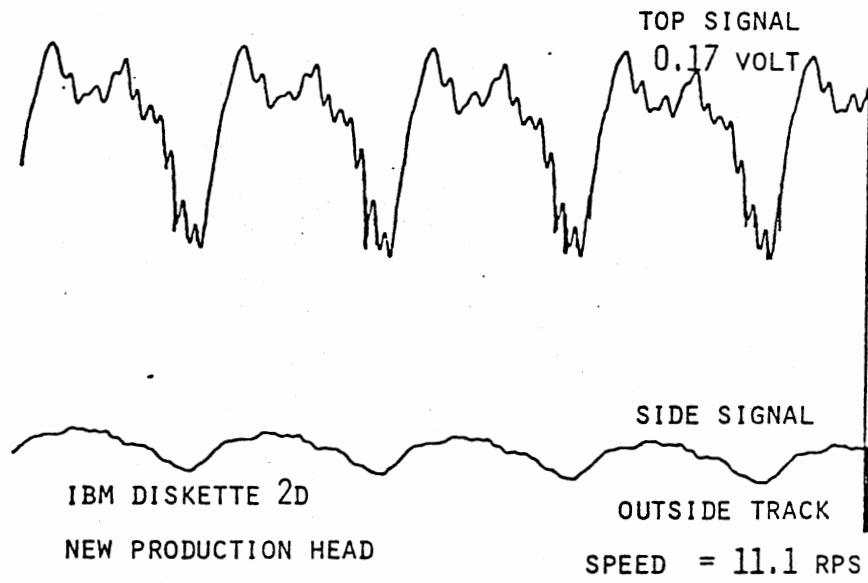
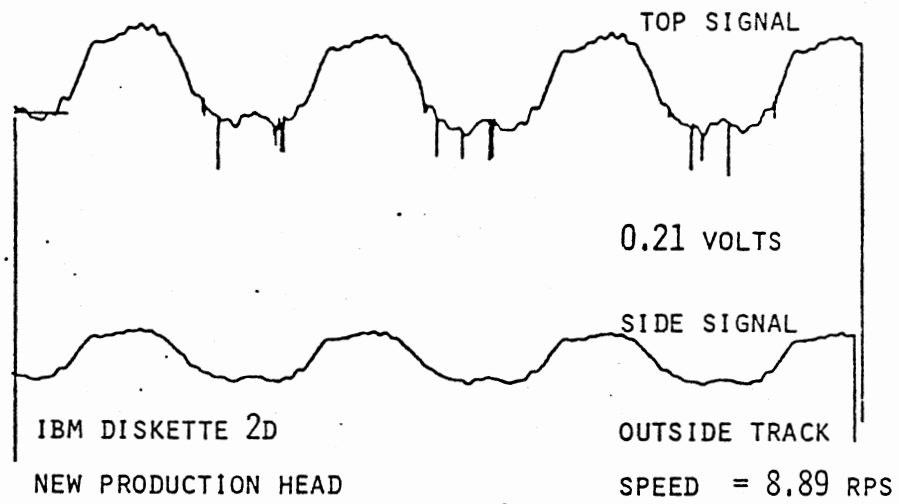


Figure 58. (Continued)

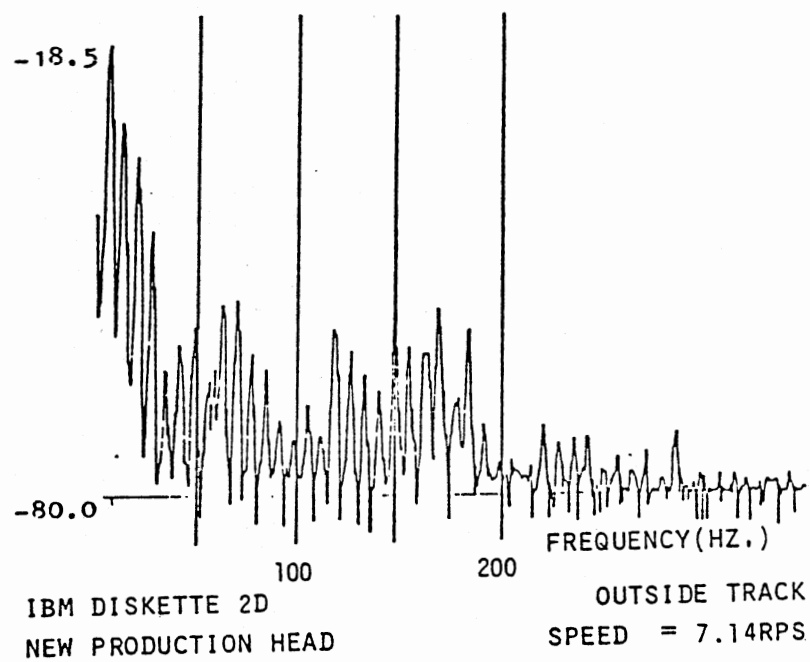
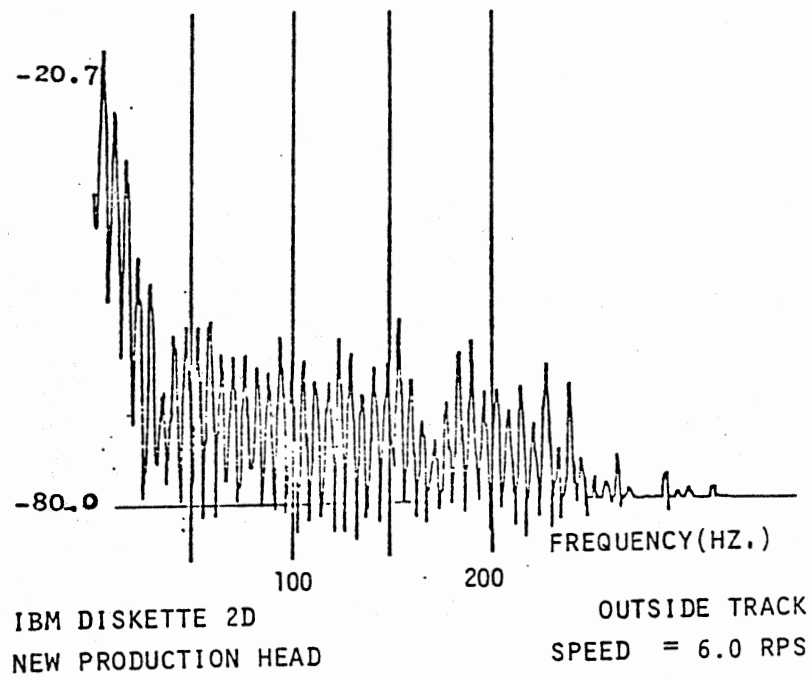
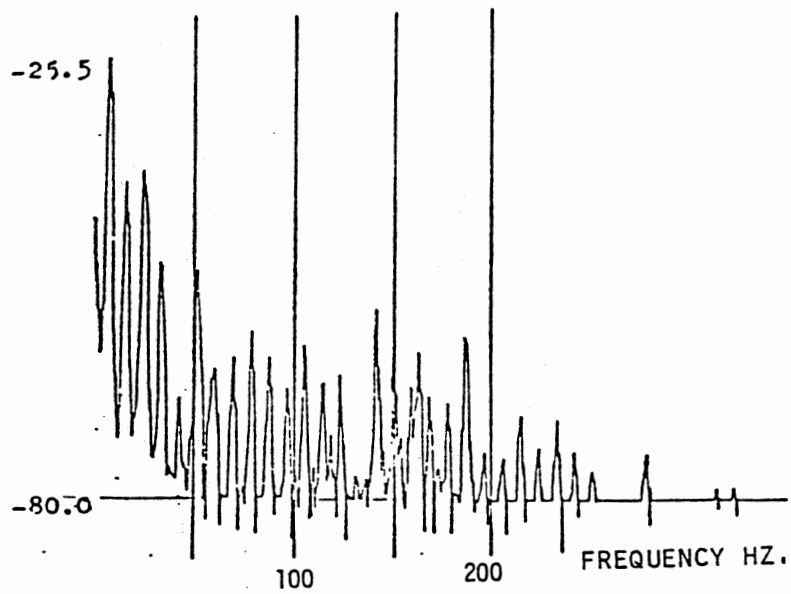
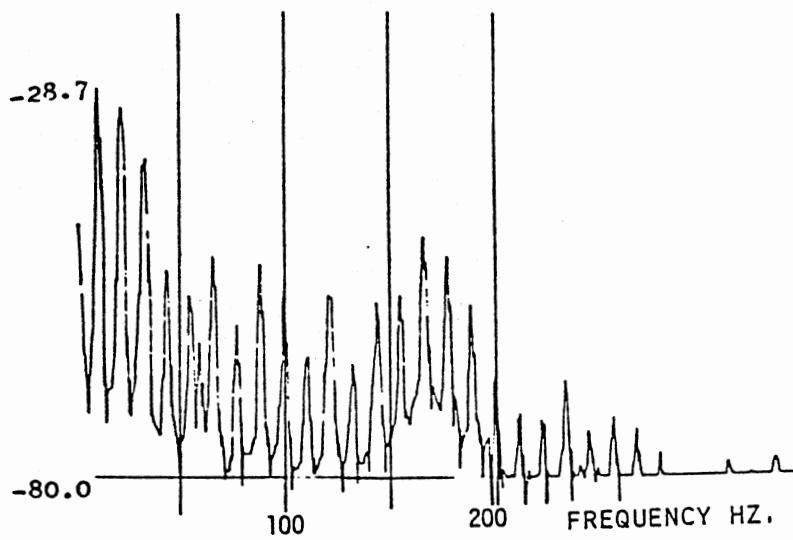


Figure 59. Spectral Plots Corresponding to Voltage versus Time Traces of Figure 58



IBM DISKETTE 2D
NEW PRODUCTION HEAD

OUTSIDE TRACK
SPEED = 8.89RPS



IBM DISKETTE 2D
NEW PRODUCTION HEAD

OUTSIDE TRACK
SPEED = 11.1RPS

Figure 59. (Continued)

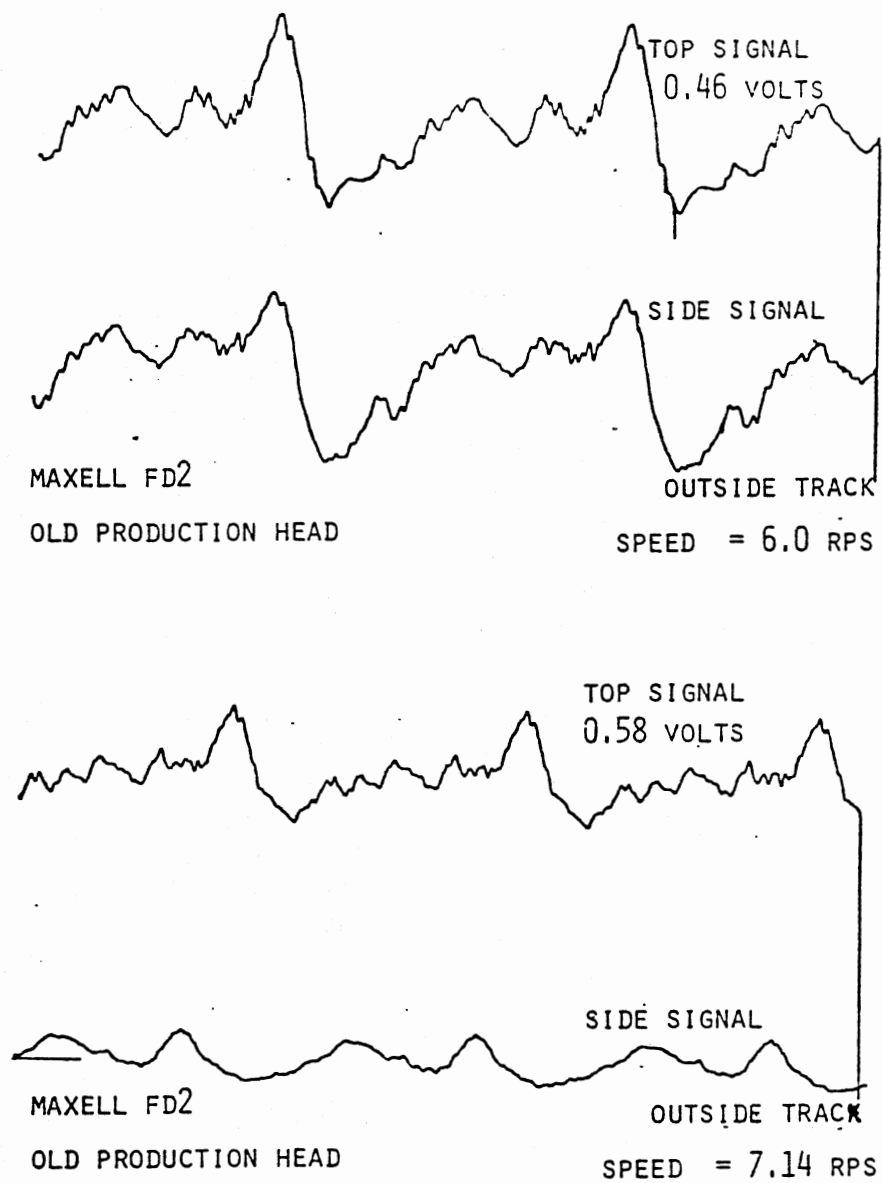


Figure 60. Voltage versus Time Traces for the Old Production Head at Various Drive Speeds

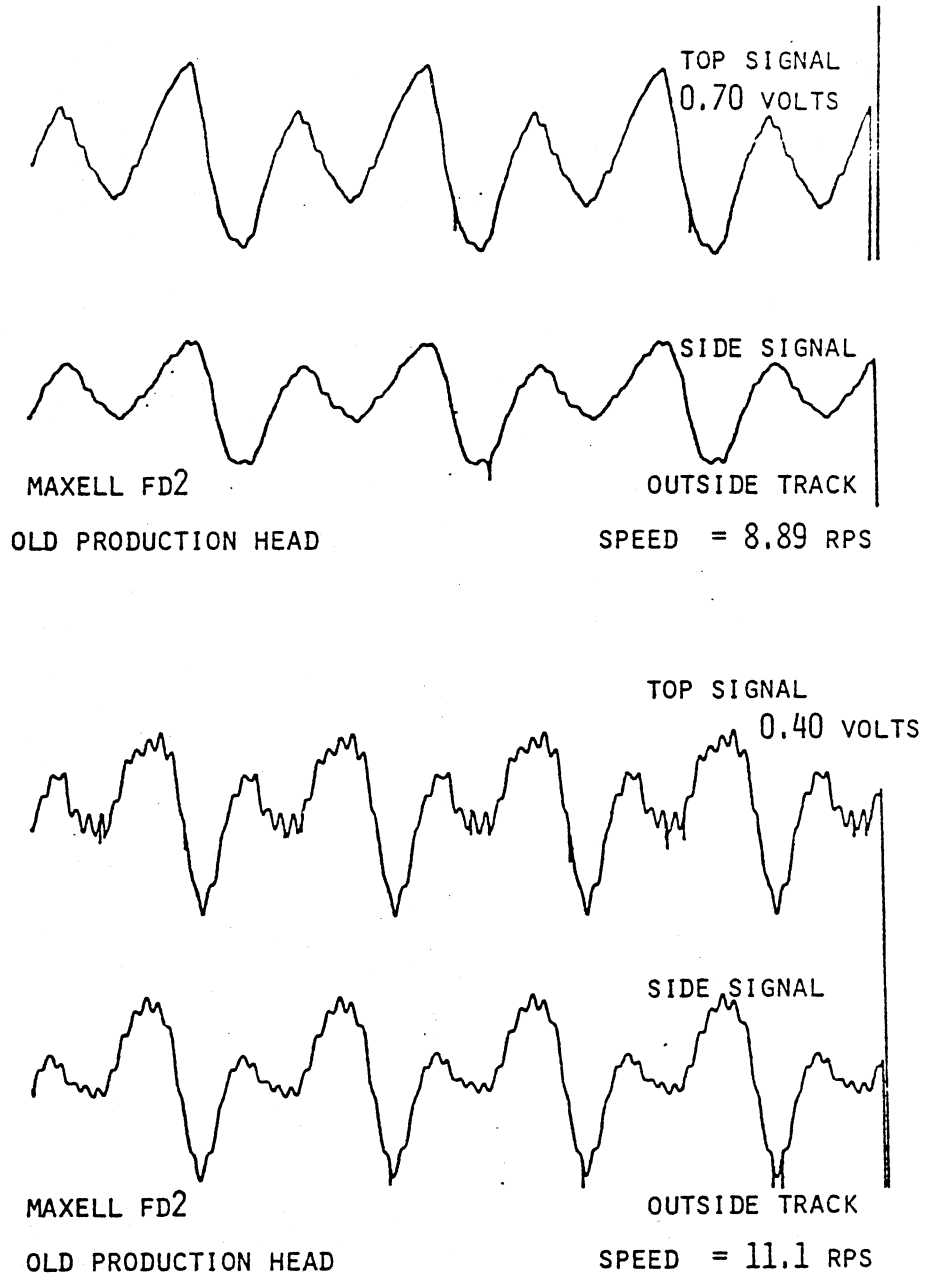


Figure 60. (Continued)

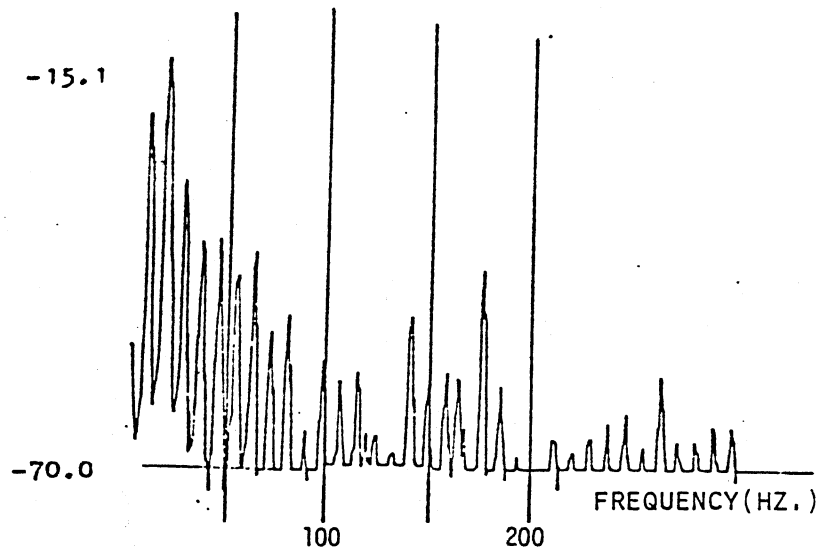
volts to 0.58 volts to 0.70 volts, respectively. At 11.1 revolutions per second, a marked decrease to 0.40 volts occurs. The waveshapes also change considerably. At one speed (8.89 RPS), the high frequency rider diminishes. Figure 61 depicts the spectral content for Figure 60. The first major frequency component is visible at approximately 175 Hz.. The amplitude of this component tends to increase with increased speed but there is an interaction with the 290 Hz. component. When one component is strong, the other tends to be weak.

The single beam LAMDA system was employed to yield qualitative information on the floppy disk system. As forementioned in Chapter V, the system was expanded to the dual beam system to obtain quantitative information. The experimental results of the dual beam system will be presented in two parts, frequency response and deflection analysis.

The frequency response data was obtained in time averaged and transient form. Time averaged spectrum for the pitch and roll modes were obtained through use of the Spectral Dynamics Real Time Analyzer forementioned in Chapter V. Transient Frequency data was collected from oscillograph recordings of signal versus time.

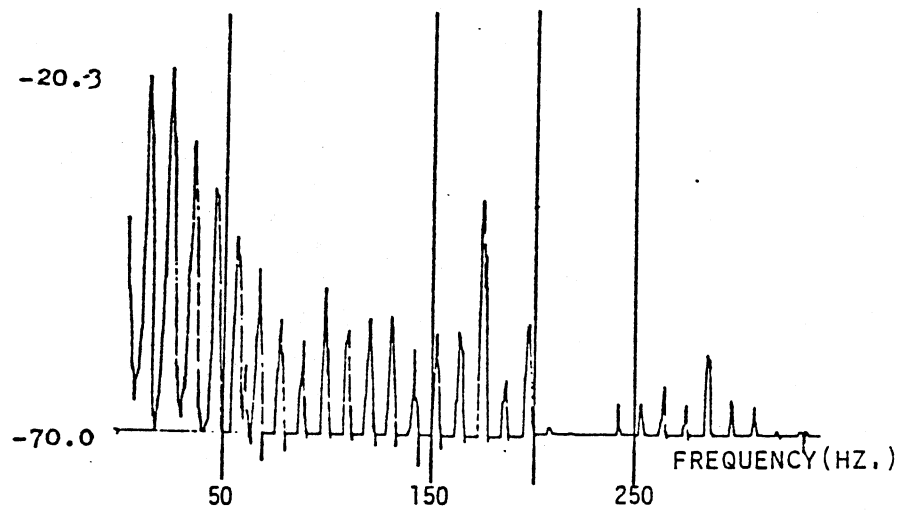
Table VII presents an overview of the resonant frequencies of the heads at an outside track on various disks. Perusal of the Table shows that the first resonant pitch frequency varies from 134.5 to 173.3 Hz. for the new production head, with an average value of 161.2 Hz. The first roll mode of the new head varies from 250.6 to 291.9 Hz., with an average value of 273.3 Hz.

Spectra for the old production head show two resonant frequencies of pitch. These frequencies lie in the 121.8 to 148.5 Hz. and the 236.3 to 263.5 Hz. ranges with average values of 138.3 and 249.9 Hz.,



MAXELL FD2
OLD PRODUCTION HEAD

OUTSIDE TRACK
SPEED = 8.89 RPS



MAXELL FD2
OLD PRODUCTION HEAD

OUTSIDE TRACK
SPEED = 11.1 RPS

Figure 61. (Continued)

TABLE VII
 RESONANT FREQUENCIES (Hz.) OF HEADS AT AN
 OUTSIDE TRACK ON VARIOUS DISKS

DISK	OLD PRODUCTION HEAD		NEW PRODUCTION HEAD	
	PITCH RESONANCE	ROLL RESONANCE	PITCH RESONANCE	ROLL RESONANCE
DYSAN 3740-2D DISKETTE	148.5 257.0	220.8	178.2	269.9
IBM DISKETTE 2D	135.6 263.5	284.1	149.8	250.6
MAXELL FD2	121.8 236.3	215.7	170.5	271.2
CONTROL DATA SAMPLE #39	147.2 244.1	235.1	162.7	285.0
CONTROL DATA SAMPLE #38	148.5 249.3	241.8	157.6	271.2
UNBURNISHED	127.9 249.3	240.2	148.5	291.9
<u>AVERAGE</u>	138.3 249.9	239.6	161.2	273.3

respectively. The roll mode ranges from 215.7 to 284.1 Hz. with an average value of 239.6 Hz.

All of the frequency spectra contained all harmonics of the disk drive speed. An explanation can be founded through the examination of the diametral modeshapes of a spinning disk. Figure 62 shows a composite modeshape for the first diametral mode. For the purpose of portrayal Figure 62 places the disk in a fixed reference system and the observer (i.e., the read/write head) is circling on an outside track at the angular velocity of the disk drive. Perusing the path of the observer it can be seen that the base period for vertical deflection or pitch rotation is equivalent to the time required for the observer to navigate the disk periphery one time. For the production disk drive this will occur every one sixth second such that the first frequency component observed would be 6 Hz..

Before results could be determined for displacement data, a method had to be resolved in which the signal voltages could be readily converted to displacements. This is particularly difficult for the Top detectors whose signals are nonlinearly dependent on both vertical displacement and pitch. In Chapter V a calibration equation relating vertical displacement to output signal was developed for the Front Top Detector for the New Production Head. For convenience, that relation is repeated:

$$F(z) = -0.243 + 42.17 z - 4333.3 z^2 \quad (6.1)$$

A calibration equation for pitch was developed in the same fashion.

$$F(\theta_{yy}) = -10.13 + 7080.0 \theta_{yy} - 990000.0 \theta_{yy}^2 \quad (6.2)$$

θ_{yy} in this equation has units of inches and represents the peak to

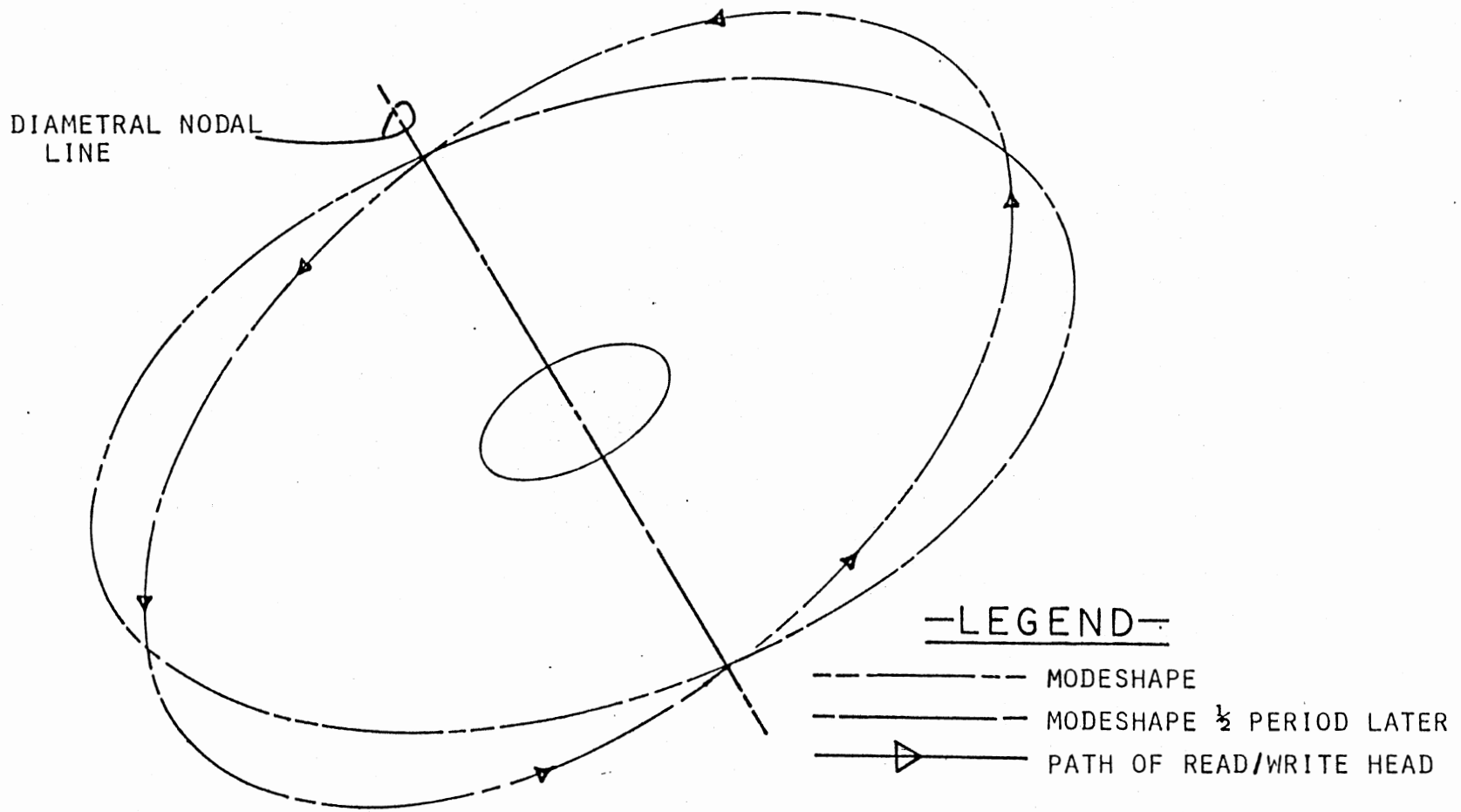


Figure 62. Composite Modeshape for First Diametral Mode of Disk

peak displacement input to the calibrating rocker device discussed in Chapter V. To convert θ_{yy} to degrees, multiply by a conversion factor of 68. $F(Z)$ and $F(\theta_{yy})$ both have units of volts. For sake of comparison substitute 0.003 inches for both Z and θ_{yy} into the relationships. This yields:

$$F(Z) = 0.063 \text{ volts} \quad (6.3)$$

$$F(\theta_{yy}) = 2.2 \text{ volts} \quad (6.4)$$

Photonic probe measurements have shown that the average peak to peak vertical displacement is approximately 0.003 inches. Peak to peak voltages from signal versus time recordings from the front top detector typically range from 0.5 to 1.0 volts. Thus it is deduced that these signals are due mainly to pitch motion.

With the knowledge that the signal was comprised mainly of pitch, a trial and error procedure was implemented to determine the pitch and translation for a given signal. For expediency, this procedure was programmed on the OSU IBM 370 computer. A flow chart of the program is shown in Figure 63. If the signal was as dependent on translation as it was on pitch the program would yield infinitely many solutions. With the increments in pitch used in the program the pitch can be resolved within 0.004 degrees. The resolution of translation cannot be determined but the translations obtained from the program were within bounds determined by photonic probe measurements.

The roll of the read/write head was much simpler to determine as the signals from the side detectors should be entirely a function of roll as forementioned in Chapter V. Again for expediency a procedure was implemented on the computer. A flow chart of this procedure is shown in Figure 64.

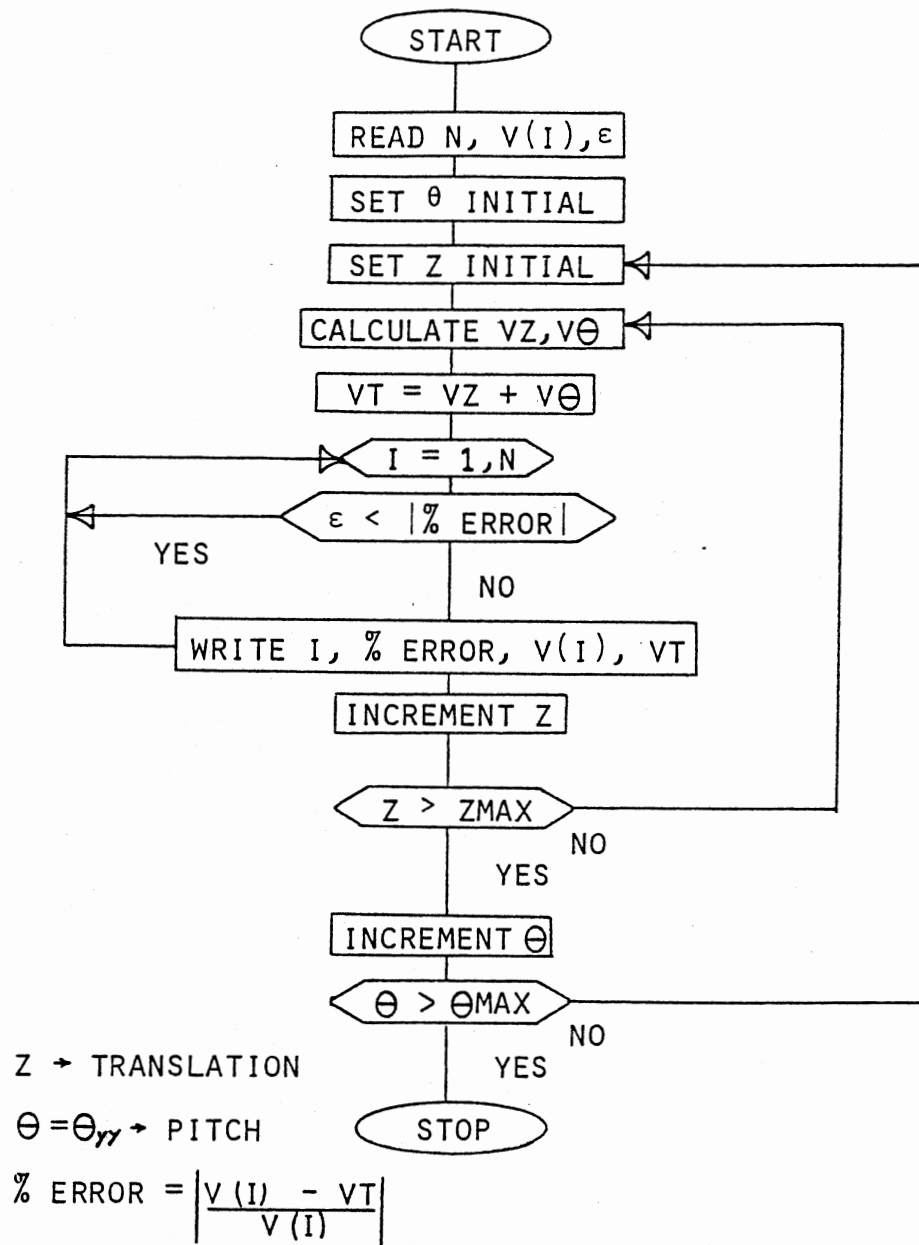
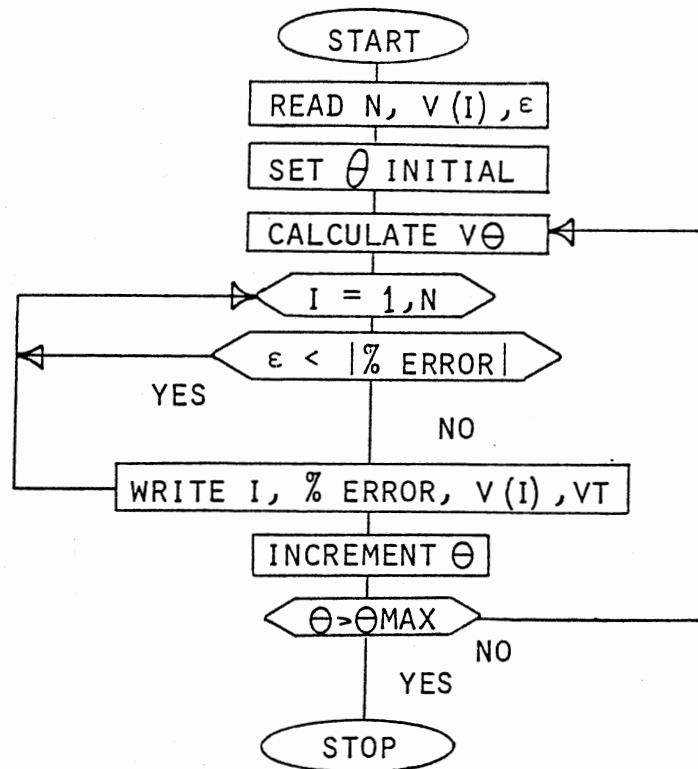


Figure 63. Flowchart to Implement Trial and Error Method to Calculate the Translation and Pitch of the Read/Write Heads



$$\theta = \theta_{xx} \rightarrow \text{ROLL}$$

$$\% \text{ERROR} = \frac{V(I) - V\theta}{V(I)}$$

Figure 64. Flowchart to Implement Trial and Error Method to Calculate the Roll of the Read/Write Heads

Figures 65 and 66 are signal versus time traces for the new production head on an outside track of a Maxell FD2 Disk. The numbers on the traces represent points at which peak to peak voltages were determined. These voltages were input to the computer program whose output can be perused in Tables VIII and IX. Results from this test and others involving the new production head show that the pitch angle (θ_{yy}) varies from about 0.145° to 0.160° . Roll (θ_{xx}) is somewhat less with maxima on the order of 0.09° to 0.10° . Figure 66 was included such that the periodicity of the signal could be examined.

Figures 67 and 68 are signal versus time traces for the old production head on an outside track of an IBM 2D Diskette. Displacements corresponding to the peak to peak voltages identified on Figure 67 are contained in Table X. Results from this test and others involving the old production head show that the pitch maxima are in the 0.2125° to 0.2175° range. Roll maxima are in the 0.0694° to 0.1523° range. The increase in pitch and roll when compared to the new production head can be attributed to the higher flexibility of the gimbaled old production head design.

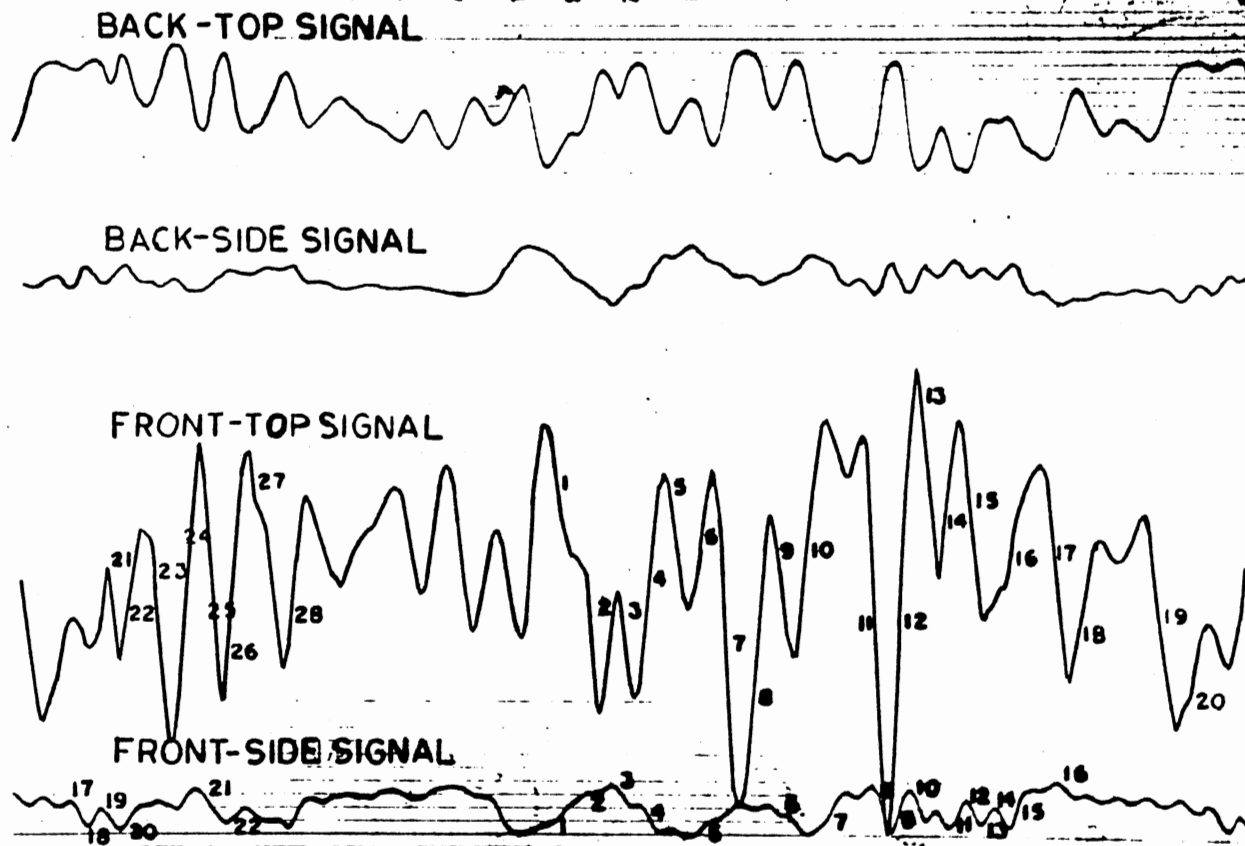


Figure 65. New Production Head on an Outside Track of a Maxell FD2 Disk. Chart Speed = 32 in/sec

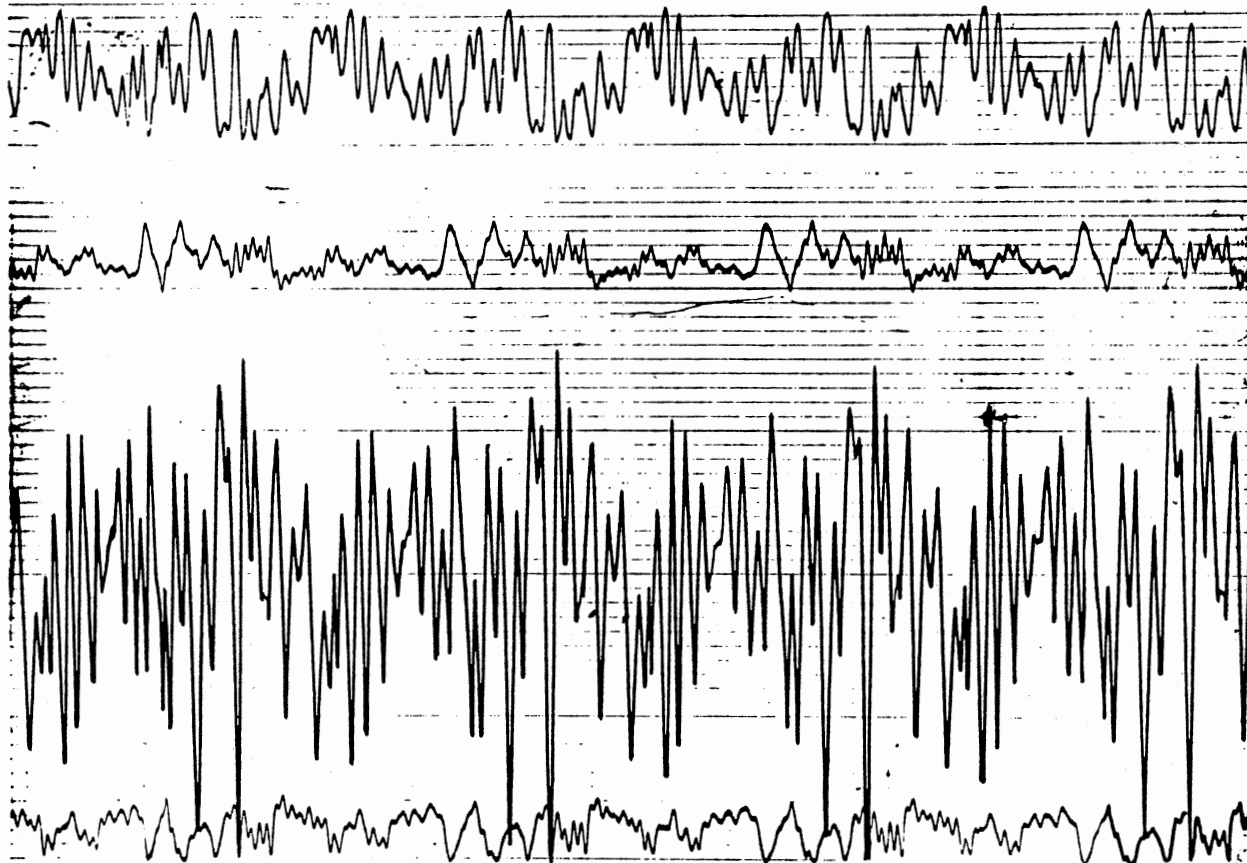


Figure 66. New Production Head on an Outside Track of a
Maxell FD2 Disk. Chart Speed = 8 in/sec

TABLE VIII

PITCH AND DISPLACEMENT OF THE NEW PRODUCTION HEAD
ON A MAXELL FD2 DISK AT AN OUTSIDE TRACK.

FRONT - TOP DETECTOR					
I	V(I) (volts)	VT (volts)	ERROR(I)	Θ_{yy} (deg.)	Z (in.)
10	0.51875	0.52165	0.00559	0.14586	0.0012
27	0.52813	0.527831	0.000567	0.14586	0.0014
19	0.54063	0.539152	0.002734	0.14586	0.0018
34	0.54375	0.544293	0.000998	0.14586	0.0020
4	0.550	0.549087	0.001661	0.14586	0.0022
25	0.59375	0.591854	0.003194	0.14756	0.0012
26	0.59375	0.591854	0.003194	0.14756	0.0012
17	0.60313	0.603868	0.001224	0.14756	0.0016
8	0.625	0.623738	0.00202	0.14756	0.0024
1	0.65626	0.65429	0.002985	0.14926	0.0010
24	0.69375	0.692703	0.00151	0.14926	0.0024
7	0.750	0.751191	0.001589	0.15096	0.0020
11	0.875	0.872304	0.003081	0.15436	0.0016
12	1.03438	1.030218	0.004024	0.15776	0.0030

TABLE IX

ROLL OF THE NEW PRODUCTION HEAD ON A
MAXELL FD2 DISK AT AN OUTSIDE TRACK.

FRONT - SIDE DETECTOR				
I	V(I) (volts)	VTHETA (volts)	ERROR(I)	Θ_{XX} (deg.)
5	0.3438	0.34356	0.00070	0.04216
13	0.04375	0.044016	0.006078	0.04896
19	0.04375	0.044016	0.006078	0.04896
14	0.05313	0.053476	0.006509	0.05576
4	0.0625	0.062736	0.003773	0.06256
17	0.0625	0.062736	0.003773	0.06256
21	0.06875	0.068196	0.008062	0.06664
10	0.07188	0.071796	0.001173	0.06936
23	0.07188	0.071796	0.001173	0.06936
24	0.0875	0.0876	0.00114	0.0816
1	0.09375	0.094416	0.0071	0.08704
7	0.09375	0.094416	0.0071	0.08704
15	0.09688	0.0961	0.008055	0.0884
9	0.10	0.099444	0.005564	0.09112
8	0.10625	0.106036	0.002017	0.09656

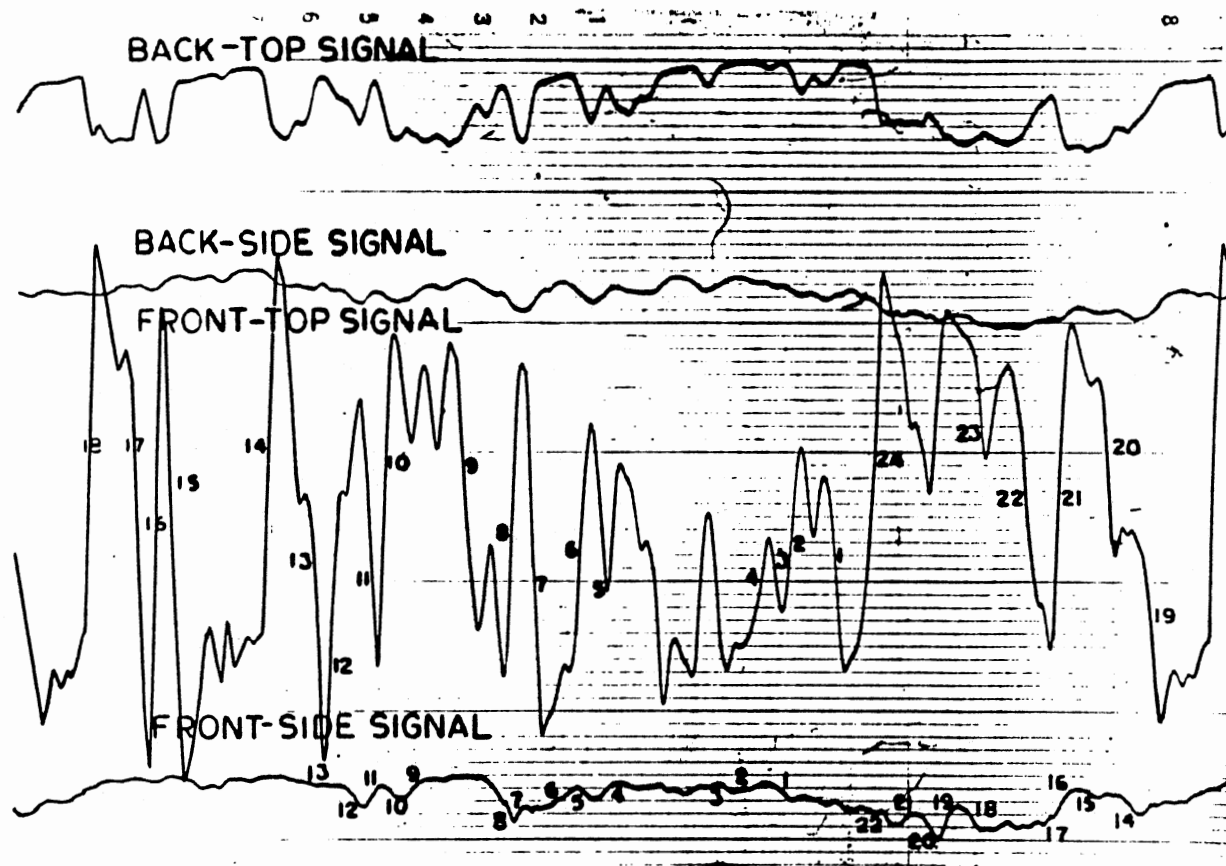


Figure 67. Old Production Head on an Outside Track
of an IBM 2d Diskette Chart Speed =
32 in/sec

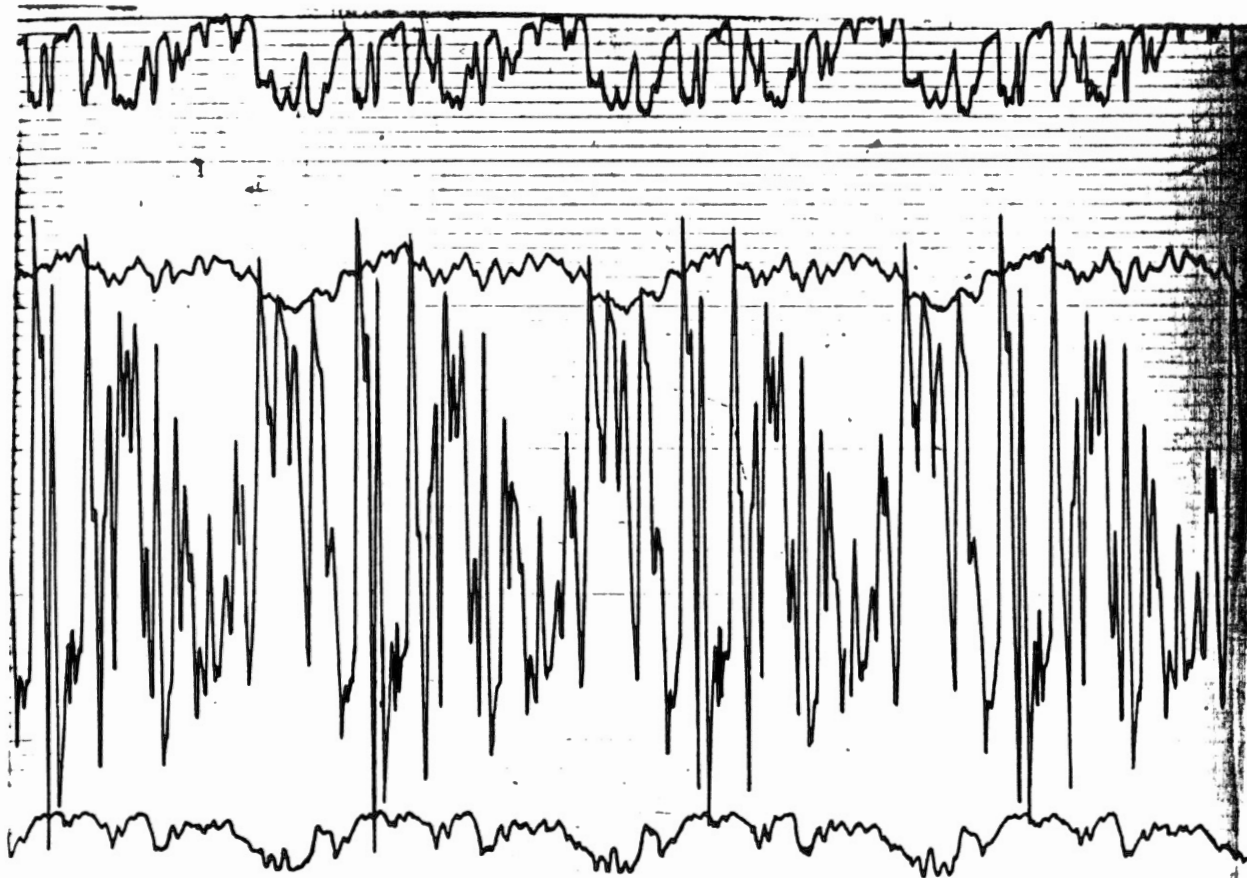


Figure 68. Old Production Head on an Outside Track
of an IBM 2D Diskette. Chart Speed =
8 in/sec

TABLE X

ROTATIONS AND DISPLACEMENT OF THE OLD PRODUCTION HEAD
ON AN IBM 2D DISKETTE AT AN OUTSIDE TRACK.

FRONT - TOP DETECTOR					
I	V(I) (volts)	VT (volts)	ERROR(I)	Θ_{yy} (deg.)	Z (in.)
7	0.89063	0.89065	0.000023	0.1258	0.0022
21	0.83125	0.831868	0.000744	0.1156	0.0010
12	0.91875	0.918868	0.000128	0.1564	0.0010
14	0.91875	0.918868	0.000128	0.1564	0.0010
24	0.9625	0.962063	0.000454	0.1581	0.0020
18	1.0375	1.037859	0.000346	0.1734	0.0026
17	1.08125	1.081171	0.000073	0.1836	0.0026
15	1.13125	1.131355	0.000093	0.2023	0.0014
16	1.175	1.174627	0.000317	0.2074	0.0018
13	1.2125	1.212527	0.000023	0.2176	0.0012
FRONT - SIDE DETECTOR					
I	V(I) (volts)	VTHETA (volts)	ERROR(I)	Θ_{xx} (deg.)	
1	0.03125	0.031498	0.007935	0.06936	
13	0.03125	0.031498	0.007935	0.06936	
17	0.03125	0.031498	0.007935	0.06936	
22	0.03438	0.034482	0.002965	0.07208	
15	0.0375	0.03745	0.001344	0.0748	
7	0.04063	0.040402	0.005613	0.07752	
6	0.04375	0.043338	0.009419	0.08024	
11	0.04375	0.043338	0.009419	0.08024	
14	0.04375	0.043338	0.009419	0.08024	
16	0.06563	0.06625	0.009443	0.1020	
19	0.06875	0.069042	0.004244	0.10472	
8	0.11563	0.115312	0.002753	0.15232	

CHAPTER VII

CORRELATION BETWEEN ANALYTICAL AND EXPERIMENTAL STUDIES

Correlation between experimental and analytic displacements is impossible, at this point in time, as there were no forced vibration studies performed analytically. This type of analysis is hampered due to the lack of knowledge with regard to the forcing function that exists between head and disk.

Correlation in the frequency domain is both possible and rewarding. For instance, using the single beam LAMDA 3system it was noted for the old production head that there were two major frequency pitch components, one at about 175 Hz. and one at about 290 Hz.. The 175 Hz. signal is due to one of the head/disk modes discussed in the analytic results and the 290 Hz. signal is undoubtedly the second pitch mode of the head which was analytically determined to be about 295 Hz.. A major point of interest is that experiments indicated that the two frequency components fluctuate with respect to time and that when one component is strong the other is comparatively weak. The transient analysis of the old production head exhibited a component at approximately 315 Hz. that died out quickly as shown in Figure 27. This substantiates the difficulty entailed in the second pitch mode existing with a lower frequency pitch mode as discussed in the analytical results. Comparing the frequency analysis results using

the dual beam LAMDA system with the analytical eigenvalue analyses gives reasonable correlation for both heads.

For the new production head, modes contributing to the pitch of the head were distinguished at 121.6, 143.5, and 163.2 Hz. by the eigenvalue analyses. The experimental data indicate pitch frequencies varying from 134.5 to 173.3 Hz. indicating that possibly all three modes are excited but one dominates, possibly depending on such parameters as disk type and waveforms imposed on the disk by the clamping mechanism. The correlation for the roll mode is not quite as good. Experimental data indicate the roll mode of the new head varies in the 250.6 to 291.9 Hz. range while the eigenvalue analyses predict a variance between 227.2 and 243.9 Hz.. While this difference is sizable it is not of concern. During tests in which the natural frequencies of the flexures were determined it was noted that the tension in the electrical leads to the stylus had a significant effect on the natural frequency (as much as 30 Hz. changes were noted for different tensions and geometries of the leads) of the first roll mode. Therefore, on present head designs the roll mode frequency will differ from one drive to another.

The old production head has eigenvalues which contribute to head pitch at 120.9, 167.3, and 169.1 Hz.. The second pitch mode of the head is at 295.3 Hz.. The experiments show pitch response in the 121.8 to 148.5 Hz. and 236.3 to 263.5 Hz. ranges. In this case the 120.9 Hz. eigenvalue may dominate while the 167.3 and 169.1 Hz. eigenvalues play a lesser role. The 295.3 Hz. eigenvalue, the second pitch mode, does not fall in the 236.3 to 263.5 Hz. range; however, it is very close to earlier data indicating a 290 Hz. signal. This drew

attention to the fact the mirrors which have been cemented to the ferrite posts, to reflect the laser signal, significantly increase the mass moment of inertia of the stylus, and the mirror used in the earlier work was much smaller than those presently used. Since the stylus rotates independently of the gimbal frame during the second pitch mode a decrease would be expected in natural frequency. As the stylus and gimbal frame rotate in phase during the first pitch mode the percentage change in mass moment of inertia is less and there by only small changes in natural frequency would be expected. For the roll mode, analyses predicted a range from 246.3 to 281.0 Hz.. Experimental values ranged from 215.7 to 284.1 Hz. which is fair correlation but still indicative of wide variances due to the tension and geometry of the electrical leads.

CHAPTER VIII

CONCLUSIONS

Overview

The finite element method provides viable solutions in the vibration analysis of read/write heads on floppy disks. The finite element analysis predicted broad band pitch response in the 120 to 170 Hz. range. Experimental frequency analyses performed on the dual beam LAMDA system verified this prediction. The finite element analysis of the old production head predicted a second pitch mode at 295 Hz. Experimental analyses indicated the second pitch mode occurred at 290 Hz., well within engineering accuracy. The results from the roll analyses are not as consistent as results from pitch analyses. This is partially due to variance in electrical lead configuration for the experimental analyses while selection of realistic boundary conditions is difficult for the finite element model. The third pitch mode of the old production head predicted by the finite element model could not be verified by the experimental apparatus as the apparatus frequency response is nonlinear above 500 Hz. High frequency analyses should include transient analyses to save cost.

Experiments run on disks of various manufacturers using the single beam LAMDA system demonstrated that vibration amplitude is affected by the make of disk. Spectral plots of the subject data depicted little variation in frequency content. Experiments in which

disk drive velocity was varied demonstrated the stability of the new production head. The old production head, in contrast, displayed some instability at increased drive speed due to excitation of the second pitch mode.

The dual beam LAMDA system helped establish maximum rotations for the new and old production heads. The maximum pitch and roll rotations of the new production head are 0.16° and 0.10° , respectively. The maximum pitch and roll rotations of the old production head are 0.22° and 0.15° , respectively.

Conclusions Regarding Design Characteristics

It is clear that read/write head design is truly an iterative process. For instance, the gimballed design of the old production head has the following advantages:

1. It has great flexibility in the pitch direction thereby allowing the to stylus follow low frequency waveshapes (0 - 350 Hz.) of the disk well.
2. The flexibility results in low disk wear.

The disadvantages are:

1. Although the gimbals allow flexibility at low frequencies, high frequency inputs to the system (i.e., the oxide surface of the disk abrading against the stylus) may excite resonances in the gimballed region.
2. These resonances may cause high frequency head pitch motion which will promote head squeal, signal loss, and increased wear of the disk surface.

The new production head, which is not gimbaled has greater stiffness than the old production head at higher frequencies. As the stylus is unable to pitch independently of the flexure the second and third pitch modes exhibited by the old head are non-existent. This provides an explanation for the old production head squealing phenomena and the absence of this phenomena for the new production head. Although the non-gimbaled design may eliminate the high frequency resonance problem, the greater stiffness may cause higher disk wear at low frequencies due to an inability to follow the disk's waveshapes as well as the flexible gimbaled design.

Recommendations for Future Designs

For low frequencies (0 - 300 Hz.) the stability of the system could be improved by increasing the dynamic stiffness of the disk locally in the read/write head region. There are several ways of accomplishing this, the easiest of which may be by inducing curvature in the disk locally as is suggested by U.S. Patent 4,120,505. The patent details a flexible disk moving over a stabilizing backing plate but it seems that this idea could be extended to enforcing a curvature into the disk jacket.

Another method of increasing localized stability of the disk would be to design a pressure pad which would encompass the read/write head. Experiments using the LAMDA system have shown that the present pressure pad does little to increase stability of the read/write head although it may help maintain the radial position of a track under the stylus. This concept could be combined with the first concept such that the pressure pad could enforce the curvature in the disk.

Work could be done in the drive clamp area to keep the clamp from forcing buckled shapes into the disk. While this could have impact on the forcing function and thereby the amplitude of vibration of the heads it would not by any means be a solution to the overall problem. Waveshapes due to eigenvalues of the disk would not be impaired significantly by clamp technique such that the read/write head would still have to encounter these waves.

For high frequencies (1000 - 3000 Hz.) the system stability can be controlled mainly by the read/write head flexure design. This is the only controllable parameter as it is unlikely the oxide surface of the disk will be changed. Certainly the new production head flexure is more stable than the old production head flexure as the gimbals were eliminated making an eigenvector, as shown in Figure 31, exist at frequencies high compared to the 1 - 3 KHz. range.

BIBLIOGRAPHY

1. The Hewlett Packard Electronics Instruments and Systems Catalogue. North Hollywood, California: Hewlett Packard, 1983.
2. Mulvaney, R. B., and L. H. Thompson, "Innovations in Disk File Manufacturers", IBM Journal of Research and Development, Vol. 25 (1981), pp. 711-723.
3. Magnetic Peripherals Inc., Informal Meeting, Oklahoma City, Oklahoma, February 5, 1981.
4. Lamb, H., and R. V. Southwell, "The Vibrations of a Spinning Disk", Proceedings of the Royal Society, London, Vol. 99, (1921), pp. 272-280.
5. Southwell, R. V., "On the Free Transverse Vibrations of a Uniform Circular Disc Clamped at Its Centre", Proceedings of the Royal Society, London, Vol. 101 (1921), pp. 133-153.
6. Prescott, J., Applied Elasticity, New York: Dover Publications, Inc., 1961, Ch. 18.
7. Tobias, S. A., "Free Undamped Nonlinear Vibrations of Imperfect Circular Disks", Proceedings of the Institute of Mechanical Engineers, Vol. 171 (1957), pp. 691-701.
8. Nominski, J. L., "Nonlinear Transverse Vibrations of a Spinning Disk", Journal of Applied Mechanics, Vol. 31. Transactions of ASME, Vol. 86, Series E (1964), pp. 72-78.
9. Iwan, W. D., and T. L. Moeller, "The Stability of a Spinning Elastic Disk with a Transverse Load System", Journal of Applied Mechanics, Vol. 43. Transactions of ASME, Vol. 98, Series E (1976), pp. 485-490.
10. Benson, R. C., "Deflection of a Transversely Loaded Spinning Disk", Microfilm copy published by University Microfilms International, Ann Arbor, Michigan. (Ph.D. thesis, Department of Mechanical Engineering, University of California, 1977).
11. Benson, R. C., and D. B. Bogy, "Deflection of a Very Flexible Spinning Disk Due to a Stationary Transverse Load", Transactions of ASME, Vol. 45 (1978), pp. 636-642.

12. Pardoen, G. C., "Static, Vibration, and Buckling Analysis of Axisymmetric Circular Plates Using Finite Elements", Computers and Structures, Vol. 3 (1973), pp. 355-375.
13. Srinivasan, V., and V. Ramamurti, "Dynamic Response of an Annular Disk to a Moving Concentrated In-Plane Edge Load", Journal of Sound and Vibration, Vol. 72 (1980), pp. 251-262.
14. Nigh, G. L., and M. D. Olson, "Finite Element Analysis of Rotating Disks", Journal of Sound and Vibration, Vol. 77 (1981), pp. 61-78.
15. Kirkhope, J., and G. J. Wilson, "Vibration and Stress Analysis of Thin Rotating Disks Using Annular Finite Elements", Journal of Sound and Vibration, Vol. 44 (1976), pp. 461-474.
16. Kennedy, W., and D. Gorman, "Vibration Analysis of Variable Thickness Discs Subjected to Centrifugal and Thermal Stresses", Journal of Sound and Vibration, Vol. 53 (1977), pp. 83-101.
17. Pelech, I., and A. H. Shapiro, "Flexible Disk Rotating on a Gas Film Next to a Wall", Journal of Applied Mechanics, December 1964, pp. 577-584.
18. Krauter, A. I., and P. Z. Bulkeley, "Effect of Central Clamping on Transverse Vibrations of Spinning Membrane Disks", Journal of Applied Mechanics, December 1970, pp. 1037-1042.
19. Lin, C., and R. F. Sullivan, "An Application of White Light Interferometry in Thin Film Measurements", IBM Journal of Research and Development, Vol. 16 (1972), pp. 269-276.
20. Houston, R. A., Physical Optics. London: Blackie and Son Limited, 1968, pp. 49-58.
21. Waddell, P., "Strain Pattern Examination", Engineering and Materials Design, Vol. 17 (1973), p. 3.
22. Stetson, K. A., and J. N. Elkins, "Optical System for Dynamic Analysis of Rotating Structures", Air Force Aero Propulsion Lab. Contract F33615-75-C-2013, AFAPL-TR-77-51 (1977).
23. MacBain, J. C., J. E. Horner, W. A. Stange, J. S. Ogg, "Vibration Analysis of a Spinning Disk Using Image-Derotated Holographic Interferometry", Experimental Mechanics, January 1979, pp. 17-22.
24. Kita, T., K. Kogure, Y. Mitsuva, T. Nakanishi, "New Method of Detecting Contact Between Floating Head and Disk", IEEE Transactions on Magnetics, Vol. 16 (1980), pp. 873-875.
25. Engh, J. T., "The IBM Diskette and Disk File", IBM Journal of Research and Development, Vol. 25 (1981), pp. 701-710.

26. Greenberg, H. J., "Flexible Disk-Read/Write Head Interface", IEEE Transactions and Magnetics, Vol. 14 (1978), pp. 336-338.
27. Adams, G. G., "Procedures for the Study of the Flexible-Disk to Head Interface", IBM Journal of Research and Development, Vol. 24 (1980), pp. 512-517.
28. National Aeronautics and Space Administration, NASTRAN User's Manual, Washington D.C.: Revised, 1978.
29. Timoshenko, S., and S. Woinowsky-Krieger, Theory of Plates and Shells, 2nd ed. New York: McGraw-Hill Book Co., 1959.
30. Shigley, J. E., Mechanical Engineering Design, 3rd ed. New York: McGraw-Hill Book Co., 1977.
31. Todd, B., Unpublished Research, School of Mechanical and Aerospace Engineering, Oklahoma State University, 1981.
32. Swedeen, R., "Vibration Analysis of a Floppy Disk Head", (Unpublished M.S. Report), School of Mechanical and Aerospace Engineering, Oklahoma State University, 1982.
33. Vickery, C. M., "An Experimental Analysis of Floppy Disk Read/Write Head Vibrations", (Unpublished M.S. Report), School of Electrical Engineering, Oklahoma State University, 1982.
34. Gerald, F. G., Applied Numerical Analysis, 2nd ed., Menlo Park, California: Addison-Wesley, 1980.

APPENDIX

COMPUTER PROGRAM LISTING OF
AUTOMATIC MESH GENERATOR

```

//U16954A JOB (?????,446-60-8155),KG,TIME=(00,5),CLASS=F,
// MSGCLASS=X,MSGLEVEL=(1,1),NOTIFY=U16954A
/*PASSWORD ????
// EXEC FORTGCG
//FORT.SYSIN DD *
    DIMENSION RAD(5000),THET(5000),BC(5000)
    REAL LAMDA,NU
    INTEGER BC
    WRITE(6,4)
    4 FORMAT(' INPUT RI,RO,QI,QF ')
    READ(5,*) RI,RO,QI,QF
    WRITE(6,5)
    5 FORMAT(' INPUT FREQM,ITYPE,OMEGA ')
    READ(5,*) FREQM,ITYPE,OMEGA
    WRITE(6,6)
    6 FORMAT(' INPUT DISK THICKNESS,YOUNGS MOD,POISSON,DENSITY ')
    READ(5,*) TH,E,NU,RHO
    CIRC=2*3.1416*RO
    LAMDA=CIRC/(FREQM*4)
    R=RO-RI
    B=LAMDA/R
    WRITE(6,*) VEL,CIRC,T1,T2,N,LAMDA
    WRITE(6,*) R;B
    IF (ITYPE.EQ.0) GO TO 30
    IF (ITYPE.EQ.1) GO TO 40
30 X1=R/LAMDA
    N1=INT(X1)
    DEL=R/N1
    N1=N1+1
    DO 35 I=1,N1
    RAD(I)=0.0
35 RAD(I)=((I-1)*DEL)+RI
    WRITE(6,*) X1,N1,DEL
    GO TO 46
40 X=1/(10**(B)-1)
    IF(X.LE.10.0) N1=10
    IF(X.GT.10.0) N1=100
    DO 45 K=1,N1
    RAD(K)=0.0
    M=K
    P=FLOAT(M)
45 RAD(K)=(ALOG10(P)*R)+RI

```

```

46 THET1=QF-QI
   THETA=(QF-QI)*3.1416/180.0
   ARC=RO*THETA
   N2=INT(ARC/LAMDA)
   T=FLOAT(N2)
   DTHETA=THET1/T
   WRITE(6,*) ARC,N2,DTHETA
   N2=N2+1
   DO 50 J=1,N2
   THET(J)=0.0
50 THET(J)=((J-1)*DTHETA)+QI
  2 FORMAT(1X,'GRID',4X,I4,4X,'3',7X,2F8.3,1X,'0.0',5X,'3',8X,I6)
   II=0
   DO 100 JJ=1,N1
   DO 100 KK=1,N2
   II=II+1
   BC(II)=6
   IF(KK.EQ.1) BC(II)=1236
   IF(KK.EQ.N2) BC(II)=1236
   IF(JJ.EQ.1) BC(II)=123456
   IF(JJ.EQ.N1) BC(II)=36
100 WRITE(6,2) II,RAD(JJ),THET(KK),BC(II)
   WRITE(6,10)
  10 FORMAT(1X,'GRID',4X,'1000',4X,'0',7X,'0.0',5X,'0.0',5X,'0.0',13X,
 *123456'/1X,'GRID',4X,'1001',4X,'0',7X,'0.0',5X,'0.0',5X,'1.0',13X,
 *'123456'/1X,'GRID',4X,'1002',4X,'0',7X,'1.0',5X,'0.0',5X,'1.0',13
 *X,'123456'/1X,'CORD1C',2X,'3',7X,'1000',4X,'1001',4X,'1002')
   N4=N2
   N3=(N2-1)*(N1-1)
   J1=1
  3 FORMAT(1X,'QUAD2',3X,I4,4X,'1',7X,I4,4X,I4,4X,I4,4X,I4,4X,'0.0')
   DO 110 NN=1,N3
   IF (N4.EQ.J1) J1=J1+1
   N5=J1-1
   IF (N4.EQ.N5) N4=N4+N2
   J2=J1+1
   J3=J1+N2
   J4=J2+N2
   WRITE(6,3) NN,J1,J2,J4,J3
110 J1=J1+1
   WRITE(6,7) TH
  7 FORMAT(1X,'QUAD2',2X,'1',7X,'1',7X,1F8.4)
   WRITE(6,8) E,NU,RHO
  8 FORMAT(1X,'MAT1',4X,'1',7X,1F8.1,8X,2F8.7)
   WRITE(6,9) FREQM
  9 FORMAT(1X,'EIGR',4X,'10',7X,'INV',7X,'0.0',F8.3,4X,'10',7X,'10',1
 *9X,'ABC'/1X,'+BC',7X,'MAX')
   STOP
   END

```

VITA ²

James Keith Good

Candidate for the Degree of

Doctor of Philosophy

Thesis: THE DEVELOPMENT OF FINITE ELEMENT MODELING AND EXPERIMENTAL TECHNIQUES FOR DYNAMIC ANALYSIS OF READ/WRITE HEAD DESIGNS ON FLOPPY DISK MEDIA

Major Field: Mechanical Engineering

Biographical:

Personal Data: Born December 17, 1955, in Bartlesville, Oklahoma, the son of Mr. and Mrs. W. D. Good.

Education: Graduated from College High School, Bartlesville, Oklahoma, in May 1973; received the Bachelor of Science in Mechanical Engineering degree in 1977 from Oklahoma State University; received the Master of Mechanical Engineering degree in 1979 from Oklahoma State University; completed the requirements for the Doctor of Philosophy degree at Oklahoma State University in July 1983.

Professional Experience: Structural Analyst, Cessna Aircraft Company, Wichita, Kansas, 1977; Consulting Engineer, Boyd and Associates, Inc., Stillwater, Oklahoma, 1978; Structural Analyst, Cessna Aircraft Company, Wichita, Kansas, 1979-1980; Instructor of Mechanical Engineering, Oklahoma State University, 1980-1983.

Professional Organizations: Pi Tau Sigma, American Society of Mechanical Engineers, Oklahoma Society of Professional Engineers.